Teoretical Model Study on the Surface-Adsorbate Reaction, GaAs Crystal Growth,and Hydrolysis Mechanism in Protein(Dissertation_全文)

AUTHOR(S):

Fukunishi, Yoshifumi

(2)

Theoretical Model Study on the Surface-Adsorbate Reaction, GaAs Crystal Growth, and Hydrolysis Mechanism in Protein

Yoshifumi Fukunishi

PREFACE

Surface modeling is a principal step in theoretical investigations of chemisorptions and catalytic reactions on a solid surface. Catalytic reactions are due to surface-adsorbate interaction. In the cluster model, a surface is represented by several solid atoms which interact directly with an admolecule. Furthermore, the interaction in chemisorption is localized within a small region and the adsorbate-substrate bond is local. Many calculations for surface reactions have been performed using the cluster model, and it has been shown to be useful for clarifying the mechanisms of chemisorption, as well as for describing active sites and electronic structures. The cluster model provides a good approximation of covalently bound material, particularly semiconductors and the reaction centers of proteins. However, this model does not adequately take into account the specific effect of the bulk solid and is influenced by the boundary effect due to its finite size. The electrostatic field in metal oxides, the so-called Madelung potential, plays an important role in the calculation of the bonding energy of the ionic crystal. Evalts summation method has been used to estimate bonding energy, but this method can not be readily adapted to the surface-adsorbate system.

Various models have been proposed to include the bulk effect. The free electron and image force are considered in the Dipped Adcluster Model proposed by Nakatsuji. The embedding method proposed by Grimley, Pisani and Ravenek, which is based on the Green's function method, attempts to represent the connection between the cluster and the underlying bulk solid. This model is particularly good for representing the change in electron density that is induced by a chemical reaction.

Part I of this thesis summarizes a theoretical model for representing surface-adsorbate interaction.

Chapter 1 describes the modeling of a metal-oxide. To estimate the electrostatic field of the crystal, many point charges must be considered in the calculation, due to the slow convergence of the electric field. This study reveals the exponential

attenuation of the field against the surface based on the periodicity of the electric field. The entire field is then well represented by considering only the first and second layers of the solid. The Madelung potential is important for reproducing the adsorbed structure and the band-gap. Furthermore, this study also describes the role of the charge polarization of the metal-oxide in the catalytic reaction.

Chapter 2 presents a modification of the ECM and its application to hydrogen adsorption on a lithium surface. In this system, due to the small difference in adsorption energy between different adsorption sites, the actual adsorption site is unclear. Furthermore, if we use the cluster model, the calculated adsorption energy largely depends on the cluster size. This study modifies the Green's function, the basis set and the convergence algorithm to produce a new ab-initio program. The modification results in an on-top adsorption of hydrogen instead of the bridge-site adsorption in the cluster model. The effect of the cluster size is also less than that of the cluster model.

Part II focuses primarily on the mechanism of GaAs epitaxial crystal growth. Gallium arsenide, a material which does not exist in nature, is a typical compound semiconductor and shows many interesting behaviors. Since gallium and arsenic have different vapor pressures, the GaAs crystal is difficult to produce and must be made by a special technique; the so-called epitaxial method. In molecular beam epitaxial (MBE) growth, a gallium atomic beam and an arsenic cluster beam composed of As_2 or As_4 are irradiated onto a GaAs surface in a vacuum chamber, and Ga and As atomic layers grow alternately. Although the surface morphology has been observed by LEED, RHEED, photoemission and so on, it was difficult to identify the species present on the surface and to clarify the mechanism of crystal growth.

Arthur, Foxon, Joys and others studied the reaction mechanisms of MBE using the reaction rate theory and showed that the mechanisms of the adsorption of As_2 and As_4 clusters differ from each other. In the process of proposing a reaction mechanism, they adopted several assumptions regarding the reaction rate. Therefore,

the explicit geometry of the adsorbate, the reaction path, and the cause of smooth epitaxial growth remain to be clarified.

Part II describes the mechanism of GaAs crystal growth in the arsenic beam epitaxy by an ab-initio theoretical method using the cluster model. Chapter 1 discusses the molecular and dissociative adsorption of As_2 on the GaAs surface, and the site effect of the surface is clarified. In Chapter 2, a new crystal growth mechanism is proposed which includes the formation of an intermediate $GaAs_2$ cluster. Chapter 3 presents a mechanism of epitaxial crystal growth using the As_4 cluster beam. Two mechanisms are examined, i.e., 1) that which involves a single As_4 cluster proposed here, and 2) that involving two As_4 clusters proposed by other experiments. The present study shows that both of these mechanisms are possible.

The main theme of Part III is the hydrolysis of guanosine-triphosphate (GTP) in ras-p21 protein. In protein reactions, some of the most important considerations involve the effect of the dynamic motion and the electrostatic field of the protein and the solvent molecules. The ras-p21 protein binds guanine nucleotide with a high affinity, and is involved in various signal transduction pathways in many cells. The p21-guanosine-diphosphate (GDP) complex receives a signal from an upstream element, and the GDP is exchanged for GTP to convert the inactive p21-GDP complex to the active p21-GTP complex. The p21-GTP is able to transmit the signal downstream to an appropriate target. The active p21-GTP complex is converted to the inactive GDP complex by hydrolysis of GTP to GDP. Thus, hydrolysis is the key reaction in the transmission of the signal. A recent study proposed that glutamine 61 (Gln61) helps to facilitate the nucleophilic attack on the γ-phosphate by activating a water molecule, i.e., Gln61 is the general base in the hydrolysis (GB61). However, despite the appealing structural evidence, this mechanism is not fully established.

In addition to the GB61 mechanism (proton-transfer from the water molecule to Gln 61), another mechanism can be assumed, (proton-transfer to an oxygen atom of the γ-phosphate). This work examines the GB61 mechanism and the new mechanism (mechanism A) by the ab-initio method using a cluster model and a molecular

dynamics simulation. The free energy difference between the intermediate of the mechanism A and that of the GB61 mechanism is estimated by the free energy perturbation method based on the molecular dynamics simulation. The lower energy barrier is given by the mechanism A and its intermediate is also more stable than that of the GB61 mechanism. The result reveals that the mechanism A is preferable to the GB61 mechanism in the hydrolysis of GTP.

Part IV discusses a small theoretical modification of the Hartree-Fock equation. If we suppose an N-electron system using the Hartree-Fock approximation, N one-electron wave-functions are required to describe the total wave function. This representation is somewhat cumbersome since the Hamiltonian and the number of one-electron wave functions depend on the number of electrons.

Several theories which incorporate this feature have been proposed, including the one-particle Green's function method, the field theory and the density equation or functional theory, whose theoretical concept is very appealing despite the problem of N representativity.

Part IV presents the Fourier transformation of the Hartree-Fock equation. This method combines the N one-electron simultaneous equations of the Hartree-Fock method, where N is the number of electrons in the system, into a single differential equation which includes only two variables: i.e., one spatial coordinate $\boldsymbol{x}$ (x, y, z) and a parameter t. Furthermore, a new representation for the exchange interaction is proposed by this transformation.

As shown in this thesis, the quantum chemical approach is useful for studying the reactions of macromolecules, such as solid surfaces and proteins. Although the methods examined in this thesis have not yet been fully developed, combining the quantum chemical method and molecular dynamics may provide valuable tools for studying solid surfaces and proteins.

January, 1994

Yoshifumi Fukunishi

Acknowledgments

The present thesis summarizes the author's studies at the Faculty of Engineering of Kyoto University from 1990 to 1995. The author initially (1990-1991) studied at the Division of Molecular Engineering, and then moved to the Department of Synthetic and Biological Chemistry (1991-1994). I am grateful to Professor H. Nakatsuji for his valuable comments, especially regarding the physical images of this work, and warm encouragement. I also thank Professor Isao Morishima, Professor Keiji Kuwata, and Dr. Toshio Kasai for their support.

Drs.Hiromi Nakai, Masahiko Hada and Minoru Saitoh participated in some of the work presented here and their generous contributions and comments are appreciated. The author would like to thank Drs. Yoshihiro Mizukami, Taketoshi Nakao, Masahiro Ehara, Manabu Sugimoto, and Tomoyuki Hamada, for their encouragement. Thanks are also due to the other members of the Quantum Molecular Science Group in this Department.

The calculations were performed using the FACOM M-780 and M-1800 computers at the Data Processing Center of Kyoto University, the HITAC M-680H at the Institute for Molecular Science and the FACOM VP-2600 at the Protein Engineering Research Institute. The author thanks the IMS computer center and PERI for providing computing time.

CONTENTS

PART I

Modeling of the metal and metal oxide surfaces

Chapter 1

Theoretical study of the hydrogen chemisorption on a ZnO surface

Abstract

Reactions of a hydrogen molecule with a ZnO surface are studied by an *ab initio* method. For simulating the ZnO ($10\bar{1}0$) surface, one ZnO molecule both with and without a Madelung potential is used. Since the electrostatic potential due to the ionic layer decreases exponentially, the effect of the layers deeper than the second one can be neglected. The Madelung potential is, therefore, expressed by the 32 point charges of ± 0.5 situated on the first and second layers. Several low-lying states of ZnO and ZnO + H_2 system have been calculated by the SAC (symmetry adapted cluster) and SAC-CI methods. It is found that the $^1\Sigma^+$ state of ZnO is the ground state and catalytic active and the other states are inactive. ZnO ($^1\Sigma^+$) reacts with H_2 and dissociatively adsorbs it with making Zn-H and O-H bonds. This occurs both with and without the Madelung potential. Without the Madelung potential, the heat of reaction is 81.3 kcal/mol and the reaction barrier is 14.0 kcal/mol. With the Madelung potential, the heat of reaction decreases to 73.5 kcal/mol and the barrier decreases to 11.5 kcal/mol. The mechanism of this reaction is the electron donation from the $2p\pi$ orbital of O to the antibonding σ_u MO of H_2 and the back-donation from the bonding σ_g MO of H_2 to the LUMO of ZnO. In the intermediate stage of the reaction, the dipole of ZnO works to increase the overlap of the

active MO's to make the reaction easier. Throughout the reaction, the in-plane $2p\pi$ orbital of O and the HOMO of ZnO are inactive and work to keep the ZnO bond stable during the catalytic process.

1. Introduction

Zinc oxide is n-type semiconductor and has a catalytic activity for hydrogenations of olefins. It is a wultzite-type crystal and has many stable surfaces. It dissociatively adsorbes hydrogen molecule and the existence of some adsorbed hydrogen species is known. Particulary, type I hydrogen shows a rapid and reversible adsorption and is responsible for the O-H and Zn-H IR peaks observed at 1710 and 3510 cm^{-1}, respectively. This species is the principal source of hydrogen for the hydrogenation of ethylene [1]. Type II hydrogen, on the other hand, contributes little to the hydrogenation of ethylene and does not give Zn-H and O-H bands, but it promotes the rate of the catalytic reaction. Type III hydrogen exists at the temperature near 78° K. This is molecularly adsorbed on the same site as the type I species [2].

On the theoretical side, some relevant papers are published in recent years. Anderson and Nichols studied the adsorption of hydrogen on the ZnO $(10\,\bar{1}\,0)$ surface by a semi-empirical molecular orbital method. They found that the heterolytic adsorption of H_2 allows a formation of a strong O-H and Zn-H bonds but the homolytic adsorption results in two weak Zn-H bonds [3]. Bauschlicher Jr and Langhoff studied low-lying electronic states of ZnO and ZnS. They calculated the spectroscopic constants and the dipole moments for the $^{1,3}\Sigma^+$ and $^{1,3}\Pi$ states of ZnO and ZnS by the configuration-interaction and coupled pair methods [4]. Dolg *et al.* studied early transition metal monoxides by the SD-CI method [5]. Gropen *et al.* calculated the diatomic oxides of Sc, Ti, Cr, Ni and Zn in order to test the reliability of the pseudo potential

methods [6]. Witko and Koutecky studied the potential curves of $ZnO + C_2H_4$ and $(ZnO + C_2H_4)^+$ systems using pseudo-potential-MRD-CI and all electron MRD-CI methods [7]. An attractive interaction has been found for several excited states of the $ZnO + C_2H_4$ system.

We here study hydrogen chemisorption on the ZnO $(10\,\bar{1}\,0)$ surface. We calculate the reaction path for the H_2 chemisorption on ZnO surrounded by a Madelung potential represented by an array of a limited number of point charges. We examine the effect of the Madelung potential on the low-lying states of ZnO and on the activity of ZnO for the dissociative adsorption of H_2. We show the reorganization of the electron density along the reaction process. Conclusion of the present study is given in the last section.

2. Computational method

The Gaussian basis for Zn atom is the (3s2p5d)/[2s2p2d] set and the Ar core is replaced by the effective core potential [8]. For O atom, we use Huzinaga-Dunning [4s2p] basis [9] plus diffuse sp functions (exponent 0.059) and polarization d functions (exponent 0.30). For H atom, we use Huzinaga-Dunning (4s)/[2s] set plus p-type functions which are the first derivatives of the [2s] set. Then, the Hellmann-Feynman theorem is satisfied for the forces acting on the hydrogen nuclei [10]. Calculating the Hellmann-Feynman forces acting on the H atoms, we examine the path of approach of H_2 onto ZnO for which the distance is fixed at 1.95 Å, an experimental value for the crystal. We calculate the potential eregy curves of the ground and excited states by the SAC (symmetry adapted cluster) /SAC-CI method [11,12]. We use 37 active orbitals, 9 orbitals being occupied and 28 orbitals being unoccupied. The linked operators in the SAC/SAC-CI calculation are selected by using the thresholds λg and λe of 1×10^{-5} and 2×10^{-5} au [13], respectively. The wave

function consists of 3000 ~ 5000 linked operators which are symmetry adapted in each spin symmetry. The Hartree-Fock calculation are performed with the use of the program GAMESS [14], and the SAC/SAC-CI calculations by the program SAC85 [15].

For simulating the ZnO (10$\bar{1}$0) surface, one ZnO molecule embeded in a Madelung potential is used. The Madelung potential is expressed by the 32 point charges of ± 0.5 situated on the first and second layers, which are illustrated in Fig. 1. The electrostatic potential due to the ionic layer decreases exponentially and the one due to the charges which are situated in z axis decreases more rapidly as shown in the appendix. Therefore, the electrostatic potential made by the 32 point charges located around the ZnO molecule reach to 92 % of the one due to 6886 point charges. The Madelung potential is proportional to the ionic charge, q, in $Zn^{+q}O^{-q}$. There are several ways of estimating this quantity, but the results are widely spread, namely, $q \sim 1$ [16], $q \sim 0.8$ [17], $q \sim 0.4$ [18]. The Mulliken's atomic charge of ZnO calculated by the Hatree-Fock method is ± 0.6. However the smaller value should be used for q because of the electron spacial distribution. We then choose point charge of ± 0.5.

3. Results and discussions

A. ZnO

We calculate the potential curves of the low-lying states of ZnO by the SAC/SAC-CI method. The results are shown in Fig. 2. The ground state is $^1\Sigma^+$ for the Zn-O distance shorter than 1.98 Å, but at a larger distance the $^3\Pi$ state becomes the ground state. The equilibrium bond length of the $^1\Sigma^+$ state is 1.76 Å which is shorter than the distance in the crystal, 1.95 Å. The bonding orbital is made of the 4s orbital of Zn and the $2p_\sigma$ orbital of O. The

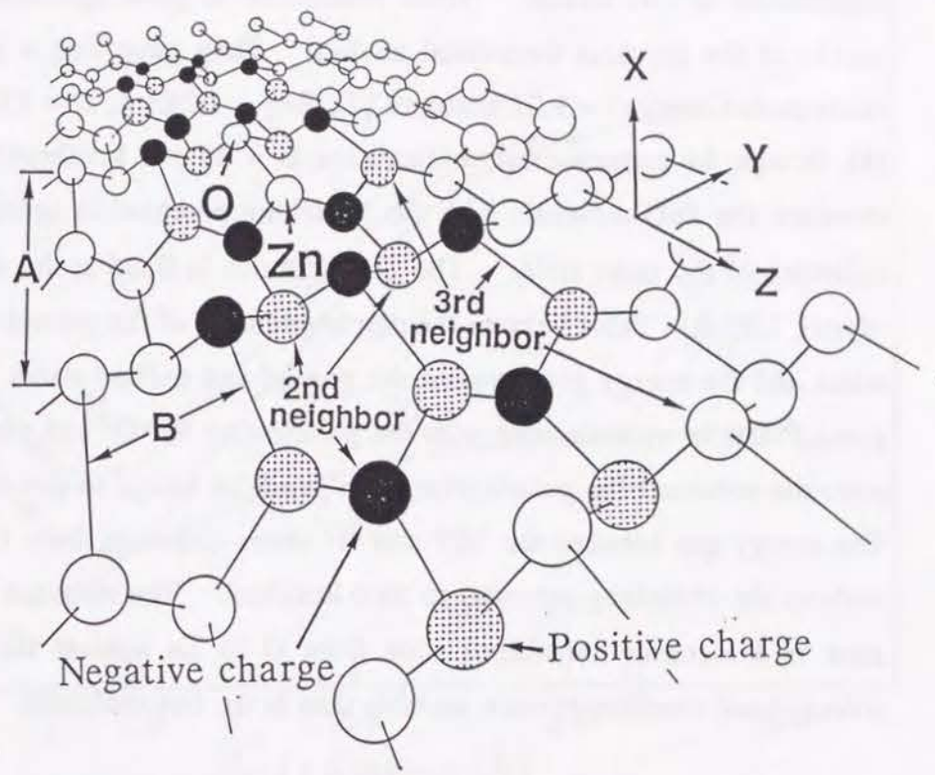

Figure 1. ZnO (10$\bar{1}$0) surface and the array of 32 point charges used in this calculation.

binding energy is 20 kcal/mol and the dipole moment at the point of equilibrium is 5.82 Debye. These results are in good agreement with the results of the previous theoretical studies. They gave Req = 1.809 Å, D (dissociation energy) = 9.22 kcal/mol [7], Req = 1.742 Å, D = 13.8 kcal/mol [5], though the experimental studies gave D = 65 ± 5 kcal/mol [19]. We calculate the ZnO molecule with the Madelung potential in order to see the influence of the outer field. The ZnO distance is fixed at the value of the crystal, 1.95 Å. Table I shows the dipole moments of the ground and excited states and the energy gap between the ground and excited states. The $^1\Sigma^+$ ground state is an ionic state with the polarization Zn^+O^- and the Madelung potential enhances the polarization from μ = 6.18 Debye to μ = 8.85 Debye. The energy gap between the $^1\Sigma^+$ and $^3\Pi$ states increases from 1.8 kcal/mol without the Madelung potential to 36.0 kcal/mol. The reason is that the Π state is a electron transferred state from O to Zn against the Madelung potential and therefore is more unstable than in the free molecule.

B. ZnO + H_2 without Madelung potential system

We examine the reaction path for the ZnO + H_2 without the Madelung potential system. The Zn-O distance is fixed at 1.95 Å. Fig. 3 is a display of the reaction path calculated by the Hartree-Fock method and the forces acting on the H atoms. Fig. 4 shows the potential energy diagram for the ground and excited states of this system calculated by the SAC/SAC-CI method. The geometry of the each point is shown in Table II. Ha is the proton on the left hand side and Hb on the other side. At the initial points 1 and 2, the H-H distance is fixed at the length of a free H_2 molecule. The points 3, 4, 5, and 6 are located successively from the force vectors acting on the H atoms at the points 2, 3, 4, and 5, respectively. The point 7 is the most stable geometry

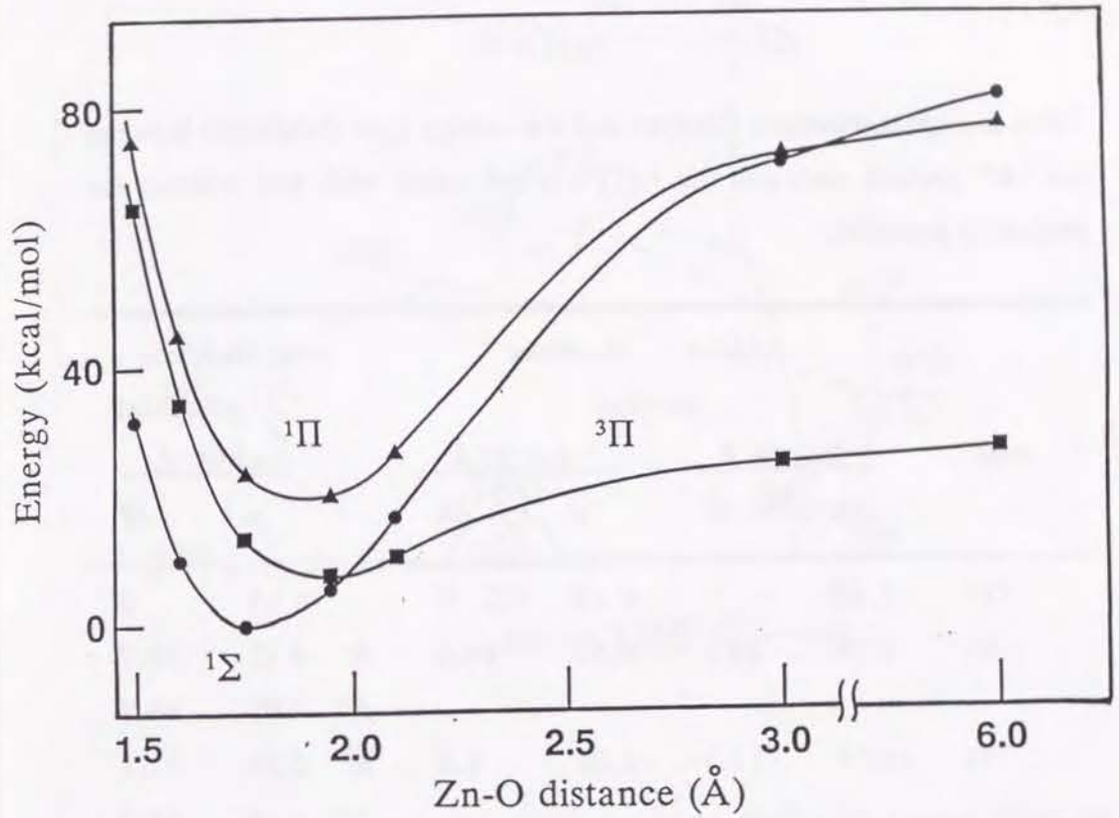

Figure 2. Potential energy curves of the lower singlet and triplet states of ZnO calculated by the SAC/SAC-CI method.

Table I. Dipole moments (Debye) and the energy gaps (kcal/mol) between the $^1\Sigma^+$ ground state and the $^{1,3}\Pi$ excited states with and without the Madelung potential.

	without Madelung potential				with Madelung potential		
state	R=1.76 Å		R=1.95 Å		R=1.95 Å		
	μ	ΔE	μ	ΔE		μ	ΔE
$^1\Sigma^+$	-5.82	0	-6.18	0		-8.85	0
$^1\Pi$	-1.73	22.9	-2.52	14.5	A'	-4.12	39.7
					A"	-4.07	46.3
$^3\Pi$	-1.58	12.9	-2.06	1.8	A'	-5.34	51.3
					A"	-4.14	36.0

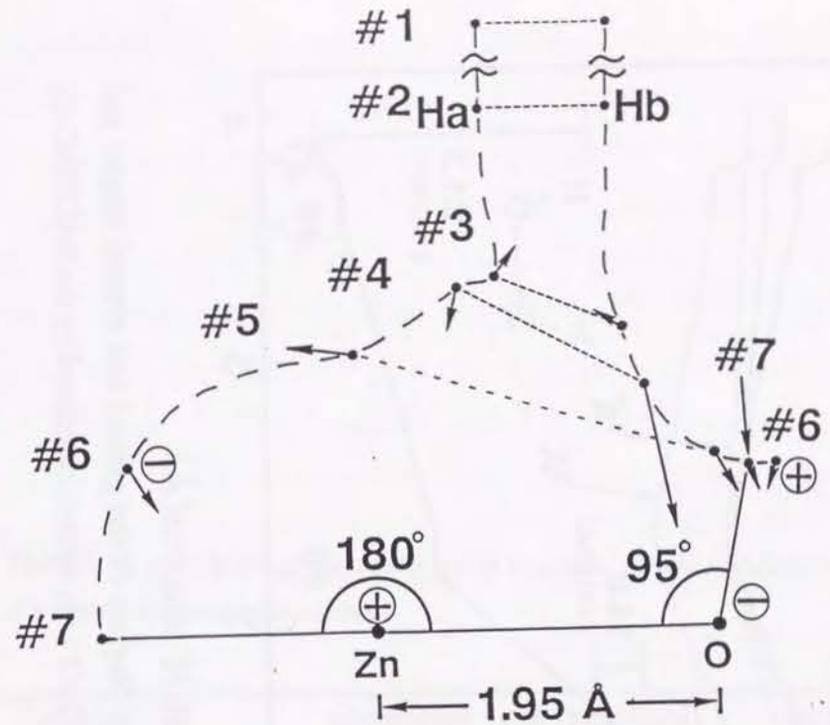

Figure 3. Force acting on the H atoms in the ZnO + H_2 system along the reaction path shown in Table II.

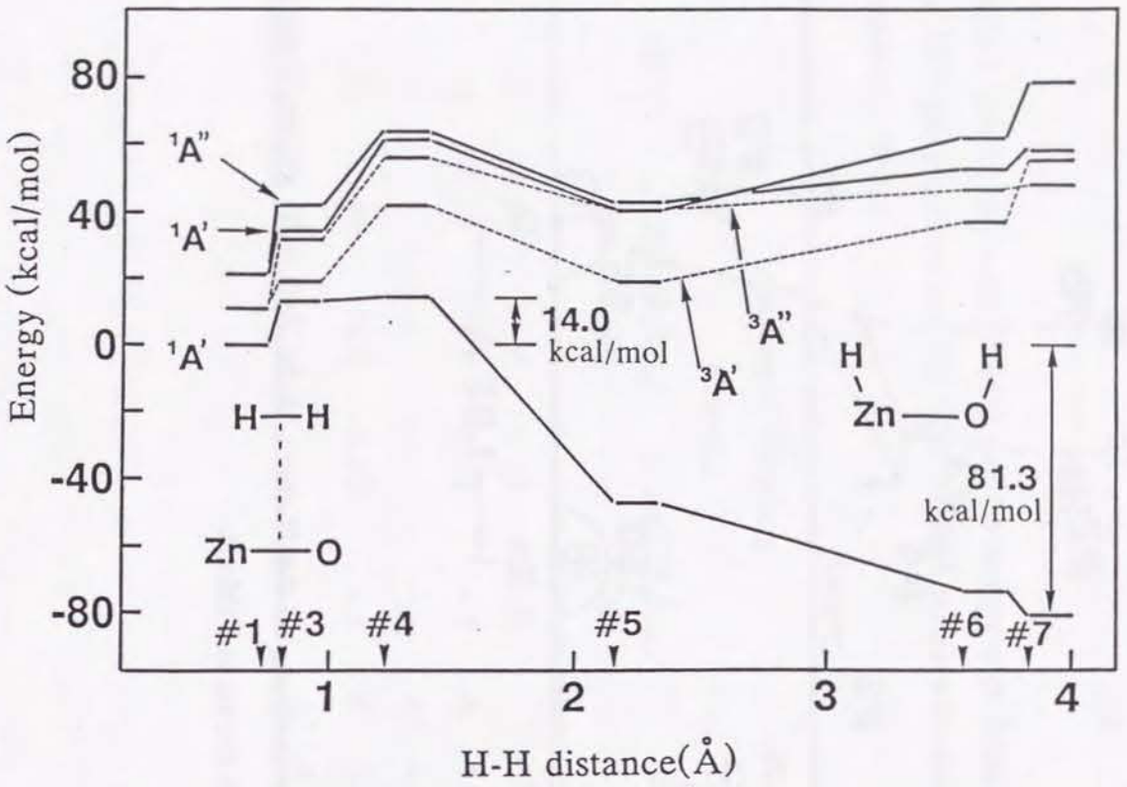

Figure 4. Potential energy diagram of the ground and several singlet and triplet excited states of the ZnO + H_2 system calculated by the SAC/SAC-CI method.

TABLE II. Adsorption energy, most stable structure, atomic populations of adsorbed H in each calculations.

cluster	adsorption site	ΔE (kcal/mol)	atomic population
Li_4 cluster	#13	-18.9	1.25
Li_{10} cluster	3-fold-hollow (#15)	-31.2	1.23
Li_{14} cluster	bridge (#14)	-14.2	1.22
embedded cluster (A)	on-top	24.7	1.29
embedded cluster (B)	on-top	34.9	1.28

from both of the Hartree-Fock and the SAC method. The transition state of the reaction exists between the points 3 and 4 as seen from Fig. 4. The H-Zn-O angle at the point 7 is 180°, which is impossible on the surface, since the hydrogen conflicts with the neighboring O on the surface.

In Fig. 4, the $^1A'$ state is the ground state and originates from the $^1\Sigma^+$ state of ZnO and the $^1\Sigma^+$ state of H_2, both being the ground states of the separated systems. It gives an exothermic potential curve with the heat of reaction of 81.3 kcal/mol and the reaction barrier of 14.0 kcal/mol. Other low-lying excited states give repulsive potential curves.

C. Two point charges plus H_2 system

To estimate the effect of the charges of ZnO on H_2, we replace Zn^+O^- by the two point charges (± 0.5) placed at the positions of Zn and O, and let H_2 approach along the reaction path shown in Fig. 3. The energy is calculated by the full-CI method. We study the role of the electrostatic polarization of ZnO at the initial stage of the reaction. The energies of the H_2 along the reaction path and the atomic charges on H are given in Table III. We see that the electrostatic potential works to stabilize the system before reaching to the barrier. The electrostatic polarization at the place of ZnO induces a polarization of the σ_g MO of H_2 on the side of Ha, and the σ_u MO on the other side. This effect increases the overlaps between the σ_g orbital of H_2 and the LUMO of ZnO and between the σ_u orbital of H_2 and the $2p\pi$ orbital of O. Therefore, the electrostatic potential makes the cleavage of H_2 easier.

D. ZnO + H_2 system with Madelung potential

We finally study the ZnO + H_2 system with including the Madelung potential. The reaction path is the same as the one shown in Fig. 3 Fig. 5 is a

Table III. Energies and atomic charges of H_2 along the reaction path in the electrostatic potential. The energy of H_2 at the equilibrium bond length and without the electrostatic potential is taken as a standard.

		with point charges		without point charges
			atomic charge	
point	$R_{H\text{-}H}$(Å)	ΔE(kcal/mol)	H_a/H_b	ΔE(kcal/mol)
2	0.7417	-0.19	-0.03/+0.03	0
3	0.7846	-10.23	0.00/0.00	0.69
4	1.2191	18.14	-0.05/+0.05	39.91
5	2.1674	43.36	-0.45/+0.45	97.70

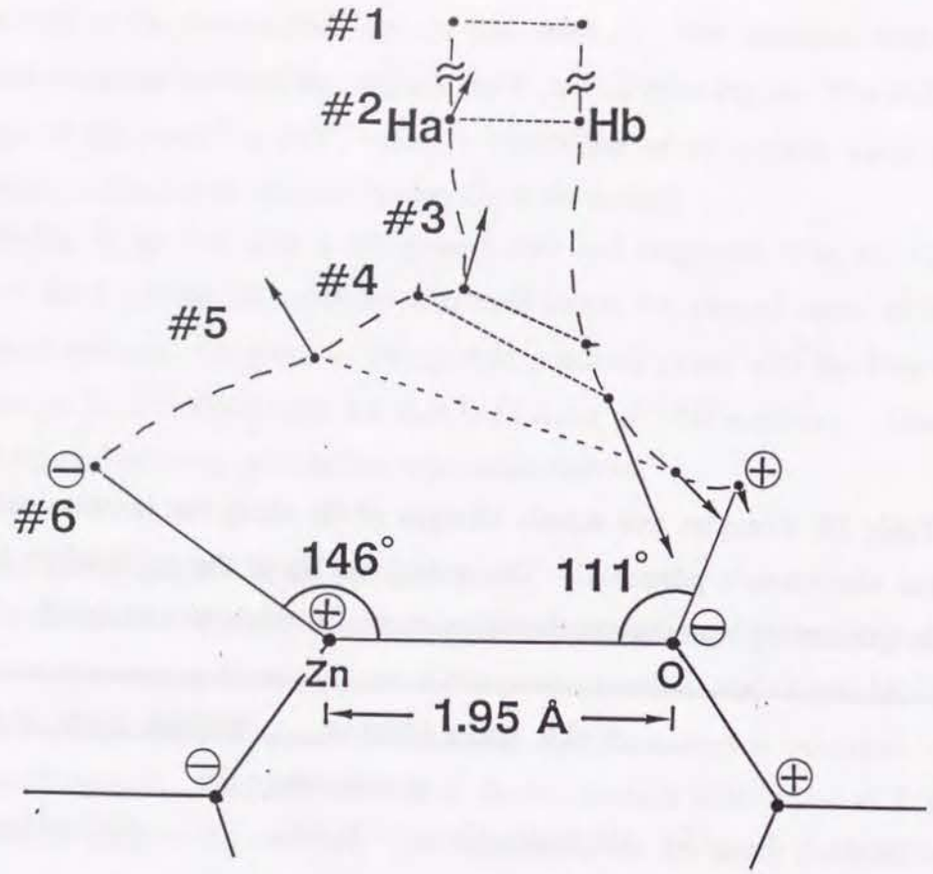

Figure 5. Force acting on the H atoms in the $ZnO + H_2$ system with the Madelung potential along the reaction path shown in Figure 3.

display of the forces acting on the H atoms along the reaction path calculated by the Hartree-Fock method. The point 6 is the equilibrium geometry calculated by the Hartree-Fock method. At this point, the H-H distance is 3.73 Å which is 5 times as large as the one of a free H_2. The H-H bond is completely broken. There the H-Zn-O angle is 146° which is different from the angle 180° obtained without the Madelung potential. The H-O-Zn angle, on the other hand, is 111° which is slightly larger than 95° obtained without the Madelung potential. The reason is the electrostatic repulsion between the adsorbed hydrogen and the surrounding Madelung potential.

The potential energies along the path calculated by the SAC/SAC-CI method are shown in Fig. 6. The energies of the ground and excited states do not change much from the one shown in Fig. 4. Again, only the ground state is exothermic and the excited states are all repulsive. The heat of reaction is 73.5 kcal/mol and the reaction barrier is 11.5 kcal/mol. The Madelung potential lowers the barrier by 2.5 kcal/mol. The calculated vibrational frequencies $\nu_{O\text{-}H}$ and $\nu_{Zn\text{-}H}$ at the point 6 are 4090 and 1730 cm^{-1}, and are similer to the experimental values of 3510 and 1710 cm^{-1}, respectively.

Fig. 7 shows the contour maps of the density difference difined by

$\Delta\rho = \rho(ZnO\text{-}H_2) - \rho(ZnO) - \rho(H) - \rho(H)$.

At point 2, the density of H_2 is polarized by the long-range electrostatic dipole field of Zn^+O^- with the right-hand side hydrogen becoming protonic. There is a large difference between the densities at 3 and 4, though there is only a little difference in geometry between 3 and 4. It indicates that the transition state exists between 3 and 4 in accordance with the potential diagram given by Fig. 4. At 5, the H-H bond is completely broken, and the Zn-H and O-H bonds are formed. Along the Zn-H bond, the density in the left region of the Zn-H bond increases and induces to the left a force acting on the hydrogen.

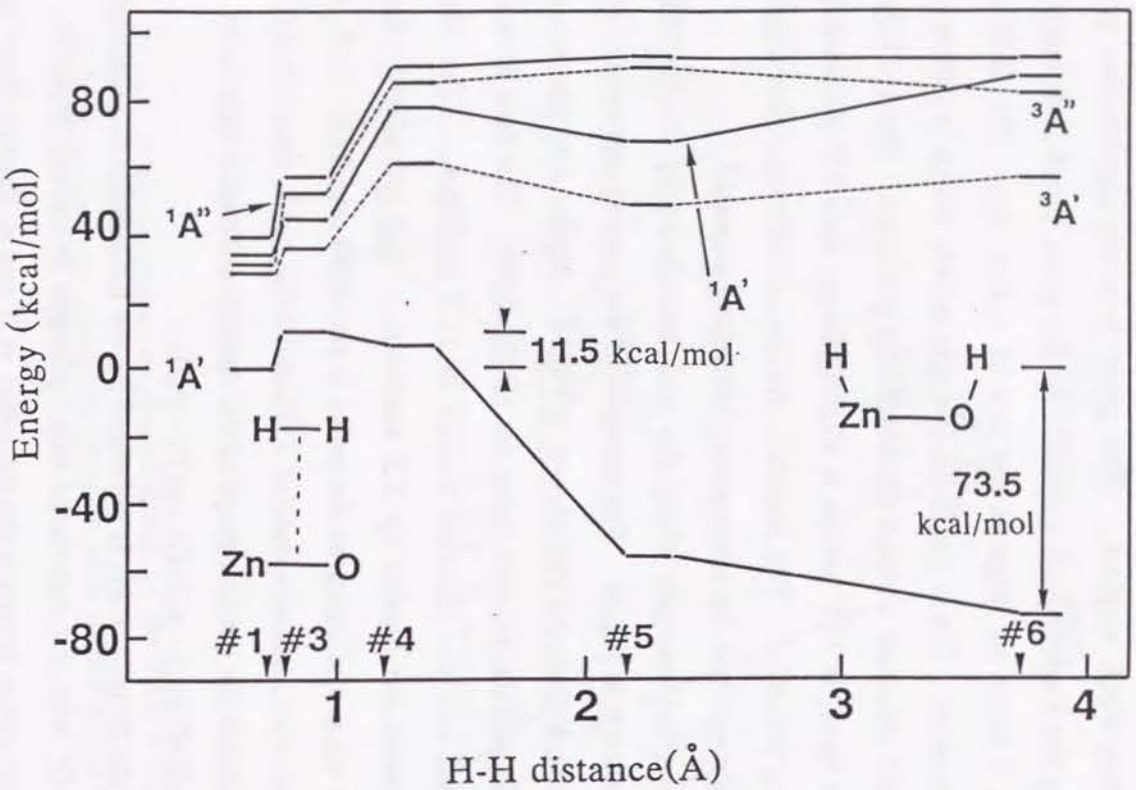

Figure 6. Potential energy diagram of the ground and several singlet and triplet excited states of the ZnO + H_2 system with the Madelung potential calculated by the SAC/SAC-CI method.

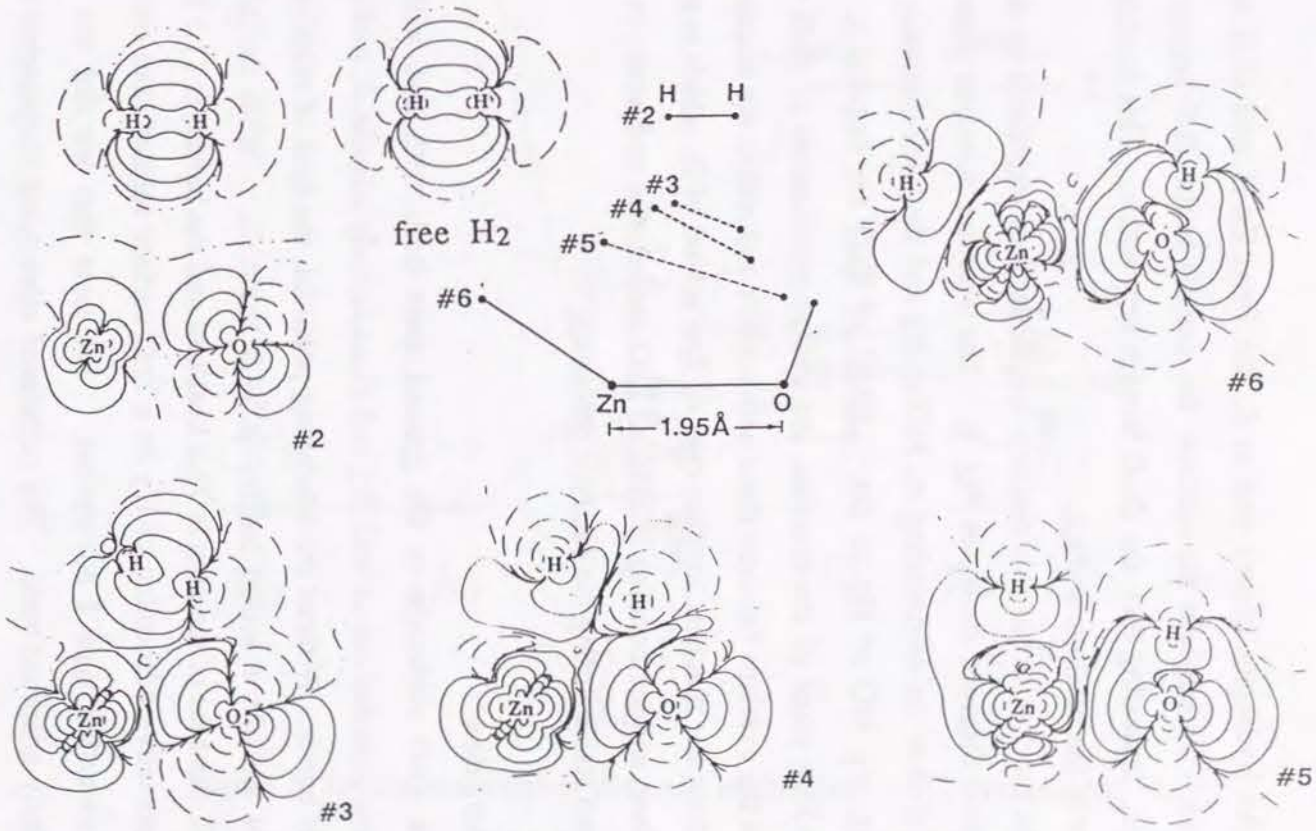

Figure 7. Reorganization of the electron density of the ZnO + H_2 system along the reaction path shown in Figure 3. The difference density is difined in the text.

Then the hydrogen moves and at 6, the final Zn-H and O-H bonds are observed. Throughout the reaction, the density in the ZnO region does not decrease, indicating that the Zn-O bond is kept stable. This is related to the stability of the catalytic surface.

The mechanism of this reaction is qualitatively explained by the orbital correlation diagram shown in Fig. 8. The electron donation from the $2p\pi$ orbital of O to the antibonding σ_u MO of H_2 and the back-donation from the bonding σ_g MO of H_2 to the LUMO of ZnO are important. In the intermediate stage of the reaction, the charge polarization of ZnO works to increase the overlaps between these active MO's and makes the reaction easier. Throughout the reaction, another type of $2p\pi$ orbital of O, which is parallel to the surface, and the bonding HOMO of ZnO are inactive and works to keep the ZnO bond stable during the catalytic processes.

4. Conclusion

The ZnO molecule in the ground state both with and without the Madelung potential reacts with H_2 and dissociatively adsorbs it, making Zn-H and O-H bonds. Without the Madelung potential, the heat of reaction is 81.3 kcal/mol and the reaction barrier is 14.0 kcal/mol. With the Madelung potential, the heat of reaction is 73.5 kcal/mol and the barrier is 11.5 kcal/mol. The dissociative adsorption of H_2 on a ZnO surface studied here corresponds to the so-called type I adsorption. We note that we did not observe molecularly adsorbed state. The calculated vibrational frequencies $\nu_{O\text{-}H}$ and $\nu_{Zn\text{-}H}$ at the dissociated geometry are 4090 and 1730 cm^{-1}, respectively and are similer to the experimental values.

The mechanism of the dissociative adsorption of H_2 on a ZnO surface is the electron donation from the $2p\pi$ orbital of O to the antibonding σ_u MO of

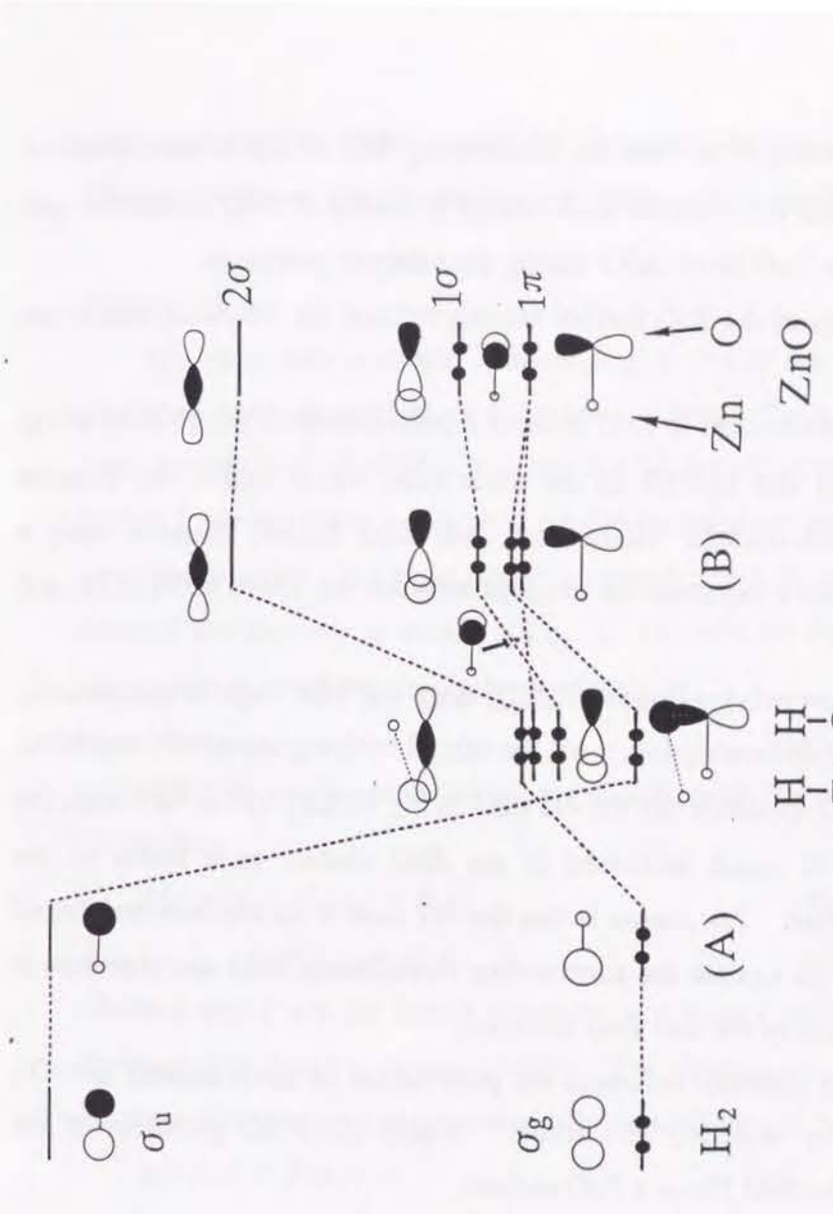

Figure 8. Orbital correlation diagram of the ZnO + H_2 system. (A) H_2 with the electrostatic field due to the poralization of Zn^+O^- at the point 3 of the H_2 + two point charges system ; (B) ZnO with the Madelung potential.

H_2 and the back-donation from the bonding σ_g MO of H_2 to the LUMO of ZnO. Throughout the reaction the bonding σ orbital of ZnO is inactive and works to keep the ZnO bond stable during the catalytic processes.

The reactivity of the ZnO surface is analyzed and the following results are notable.

a) The charge polarization in ZnO induces a polarization of the HOMO of H_2 on the side of O and LUMO on the other side, which makes the electron transfer and back-transfer interaction with ZnO easier, because such a deformation of MO's increases the overlaps between the active MO's of H_2 and ZnO.

b) Among the lower-lying states of ZnO, only the $^1\Sigma^+$ state is catalytically active for the H_2 chemisorption. All the other low-lying states are repulsive. While a free ZnO molecule has the $^3\Pi$ state in the vicinity of the $^1\Sigma^+$ state, the energy separation much increases in the ZnO cluster as a effect of the Madelung potential. The reason is that the $^3\Pi$ state is an electron transferred state from O to Zn against the surrounding electrostatic field and therefore is more unstable than in the free ZnO molecule.

c) The Madelung potential enhances the polarization of ZnO, namely Zn^+-O^-, and the reactivity with H_2 as a result. It also affect the geometry of the dissociatively adsorbed H_2 on a ZnO surface.

Acknowledgements

The calculations have been carried out with the FACOM M/780 computer at the Data Processing Center of Kyoto University and the HITAC M-680H at the Institute for Molecular Science. The authors thank the IMS computer center for the grants of compueting time. Part of this study has been supported by the Grant-in-Aid for Scientific Research from the Japanese Ministry of Education, Science, and Culture, and by the Kurata Foundation.

Appendix

We show here a simple mathematical forms of the electrostatic potential due to an array of charges on a surface. Though Evalt, Kohnfeld and others have shown the method of calculating the Madelung potential [20-22], they are for the inner region of a solid and are too complicated for the present purpose.

We consider a y-z plane in which positive and negative point charges are situated alternatively as shown in Fig. 1. Let ϕ be the scalar potential. In the region above the plane, the Poisson equation is

$$\Delta\phi = 0, \tag{1}$$

since there is no charge distribution. Considering the translational symmetry of the plane,

$$\phi(x,y,z) = \phi(x,y+ \text{n } B,z) \tag{2}$$

$$= \phi(x,y,z+ \text{m } A) \tag{3}$$

where A and B are the lattice constants along the z and y axes, respectively, shown in Fig. 1 and n, m are integers. The charges are symmetrically located for the z-x plane and anti-symmetrically located for the x-y plane,

$$\phi(x,y,z) = \phi(x,-y,z) \tag{4}$$

$$= - \phi(x,y,-z). \tag{5}$$

Any periodic value is represented by the summation of the sine waves by the Fourier's theorem. We suppose a function which satisfies Eqs. (2) ~ (5).

$$\phi(x,y,z) = \sum_{n=1,m=0} F_{n,m}(x)\, sin(k_a nz)\, cos(k_b my)\,, \tag{6}$$

where $k_a = 2\pi/A$, $k_b = 2\pi/B$.

The terms with $n = 0$ do not satisfy the Eq. (5), so they should be excluded.

It is easy to show the mathematical form of $F_{n,m}(x)$. Substituting Eq. (6) into Eq. (1), and operating Δ on ϕ term by term, we see that Eq. (1) holds only when

$$(\frac{\partial^2}{\partial x^2}+\frac{\partial^2}{\partial y^2}+\frac{\partial^2}{\partial z^2})\, F_{n,m}(x)sin(k_anz)\, cos(k_bmy)$$

$$=\frac{d^2}{dx^2} F_{n,m}(x)\, sin(k_anz)\, cos(k_bmy)$$

$$- ((k_an)^2 + (k_bm)^2)\, F_{n,m}(x)\, sin(k_anz)\, cos(k_bmy)$$

$$= 0 \qquad (7)$$

Thus,

$$F_{n,m}(x) = C_{n,m}\, exp(\pm\sqrt{(k_an)^2 + (k_bm)^2}\ |x|)\, sin(k_anz)\, cos(k_bmy) \quad (8)$$

where $C_{n,m}$ is a constant. The potential should vanish at $\pm\infty$, then the sign of Eq. (8) must be minus,

$$F_{n,m}(x) = C_{n,m}\, exp(-\sqrt{(k_an)^2 + (k_bm)^2}\ |x|)\, sin(k_anz)\, cos(k_bmy) \quad (9)$$

We need a boundary condition for determining the constant $C_{n,m}$. If x is large enough, ϕ would be nearly proprotional to $sin(k_az)$ for fixed x and $\partial\phi / \partial y \sim 0$. So we suppose a boundary condition for a large enough fixed x_0 as,

$$\phi(x_0,y,z) = C'\, sin(k_az). \qquad (10)$$

The solution of Eq. (1) which satisfies Eq. (10) is

$$\phi(x,y,z) = C\ exp(-\ k_ax)\ sin(k_az). \qquad (11)$$

Eq. (11) suggests that the electrostatic potential due to the ionic layer decreases exponentially. The 3rd and 4th layers give 10.5 % of the total electrostatic potential at the surface, and 5th and 6th layers give only 0.6 %, so the effect of deeper layer than the second one may be neglected. We take into account the charges situated in the first and second layers alone.

We next consider the electric potential along the z axis. We consider a linear array which is made by the positive and negative point charges alternatively situated on the z axis as shown in Fig. (1). $\Delta\phi = 0$ is supposed as

the previous discussion. Using the cylindrical symmetry around the z axis, $\Delta\phi = 0$ is read as

$$(\frac{\partial^2}{\partial r^2} + \frac{1}{r}\frac{\partial}{\partial r} + \frac{\partial^2}{\partial z^2})\ \phi(r,z) = 0 \qquad (12)$$

where r is a radius from the z axis. Considering the translational symmetry of the plane,

$$\phi(r,z) = \phi(r,z+ \text{n } A) \qquad (13)$$

where A is the lattice constants along z axes shown in Fig. 1 and n is integer. The charges are anti-symmetrically located ,

$$\phi(r,z) = -\ \phi(r,-z). \qquad (14)$$

We suppose the function

$$\phi(r,z) = \sum_{n=1} F_n(r)\, sin(\frac{2\pi nz}{A}) \qquad (15)$$

as the one which satisfies Eqs. (13) and (14). The term with $n = 0$ does not satisfy the Eq. (14) and so should be excluded.

Substituting Eq. (15) into Eq. (12), and operating Δ on ϕ term by term, we see that Eq. (12) holds only when

$$(\frac{\partial^2}{\partial r^2} + \frac{1}{r}\frac{\partial}{\partial r} + \frac{\partial^2}{\partial z^2})\ F_n(r)\ sin(knz)$$

$$=\frac{d^2}{dr^2} F_n(r)\ sin(knz) + \frac{1}{r}\frac{d}{dr} F_n(r)\ sin(knz) - (kn)^2\, Fn(r)\ sin(knz)$$

$$= 0 \qquad (16)$$

where $k = 2\pi / A$.

Thus,

$$F_n(r) = \frac{C_n}{\sqrt{r}} exp(-knr)\ (1 - \frac{1}{4\ (knr)^2} + \frac{1}{(knr)^3} - \ldots) \quad (17)$$

where C_n is a constant. We need a boundary condition for determining the constant C_n. If r is large enough, ϕ would be nearly proprotional to $sin(kz)$ for fixed r. So we suppose a boundary condition for a large enough r_0 as,

$$\phi(r_0,z) = C'\ sin(kz)\ . \qquad (18)$$

The solution of Eq. (12) is

$$\phi(r,z) = \frac{C}{\sqrt{r}}\, cos(kz)\, exp(-kr)\, (1 - \frac{1}{4\,(kr)^2} + \frac{1}{(kr)^3} - \ldots). \quad (19)$$

If $r > A$, the first term of this expansion is dominant. So,

$$\phi(r,z) = \frac{C}{\sqrt{r}} cos(kz)\, exp(-kr) \quad (20)$$

approximates the electrostatic potential. Eq. (20) suggests that the electrostatic potential decreases more rapidly than exponential. The 2nd neighbour array shown in Fig. 1 gives 7.4% of the total electrostatic potential at the position of ZnO interacting with H_2, and the 3rd neighbour array gives 0.8%, the 4th neighbour array gives 0.1% and so on. Therefore, we take into account the charges situated only in the first, second and third neighbour linear array.

Reference

[1] A. L Dent and R. J. Kokes, J. Phys. Chem. **73**, 3781 (1969).

[2] W. C. Conner, Jr. and R. J. Kokes, J. Catal. **36**, 199 (1975).

[3] A. B. Anderson and J. A. Nichols, J. Am. Chem. Soc. **108**, 4742 (1986).

[4] C. W. Bauschlicher, Jr. and S. R. Langhoff, Chem. Phys. Let. **126**, 163 (1986).

[5] M. Dolg, U. Wedig and H. Preuss, J. Chem. Phys. **86**, 2123 (1987).

[6] O. Gropen, U. Wahlgren and L. Pettersson, Chem. Phys. **66**, 459 (1982).

[7] M. Witko and V. B. Koutecky, Int. J. Quantum Chem. **24**, 1535 (1986).

[8] P. J. Hay and W. R. Wadt, J. Chem. Phys. **82**, 270 (1985).

[9] (a) S. Huzinaga, J. Chem. Phys. **42**, 1293 (1965); (b) T. H. Dunning, Jr., *ibid.* **53**, 2823 (1970).

[10] (a) H. Nakatsuji, K. Kanda and T. Yonezawa, Chem. Phys. Lett. **75**, 340 (1980);

(b) H. Nakatsuji, T. Hayakawa and M. Hada, *ibid.* **80**, 94 (1981).

[11] H. Nakatsuji and K. Hirao, J. Chem. Phys. **68**, 2053 (1978).

[12] H. Nakatsuji, Chem. Phys. Lett. **59**, 362 (1978); **67**, 329, 334 (1979).

[13] H. Nakatsuji, Chem. Phys. **75**, 425 (1983).

[14] B. R. Brooks, P. Saxe, W. D. Laidig, and M. Dupuis, Program Library No. 481,

Computer Center of the Institute for Molecular Science, (1981).

[15] H. Nakatsuji, Program Library No. 146 (Y4/SAC), Data Processing Center of Kyoto University, (1985); Program Library SAC85, No. 1396, Computer Center of the Institute for Molecular Science, (1981).

[16] G. Heiland, P. Kurstman and H. Pfister, Z. Physik. **176**, 485 (1963).

[17] W. A. Harrison, Phys. Rev. B **10**, 767 (1974).

[18] J. C. Phillips, *Covalent Bonding in Crystarls, Molecular and Polymers* (University of Chicago Press, Chicago, 1969).

[19] (a) B. G. Wicke, J. Chem. Phys. **78**, 6036 (1983); (b) D. F. Anthrop and A. W. Searcy, J. Phys. Chem. **68**, 2335 (1964).

[20] (a) P. P. Evald, Ann. Physik. **64**, 253 (1921) ; (b) H. Kornfeld, Z. Physik. **22**,

27 (1924).

[21] R. W. Nosker, P. Mark and J. D. Levine, Surf. Sci. **19**, 291 (1970).

[22] R. E. Watson, M. L. Perlman and J. W. Davenport, Surf. Sci. **115**, 117 (1982).

Chapter 2

Modifications for ab-initio calculations of the moderately large-embedded-cluster model. Hydrogen adsorption on a lithium surface

Abstract

Moderately large-embedded-cluster (MLEC) model of Grimley, Pisani, Ravenek and others are modified so that the model is more easily applicable to *ab-initio* calculations. We give a line width to each discrete energy level of a cluster for simulating the density of states of a bulk metal and for preventing from the singularity. The dependence of the calculated results on this line width is shown to be small. Symmetric orthogonalization of basis set and new convergence algorithm are adopted in writing up our *ab-initio* program. These modifications give a rapid convergence of density matrix in the self-consistent-field calculation. Test calculations are performed for hydrogen adsorption on a Li (100) surface with the use of the several cluster models and embedded cluster models.

1. Introduction

Cluster model is based on the locality of surface-molecule interactions. Large number of cluster model calculations have been performed for studying surface reactions and it is proved that the cluster model is useful for clarifying the mechanism of chemisorption and electronic structures of active sites. In previous *ab-initio* calculations on small Li clusters, various adsorption sites were compared. The bridge or hole site of the Li (100) surface have been found to be most favorable, though the energy differences among the bridge, hole, and on-top sites were rather small. The cluster model does not include the enough effect of the bulk solid and is not prevented from an artificial boundary effect due to a finite size of the cluster. The calculated adsorption energy depends on the cluster size. The heats of atomic hydrogen adsorption on a Li cluster are reported to vary from 5 to 70 kcal/mol for different Li clusters. [1-8]

Some models have been proposed for including the effect of bulk metal. For surface-molecule interactions in which electron transfer between surface and adsorbate is important, the dipped adcluster model is proposed from this laboratory.[9] The adcluster, which is a combined system of adsorbate and cluster, is dipped on to the electron bath of a solid surface and is made equilibrium for electron exchange. The electrostatic image force between adsorbate and surface is also taken into account. This model has been applied successfully to O_2 chemisorptions on palladium and silver surfaces.[9,10]

On the other hand, Grimley and Pisani proposed earlier the method in which the surface-adsorbate system is embedded on a surface (actually on a larger cluster) and is attempted to connect with the outer surface region. This embedded cluster model has been extended by many authors.[11-44] This model is intuitively so charming that we tried to use this model by preparing an *ab-inito* program.

In this work, we adopt the moderately large-embedded-clusetr (MLEC) method of Grimley, Pisani, Ravenek, and Geurts based on the Green's function method.[11-20] For *ab-initio* calculations, the size of the metal cluster appearing in the model is very important; it is difficult to use a moderately large cluster for representing the solid. We therefore modify the MLEC method such that the calculational labour is reduced by modifying the Green's function method and some other computational techniques. We have coded an *ab-initio* program based on the program "GAMESS".[45]

Section II gives a brief derivation of the MLEC method proposed by Pisani.[13] In section III, a formalism of symmetric orthogonalization are presented instead of the orthogonalization of basis set by Ravenek and Geurts,[20] and in section IV, a new convergence algorithm is summarized. In section V, we modify the Green's function method so that it is able to take into accounts the line width of the energy levels of a cluster. In section VI, additional terms in the Fock matrix due to the electrostatic potential, and in section VII, the behavior of the coupling matrix in the present calculations are presented. In section VIII, the calculation of the hydrogen adsorption on a Li (100) surface is performed with the use of the several cluster and embedded cluster models; Li_4 , Li_{10} and Li_{14} clusters, and Li_4 embedded in Li_6 and Li_{10} clusters. The calculated results and the comparison between the two models are given.

2. Method

We explain here the MLEC model of Pisani *et. al.* which is the starting basis of the present study. The surface-adsorbate system is illustrated in Fig. 1, where the adsorbate is represented by A and the solid surface by $B \cup D$. In the cluster model, the system is represented by the cluster B interacting with the adsorbate A. In the embedded cluster model, the self-consistent-field (SCF) calculation on $A \cup B$ region is performed with considering the effect of D. The

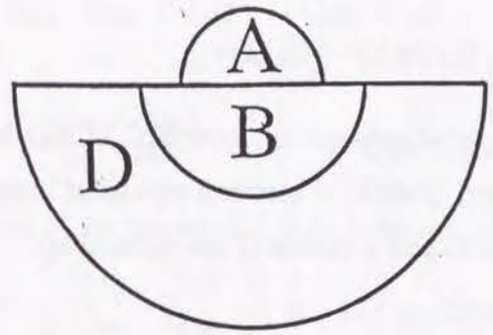

Figure 1. Schematic representation of the embedded cluster model. A is the adsorbate, B the cluster, and D represents the solid.

embedding scheme is performed based on the restricted Hartree-Fock (RHF) approximation.

The Fock matrix F in the RHF-Roothaan method and it's total energy E are given as a functional of the one-electron density P as,

$$F(P)\,C = S\,C\,\varepsilon \tag{1}$$

$$E = \sum_{\lambda\sigma} P_{\lambda\sigma}\,(H + F(P))_{\lambda\sigma} \tag{2}$$

where

$$F_{\mu\nu} = H_{\mu\nu} + \sum_{\lambda\sigma} P_{\lambda\sigma}\,[(\mu\nu|\sigma\lambda) - \frac{1}{2}(\mu\lambda|\sigma\nu)]\,, \tag{3}$$

and H, S, C and ε are core-Hamiltonian, overlap, LCAO-MO coefficient and orbital energy matrices and $(\mu\nu|\sigma\lambda)$ is electron repulsion integral.

The Green's function G and a matrix Q are defined by:

$$Q(z)\,G(z) = 1 \tag{4}$$

$$Q(z) = z\,S - F\,. \tag{5}$$

So, the Green's function G is given by :

$$G(z) = (z\,S - F)^{-1} \tag{6}$$

$$G_{\lambda\sigma}(z) = \sum_i \frac{C_{\lambda i}\,C_{\sigma i}}{z - \varepsilon_i}\,. \tag{7}$$

The density matrix is given as a integral of the Green's function:

$$P_{\lambda\sigma} = \frac{1}{2\pi\,i} \oint G_{\lambda\sigma}(z)\,dz \tag{8}$$

where the integral path is around the poles corresponding to the occupied orbitals.

Let the interaction between A and D is small enough to approximate:

$$Q_{AD} = 0,\ Q_{DA} = 0,\ G_{AD} = 0,\ \text{and}\ G_{DA} = 0\,, \tag{9}$$

then Eq. (4) becomes :

$$\begin{pmatrix} Q_{AA} & Q_{AB} & 0 \\ Q_{BA} & Q_{BB} & Q_{BD} \\ 0 & Q_{DB} & Q_{DD} \end{pmatrix}\begin{pmatrix} G_{AA} & G_{AB} & 0 \\ G_{BA} & G_{BB} & G_{BD} \\ 0 & G_{DB} & G_{DD} \end{pmatrix} = \begin{pmatrix} 1 & 0 & 0 \\ 0 & 1 & 0 \\ 0 & 0 & 1 \end{pmatrix}. \tag{10}$$

After a matrix manipulation, we obtain:

$$\begin{pmatrix} Q_{AA} & Q_{AB} \\ Q_{BA} & Q_{BB} \end{pmatrix}\begin{pmatrix} G_{AA} & G_{AB} \\ G_{BA} & G_{BB} \end{pmatrix} = \begin{pmatrix} 1 & 0 \\ 0 & 1 - Q_{BD}G_{DB} \end{pmatrix}, \tag{11}$$

in which the elements on the left-hand-side belong only to the $A \cup B$ region.

Supposing that in the adsorption of A on B, the interaction between B and D is constant:

$$Q_{BD}\,G_{DB} = Q_{BD}^{f}\,G_{DB}^{f} \tag{12}$$

where the superscript f specifies the value for the free solid $B \cup D$ without the adsorbate A. Eq. (11) then becomes:

$$\begin{pmatrix} Q_{AA} & Q_{AB} \\ Q_{BA} & Q_{BB} \end{pmatrix}\begin{pmatrix} G_{AA} & G_{AB} \\ G_{BA} & G_{BB} \end{pmatrix} = \begin{pmatrix} 1 & 0 \\ 0 & 1 - Q_{BD}^{f}G_{DB}^{f} \end{pmatrix} \tag{13}$$

$$\begin{pmatrix} G_{AA} & G_{AB} \\ G_{BA} & G_{BB} \end{pmatrix} = \begin{pmatrix} Q_{AA} & Q_{AB} \\ Q_{BA} & Q_{BB} \end{pmatrix}^{-1}\begin{pmatrix} 1 & 0 \\ 0 & 1 - Q_{BD}^{f}G_{DB}^{f} \end{pmatrix}. \tag{14}$$

We denote the inverse of the matrix Q (Q^{-1}) in eq. (14) by $\overline{G}$:

$$\begin{pmatrix} G_{AA} & G_{AB} \\ G_{BA} & G_{BB} \end{pmatrix} = \begin{pmatrix} \overline{G_{AA}} & \overline{G_{AB}} \\ \overline{G_{BA}} & \overline{G_{BB}} \end{pmatrix}\begin{pmatrix} 1 & 0 \\ 0 & 1 - Q_{BD}^{f}G_{DB}^{f} \end{pmatrix} \tag{15}$$

We can get the density matrix with embedding effect as follows.

Step. (1) The matrices Q^f and G^f are given by the HF calculation for the free $B \cup D$, and the initial value of $\overline{G}$ is given by the HF calculation for the $A \cup B$ region.

Step. (2) G is calculated from $\overline{G}$ by Eq. (15), and the density matrix P with embedding effect is given by Eq. (8).

Step. (3) The F matrix in Eq. (1) is calculated from the new density matrix P.

Step. (4) Performing the steps. (2) and (3) iteratively until P converges.

We adopt the scheme of Ravenek and Geurts[20] who exclude the numerical integration in Eq. (8) and give the analytic form of the density matrix P. Using Eqs. (7), (8) and (14), we obtain the analytic form of the density matrix in the RHF approximation as,

$$P_{rs} = 2\sum_{i}^{occ} C_{ri}\, C_{si} \qquad r \in A \cup B,\ s \in A$$

$$P_{rs} = 2\sum_{i}^{occ} C_{ri}\, C_{si} + 2\sum_{i}^{occ}\sum_{a}^{B} C_{ri}\, C_{ai}\, X(a,s,i)$$

$$- 2\sum_{i}^{uoc}\sum_{a}^{B} C_{ri}\, C_{ai}\, X(a,s,i) \qquad r \in A \cup B,\ s \in B \qquad (16)$$

$$X(a,s,i) = \begin{cases} \sum_{b}^{D}\sum_{j}^{uoc} \dfrac{C_{bj}^{f}\, C_{sj}^{f}\, [F^{f} - \varepsilon_j^{f} S^{f}]_{ab}}{\varepsilon_i - \varepsilon_j^{f}} & \varepsilon_i \in occ \\ \sum_{b}^{D}\sum_{j}^{occ} \dfrac{C_{bj}^{f}\, C_{sj}^{f}\, [F^{f} - \varepsilon_j^{f} S^{f}]_{ab}}{\varepsilon_i - \varepsilon_j^{f}} & \varepsilon_i \in uoc \end{cases}, \qquad (17)$$

where occ and uoc denote the occupied and unoccupied orbitals, respectively. We introduce the coupling matrix M which is defined by:

$$P_{rs} = \sum_{k}^{all}\sum_{a}^{B} C_{rk}\, C_{ak}\, M_{sa}(\varepsilon_k) \qquad (18)$$

$$M_{sa}(\varepsilon) = \begin{cases} 2\delta_{sa} + 2\sum_{b}^{D}\sum_{j}^{uoc} \dfrac{C_{bj}^{f}\, C_{sj}^{f}\, [F^{f} - \varepsilon_j^{f} S^{f}]_{ab}}{\varepsilon - \varepsilon_j^{f}} & \varepsilon \le \varepsilon^{f} \\ -2\sum_{b}^{D}\sum_{j}^{occ} \dfrac{C_{bj}^{f}\, C_{sj}^{f}\, [F^{f} - \varepsilon_j^{f} S^{f}]_{ab}}{\varepsilon - \varepsilon_j^{f}} & \varepsilon > \varepsilon^{f} \end{cases}. \qquad (19)$$

In the cluster model, the coupling matrix elements are:

$$M_{sa}(\varepsilon) = \begin{cases} 2\theta(\varepsilon - \varepsilon^{f}) & \varepsilon \le \varepsilon^{f} \\ 0 & \varepsilon > \varepsilon^{f} \end{cases} \qquad (20)$$

where ε^{f} is a Fermi energy and θ is a step function.

3. Basis set

In *ab-initio* calculations of the embedded cluster model, the basis set is very important since we have to divide the cluster B from the larger cluster B ∪ D and this division is usually defined by classifying the basis functions into those

belonging to either B or D region. The coupling matrix, for example, depends on the basis set, since the definition of the B and D regions depends on the classification of the basis set used. In the non-orthogonal basis, since there are overlaps between the basis in the B region and the one in the D region, the coupling matrix elements become large and strongly dependent on the orbital energy: this gives a difficulty in the convergence of the SCF calculation. The orthogonalization of the basis of the B ∪ D region improves the behavior of the coupling matrix.[20] We perform the symmetric-orthogonalization method described below which localizes each basis on each atom.

We define the overlap matrix S and the transformation matrix Q as,

$$Q^{\dagger} S Q = 1$$

$$Q = S^{-1/2} \qquad (21)$$

$$\begin{pmatrix} Q_{BB} & Q_{BD} \\ Q_{DB} & Q_{DD} \end{pmatrix}^{\dagger} \begin{pmatrix} S_{BB} & S_{BD} \\ S_{DB} & S_{DD} \end{pmatrix} \begin{pmatrix} Q_{BB} & Q_{BD} \\ Q_{DB} & Q_{DD} \end{pmatrix} = \begin{pmatrix} 1 & 0 \\ 0 & 1 \end{pmatrix}. \qquad (22)$$

We transform the basis χ as,

$$\chi' = \chi\, W, \quad W = \begin{pmatrix} 1 & 0 & 0 \\ 0 & Q_{BB} & Q_{BD} \\ 0 & Q_{DB} & Q_{DD} \end{pmatrix}. \qquad (23)$$

Namely, with the matrix W, only the elements of the B ∪ D region in the system A ∪ B ∪ D are orthogonalized:

$$\begin{pmatrix} 1 & 0 & 0 \\ 0 & Q_{BB} & Q_{BD} \\ 0 & Q_{DB} & Q_{DD} \end{pmatrix}^{\dagger} \begin{pmatrix} S_{AA} & S_{AB} & 0 \\ S_{BA} & S_{BB} & S_{BD} \\ 0 & S_{DB} & S_{DD} \end{pmatrix} \begin{pmatrix} 1 & 0 & 0 \\ 0 & Q_{BB} & Q_{BD} \\ 0 & Q_{DB} & Q_{DD} \end{pmatrix} = \begin{pmatrix} S_{AA} & S'_{AB} & S'_{AD} \\ S'_{BA} & 1 & 0 \\ S'_{DA} & 0 & 1 \end{pmatrix} \qquad (24)$$

Since the new basis χ'_D is localized on the atoms of the D region, the elements S'_{AD} and S'_{DA} should be small enough, so that we assume $S'_{AD} = 0$ and $S'_{DA} = 0$. Thus this transformation satisfies Eq. (9). Using Eq. (24) , Eq. (17) becomes,

$$X(a,s,i) = \begin{cases} \sum_{b}^{D} \sum_{j}^{uoc} \frac{C_{bj}^{f} C_{sj}^{f} F_{ab}^{f}}{\varepsilon_i - \varepsilon_j^{f}} & \varepsilon_i \in occ \\ \sum_{b}^{D} \sum_{j}^{occ} \frac{C_{bj}^{f} C_{sj}^{f} F_{ab}^{f}}{\varepsilon_i - \varepsilon_j^{f}} & \varepsilon_i \in uoc \end{cases} . \quad (25)$$

4. Modification of the density matrix calculation

There are some difficulties in the SCF process of the embedded cluster model calculation.

1) Large number of operations for calculating density matrix elements. The calculation of density matrix elements in Eq. (16) involves n^3 operations.[20]

2) Slow convergence in the SCF calculation. The variables for calculating the density matrix are not only the LCAO coefficients but also their orbital energies. The increase of the variables leads to a slow convergence.

We therefore modify the algorithm of the density matrix calculation. We divide the convergence process of the LCAO coefficients from that of the orbital energies. The scheme is summarized in the following steps.

Step 1. The matrix X in Eq. (25) is produced from C^f, ε^f and F^f with ε_i fixed.

The orbital energy ε_i calculated for the cluster $A \cup B$ is chosen as the initial value of ε_i.

Step 2. SCF calculations are performed until P converges with fixed X.

After the convergence, we get a new set of ε_i which are different from the old ε_i .

Step 3. Replacing old ε_i by new ε_i, X in Eq. (25) is reproduced.

Step 4. Steps 2 and 3 are done iteratively until P and ε_i converge.

Although the convergence depends on the initial values of P, C and ε, the SCF cycle in Step 2 costs 1/3 ~ 1/5 times of the CPU time for the calculation without this scheme. Without this scheme, the embedded cluster model calculation oscillated and did not show a convergence of the density matrix in the following calculations for the Li_nH_2 system. However, with this scheme, the embedded cluster calculations converged and several trial calculations using different initial MOs gave the same unique stable result, that is the ground state. In step 2, the calculation of density matrix elements involves n^2 operations.

5. Modification of the Green's function

For *ab-initio* calculations of surface-molecule interactions, it is usually difficult to use large enough cluster for representing a solid surface. In a bulk metal, the conduction and the valence bands are continuous, but in the cluster model, the energy levels are discrete and there is a HOMO-LUMO gap. Since the analytic form of the coupling matrix in Eq. (19) is different between the regions $\varepsilon < \varepsilon^f$ and $\varepsilon > \varepsilon^f$, and includes the term $1/(\varepsilon - \varepsilon_j^f)$ which is singular at $\varepsilon = \varepsilon_j^f$, the matrix elements are not smooth near the Fermi energy level. We then attempt to modify the term $1/(\varepsilon - \varepsilon_j^f)$ in order to prevent from the singularity. We try to simulate the density of states of a bulk metal by adding a line width to each energy level of the cluster and modify the embedded cluster model by requiring the Green's function to consider the line width of each energy level. The energy gap κ

$$\kappa = \varepsilon_{HOMO} - \varepsilon_{LUMO} \quad (26)$$

in the bulk metal should be zero, but is actually non-zero because of a finite size of the cluster $B \cup D$. We therefore modify the density of states so that the value is non-zero in the neighborhood of the Fermi level.

The density matrix in Eq. (8) can be written by using the δ function as,

$$P_{\lambda\sigma} = \int_{-\infty}^{\varepsilon^f} d\varepsilon \sum_{n}^{all} C_{\lambda n}\, C_{\sigma n}\, \delta(\varepsilon-\varepsilon_n) \ , \qquad (27)$$

and the δ function is rewritten as below by using the Lorentz type function,

$$\delta(z - \varepsilon_n) = \lim_{\kappa\to 0} \frac{1}{\pi} \frac{\kappa}{(z - \varepsilon_n)^2 + \kappa^2}$$

$$= \lim_{\kappa\to 0} \frac{1}{\pi} \mathrm{Im}[\frac{\kappa}{z - \varepsilon_n + i\kappa}] \qquad (28)$$

where i is the imaginary unit. We put Eq. (28) into Eq. (27), and obtain

$$P_{\lambda\sigma} = \lim_{\kappa\to 0} \frac{1}{\pi} \int_{-\infty}^{\varepsilon^f} dz\ \mathrm{Im} \sum_{n} [\frac{C_{\lambda n}\, C_{\sigma n}}{z - \varepsilon_n + i\kappa}]$$

$$= \lim_{\kappa\to 0} \mathrm{Re}[\frac{1}{2\pi i} \oint d\, z \sum_{n} \frac{C_{\lambda n}\, C_{\sigma n}}{z - \varepsilon_n + i\kappa}] \ , \qquad (29)$$

where the integral path is taken around the poles corresponding to the occupied orbitals.

Let each orbital energy has a Lorentz type distribution whose half value is equal to κ' ,

$$\kappa' = \frac{\varepsilon_{HOMO} - \varepsilon_{LUMO}}{2}, \qquad (30)$$

then the density of states for the cluster B ∪ D has no energy gap. We put $\kappa = \kappa'$ instead of $\kappa \to 0$ in Eq. (29). From a comparison of Eqs. (8) and (29), the Green's function is written as:

$$G_{\lambda\sigma}(z) = \mathrm{Re}[\sum_{n} \frac{C_{\lambda n}\, C_{\sigma n}}{z - \varepsilon_n + i\kappa}] \ . \qquad (31)$$

Using Eq. (31) instead of eq. (7), we get the density matrix as,

$$P_{rs} = \sum_{i}^{occ} C_{ri}\, C_{si} \qquad r \in A \cup B, s \in A$$

$$P_{rs} = \sum_{i}^{occ} C_{ri}\, C_{si} + \sum_{i}^{occ} \sum_{a}^{B} C_{ri}\, C_{ai}\, X(a,s,i)$$

$$- \sum_{i}^{uoc} \sum_{a}^{B} C_{ri}\, C_{ai}\, X(a,s,i), \qquad r \in A \cup B, s \in B \qquad (32)$$

where

$$X(a,s,i) = \begin{cases} \sum_{b}^{D} \sum_{j}^{uoc} \dfrac{C_{bj}{}^f\, C_{sj}{}^f\, F^f{}_{ab}}{\varepsilon_i - \varepsilon_j{}^f + \dfrac{\kappa^2}{\varepsilon_i - \varepsilon_j{}^f}} & \varepsilon_i \in occ \\ \sum_{b}^{D} \sum_{j}^{occ} \dfrac{C_{bj}{}^f\, C_{sj}{}^f\, F^f{}_{ab}}{\varepsilon_i - \varepsilon_j{}^f + \dfrac{\kappa^2}{\varepsilon_i - \varepsilon_j{}^f}} & \varepsilon_i \in uoc \end{cases} . \qquad (33)$$

If the cluster is large enough, then $\kappa' \to 0$ and the modified Green's function becomes equivalent to the original one, else the density matrix and the electronic energy depend on the value of κ'.

We examine the κ' dependence for the adsorption energy. The Li crystal has a body centered cubic lattice with the lattice constant of 3.52 Å. We use a Li_{10} cluster shown in Fig.2 as the large cluster B ∪ D which is supposed to represent the Li (100) surface. The shaded four atoms represent the B region and the others represent the D region. For Li atom, STO-3G basis plus diffuse s function ($\zeta = 0.076$) are used.[6]

We set the Fermi energy ε^f and κ' as :

$$\varepsilon^f = \frac{\varepsilon_{HOMO} + \varepsilon_{LUMO}}{2} = -0.027 \text{ au} \qquad (34)$$

$$\kappa' = \frac{\varepsilon_{LUMO} - \varepsilon_{HOMO}}{2} = 0.0649 \text{ au} \qquad (35)$$

where the values of ε_{HOMO} and ε_{LUMO} are due to the Li_{10} cluster calculation.

Fig. 3 shows the κ' dependence of the total and adsorption energies for the Li_4 embedded in Li_6 cluster model. Since Eq. (33) depends on not κ' but κ'^2, the energies are plotted against κ'^2 in the range of $0.02 \le \kappa' \le 0.1$ au. If the value of κ' is less than 0.02 au, the embedded cluster model did not show

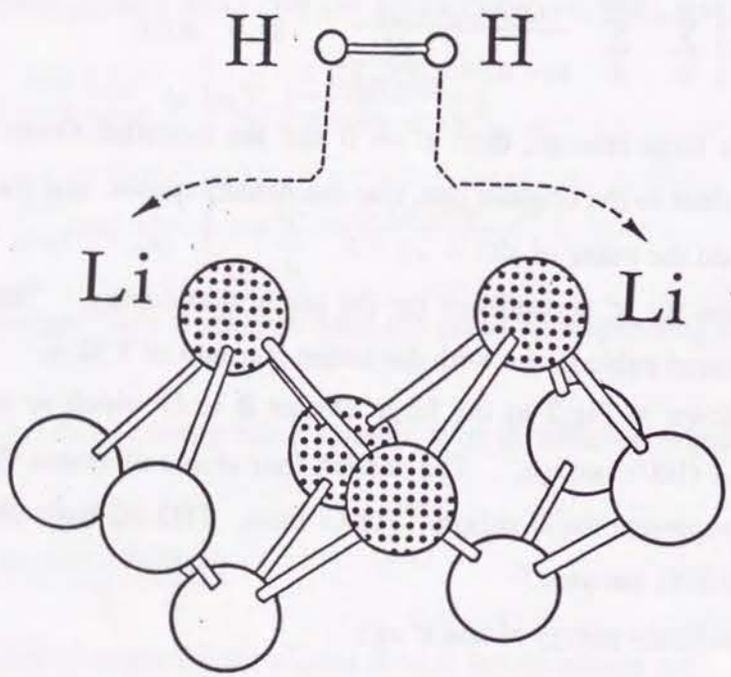

Figure 2. Li_{10} cluster interacting with H_2. The four shaded Li atoms compose the B region and the other Li atoms the D region and H_2 is the adsorbate A in Fig. 1.

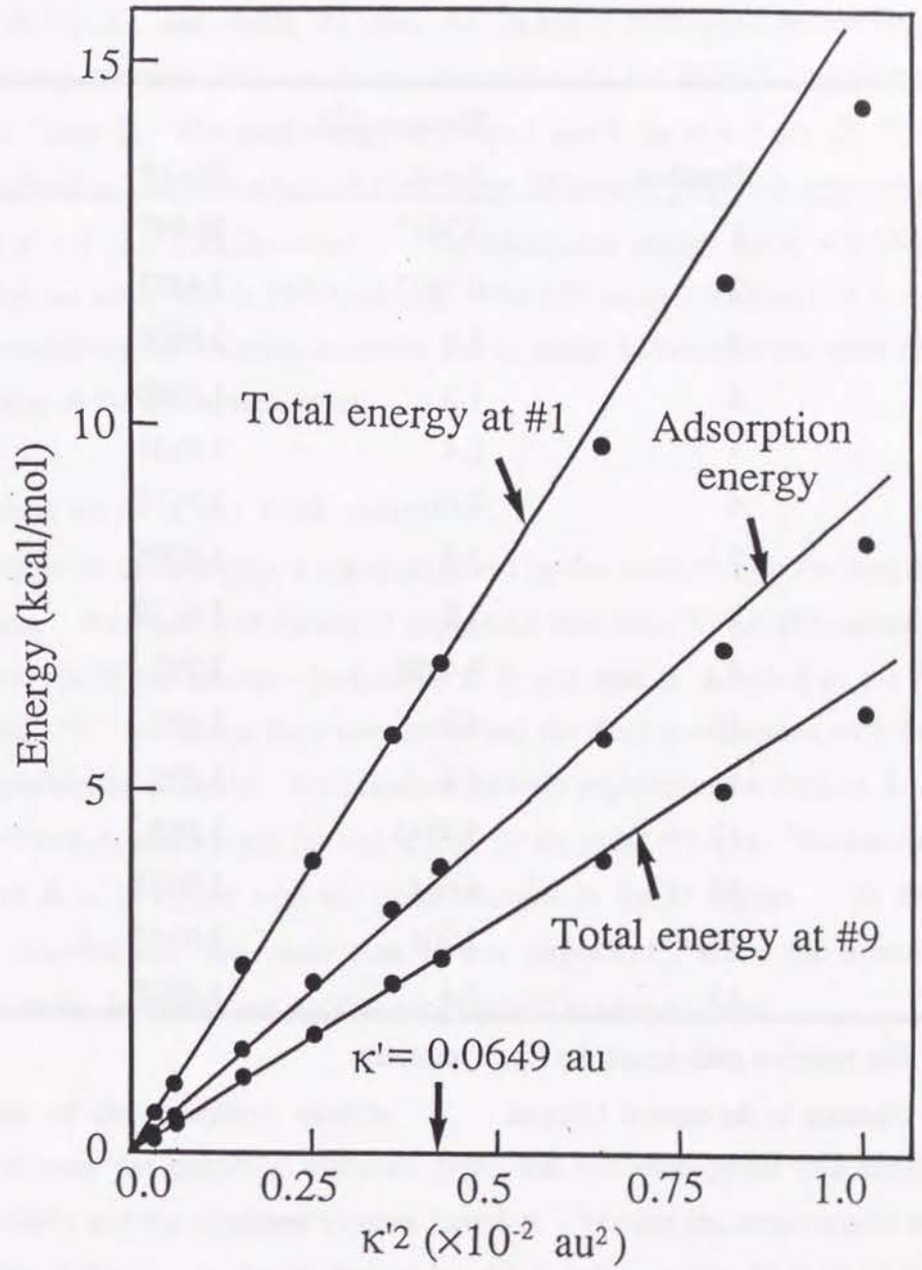

Figure 3. κ' dipendence of total and adsorption energies. The energies are plotted versus κ'2. Each value for κ' = 0 is taken to be zero.

TABLE I. Geometries of the points 1- 15 along the reaction path shown in Fig. 8[a].

	Distance (Å)	
Position	R_{H-H}	R_{Li-H}[b]
1	0.7417	20.047
2	0.7417	2.4273
3	1.0	2.0600
4	1.2	1.9290
5	1.4	1.8134
6	2.0	1.7610
7	2.5	1.6705
8	3.0	1.6139
9	3.4928	1.595
10	4.0	1.595
11	4.6	1.595
12	5.4742	1.595
13	6.644	1.5952
14	7.208	2.0147
15	7.3	1.9815

[a] The reaction path keeps the C_{2v} symmetry.

[b] Distance to the nearest Li atom

convergence and the total energy was not obtained. The extrapolation of the energies for several values of κ' gives the energies for $\kappa' = 0$ that are taken to be the origin of Fig. 3. The points "#1" and "#9" in Fig. 3 correspond to free H_2 + Li_{10} and on-top adsorbed H_2Li_{10} system, respectively (the explicit coordinates are given in Table I). The total energy at points 1 and 9 for $\kappa' = 0$ are -29.7919 au and -29.8416 au respectively, and the energy difference gives the adsorption energy for $\kappa' = 0$, *i.e.* , 31.2kcal/mol. The adsorption energy for $\kappa' = 0.0649$ au defined in the same way is 34.9 kcal/mol. The difference 3.92 kcal/mol is the effect of modifying the Green's function, but is small in comparison with the absolute value of the adsorption energy.

6. Additional term in the Fock matrix

The bulk effect on the B region is not represented by the correction of the density matrix alone. Ravenek and Geurts[20] suggested that there is an electrostatic contribution due to the charge distribution in D and that is included in the H matrix in Eq. (3). We adopt their correction and the field is estimated with the use of the population analysis. We calculate Löwdin-population for the free B $\cup$ D region without A, and replace the atoms in D by the point charges. We use the H matrix of A $\cup$ B region with the point charges in the D region. In the following calculations, this correction is not important , since the atomic populations in the D region are -0.06 ~ +0.15 which are not so large.

7. Behavior of the coupling matrix

We compare the coupling matrices using the non-orthogonal and semi-orthogonal basis and the modified Green's function. We use the same model as before shown in Fig. 2. In the cluster model, the coupling matrix M is given by Eq. (20).

Some elements of the coupling matrix by the non-orthogonal basis are shown in Fig. 4 . The diagonal and off-diagonal elements show an energy dependence

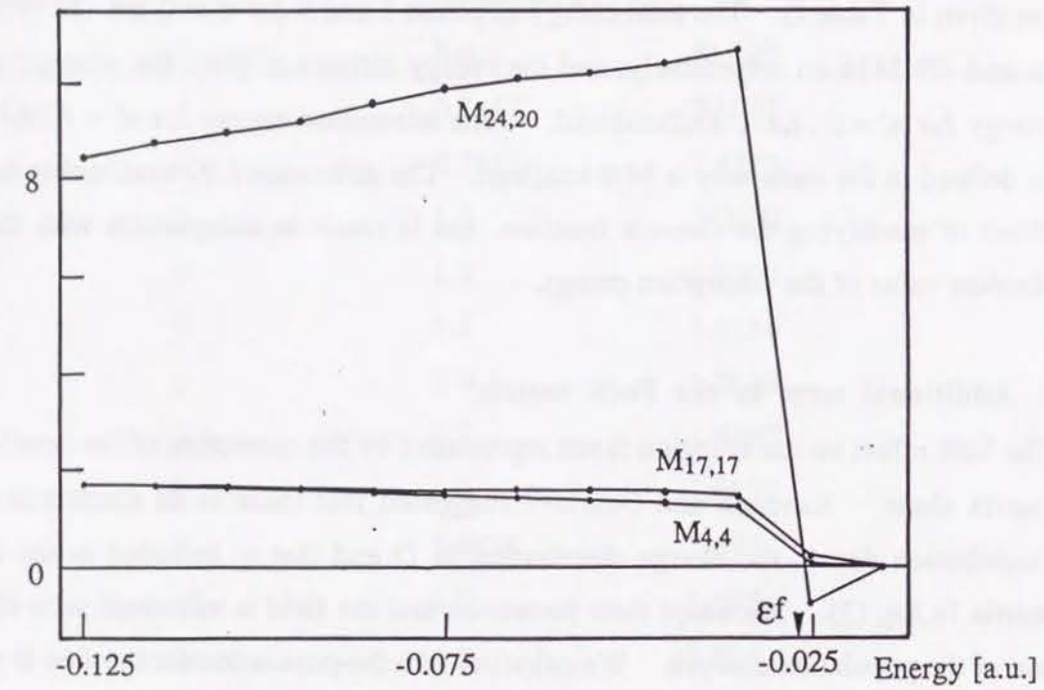

Figure 4. Coupling matrix elements for the non-orthogonal basis.

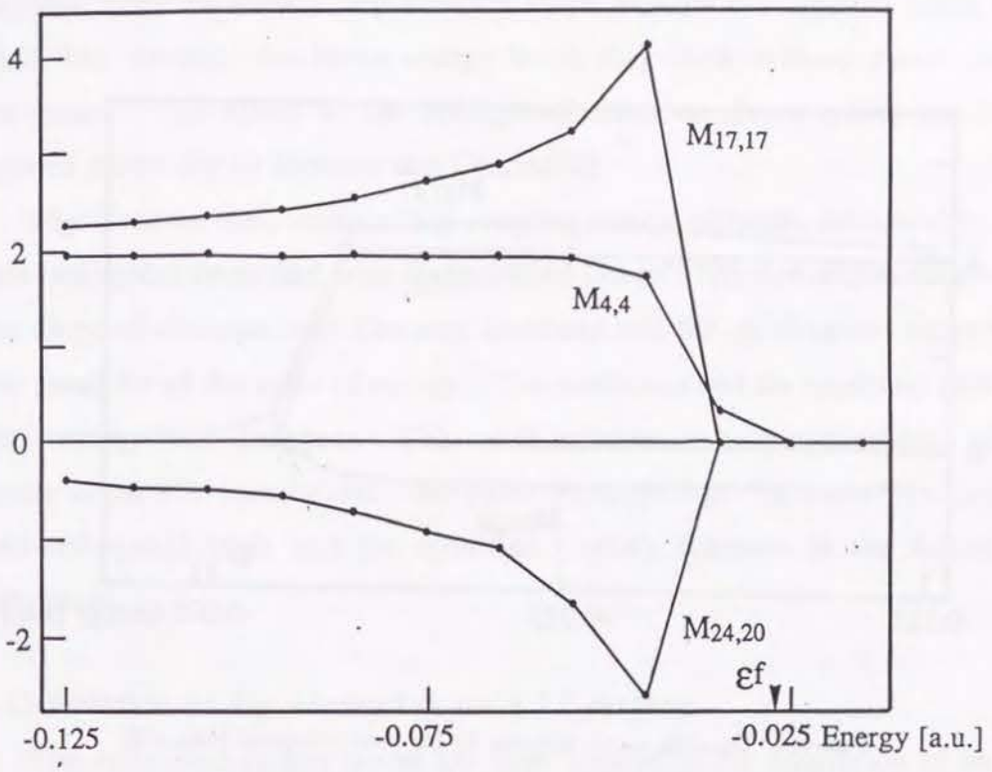

Figure 5. Coupling matrix elements for the semi-orthogonal basis.

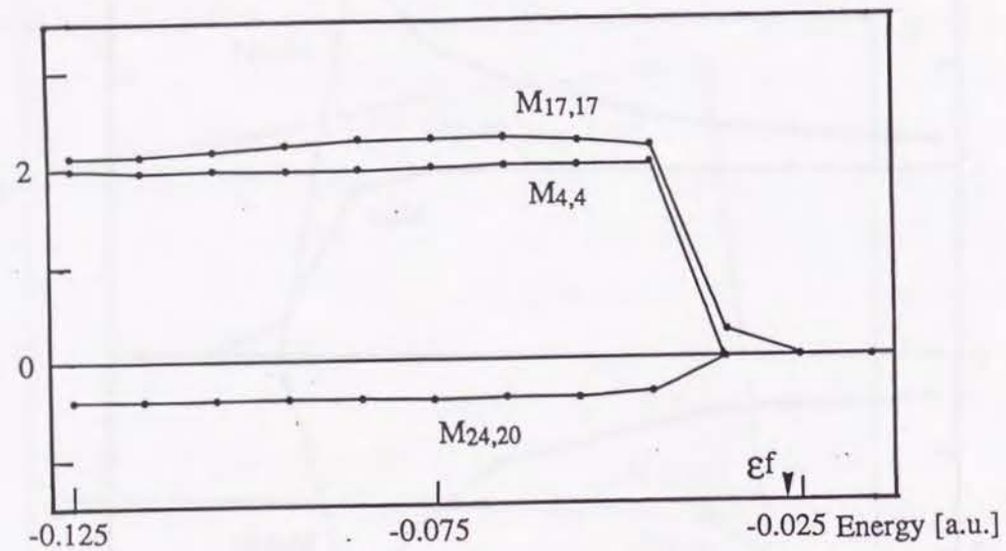

Figure 6. Coupling matrix elements for the semi-orthogonal basis with modified Green's function.

and the off-diagonal element is quite large. The corresponding coupling matrix elements obtained by the semi-orthogonal basis are shown in Fig. 5 . The diagonal elements show a step-function shape and the off-diagonal element is small, but around the Fermi energy level, they show a sharp maximum or minimum. The effect of the orthogonalization on the coupling matrix is reported previously by Ravenek and Geurts.[20]

Fig. 6 shows the corresponding coupling matrix elements calculated by the semi-orthogonal basis and with the modified Green's function explained above. The diagonal elements look like step functions and the off-diagonal element is very small for all the value of energy. The maximum and the minimum near the Fermi energy level disappear. This result indicates an easy convergence of the density in the SCF calculations. We therefore adopt Eqs. (32) and (33) using the semi-orthogonal basis and the modified Green's function in the following calculations.

8. Calculation of H_2 adsorption on a Li surface

The embedded cluster model has been applied to the adsorption of an H_2 molecule on a Li (100) surface. Ravenek and Geurts[20] studied Li-H system using the embedded cluster model.

We use Li_{10} and Li_{14} cluster shown in Figs. 2 and 7, respectively, as the B $\cup$ D region. The shaded four atoms represent the B region and the others the D region. The clusters are supposed to represent the Li (100) surface and to hold the bulk lattice structure throughout the hydrogen-adsorption processes. The H_2 molecule is assumed to approach horizontally, and interacts mainly with the shaded atoms. The Gaussian basis set for the Li atom is the same as the one used in the previous section, and for the H atom, the double zeta (4-31G) set is used.

We perform five different calculations for the cluster and embedded cluster calculations in order to clarify the embedding effect; they are Li_4 cluster, Li_4 embedded in Li_6 and Li_{10} clusters giving respectively Li_{10} and Li_{14} B $\cup$ D

clusters, and Li_{10} and Li_{14} full-cluster models. The two embedded cluster calculations are thought to have to simulate respectively the last two cluster calculations. These five calculations are performed on the same reaction path shown in Fig. 8. Several coordinates along the reaction path are shown in Table I. At points 1 and 2, the H-H distance is kept at the equilibrium bond length of a free H_2 molecule. From 7 to 10, the Li_2-H_2 distance is kept to 1.595 Å which is the Li-H equilibrium distance for the on-top adsorption. From 10 to 12, the Li-H distance is kept at 1.595 Å. In order to satisfy the condition of Eq. (9) for the embedded cluster model, the hydrogen is moved keeping the direct interaction with the Li atoms in the D region as small as possible. The distance from the point 9 to 12 is only 0.2536 Å which is small in comparison with the Li-Li distance, 3.4928 Å. Beyond the point #12, the present embedded model calculation is limited, because there the direct interaction between A and D is not negligible. We therefore perform only cluster model calculations in this region.

The potential energy curves along the reaction path are shown in Fig. 9. The results are summarized in Table II. The energy at point 1 is chosen as a standard, namely to be zero. The solid, broken and dotted lines represent the results of the embedded cluster model calculations, Li_{10} and Li_{14} cluster model calculations, and Li_4 cluster model calculations, respectively.

By embedding the Li_4 cluster onto the larger cluster, the curve for the Li_4 cluster model is shifted up to those for the Li_4 embedded cluster models. This is reasonable in comparison with the curves obtained by the full-cluster model calculations. The value and the position of the energy barrier in the cluster model are strongly dependent on the cluster size, but in the embedded model they are less dependent on the size of the D region. The energy difference between the two embedded cluster models are less than 10kcal/mol all over the reaction path and their potential curves are similar. The embedded cluster models give the sharp barrier of the height of 98~101 kcal/mol at the point 5 and the local minimum corresponding to the on-top adsorption at the point 9. The energy

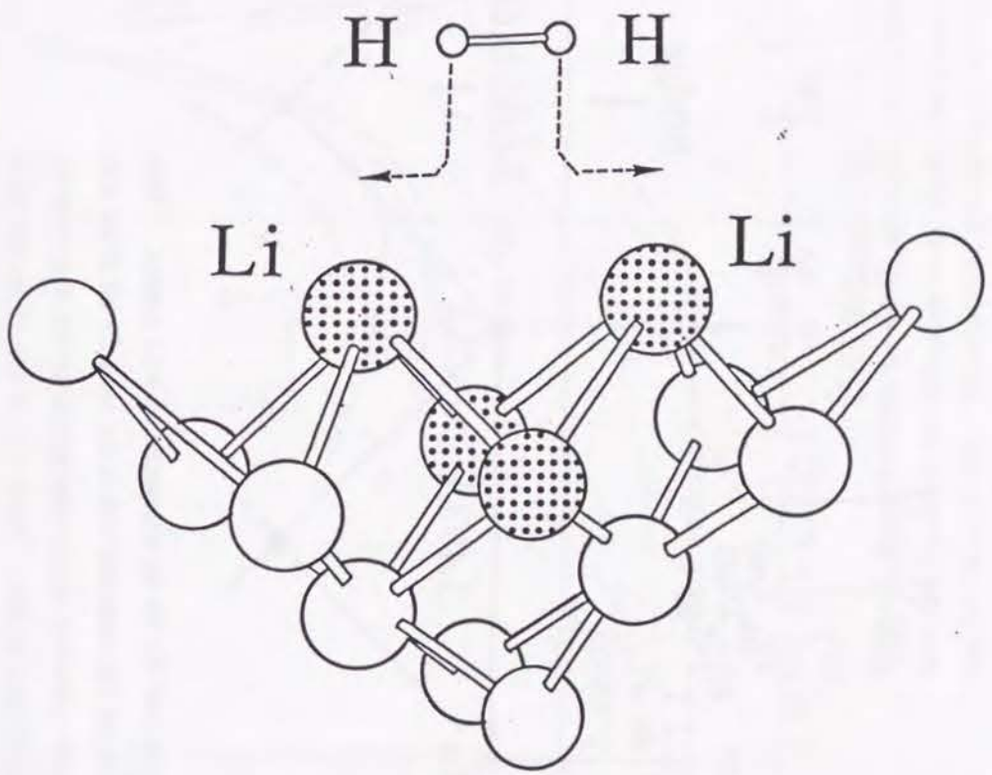

Figure 7. Li_{14} cluster interacting with H_2. The four shaded Li atoms compose the B region and the other Li atoms the D region and H_2 is the adsorbate A in Fig. 1.

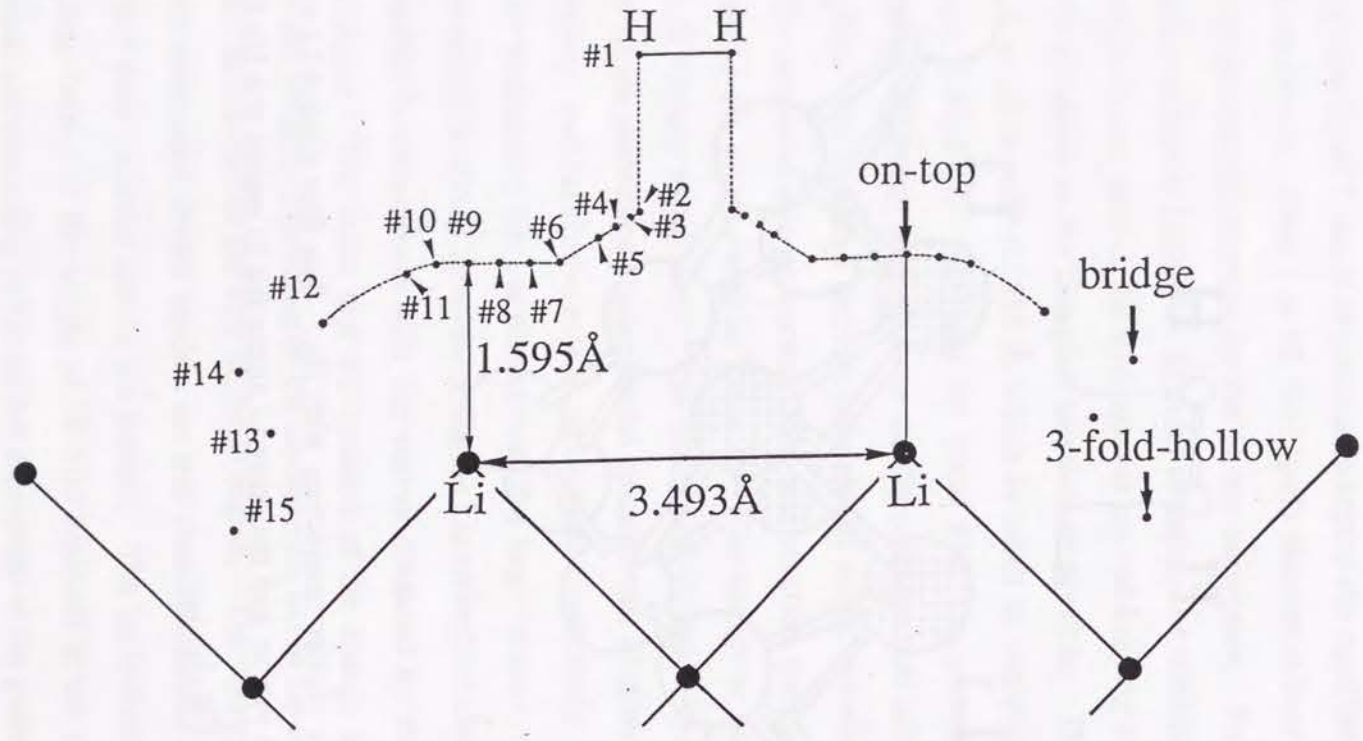

Figure 8. Reaction path for the H_2 adsorption on a Li surface. This reaction path keeps the C_{2v} symmetry and is the same for all of the five different cluster and embedded cluster calculations except that some Li atoms are missing in some models. Points 13, 14 and 15 are the most stable structures for the Li_4H_2, $Li_{14}H_2$ and $Li_{10}H_2$ cluster models, respectively.

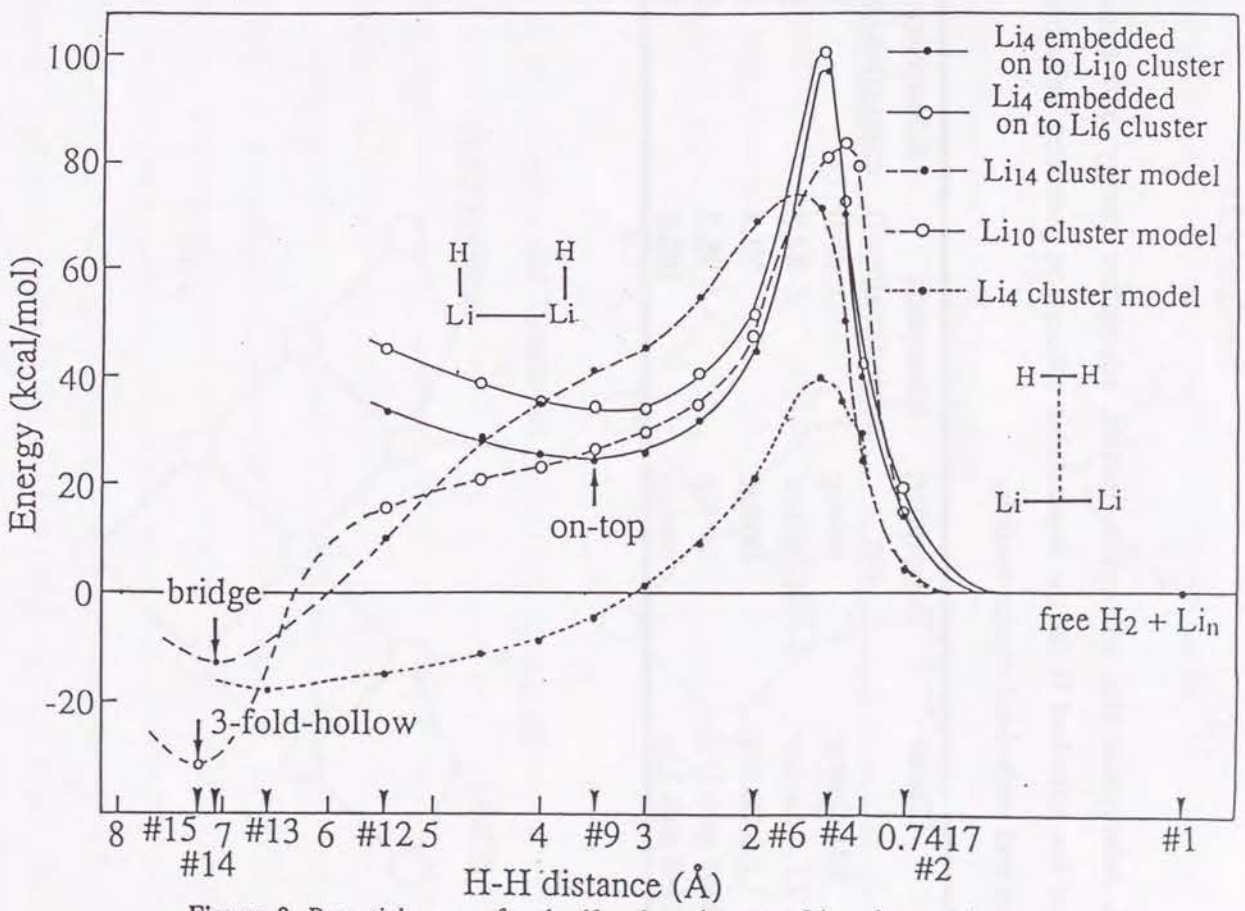

Figure 9. Potential curves for the H_2 adsorption on a Li surface. The solid line represents the embedded cluster model, the broken and dotted line the cluster model. The most stable geometries for the cluster models which are #13 ~ #15 geometries are shown in Fig.10.

TABLE II. Adsorption site, adsorption barrier, adsorption energy, and atomic population of the adsorbed H for the most stable adsorption geometry calculated by the cluster and embedded cluster models.

Cluster	Adsorption site	Adsorption barrier(kcal/mol)	Adsorption energy(kcal/mol)
Li_4 cluster	on-top	40.0	18.9
Li_{10} cluster	3-fold-hollow	84.8	31.2
Li_{14} cluster	bridge	72.3	14.2
Li_4 embedded onto Li_{10}	on-top	98.2	-24.7
Li_4 embedded onto Li_6	on-top	100.8	-34.9

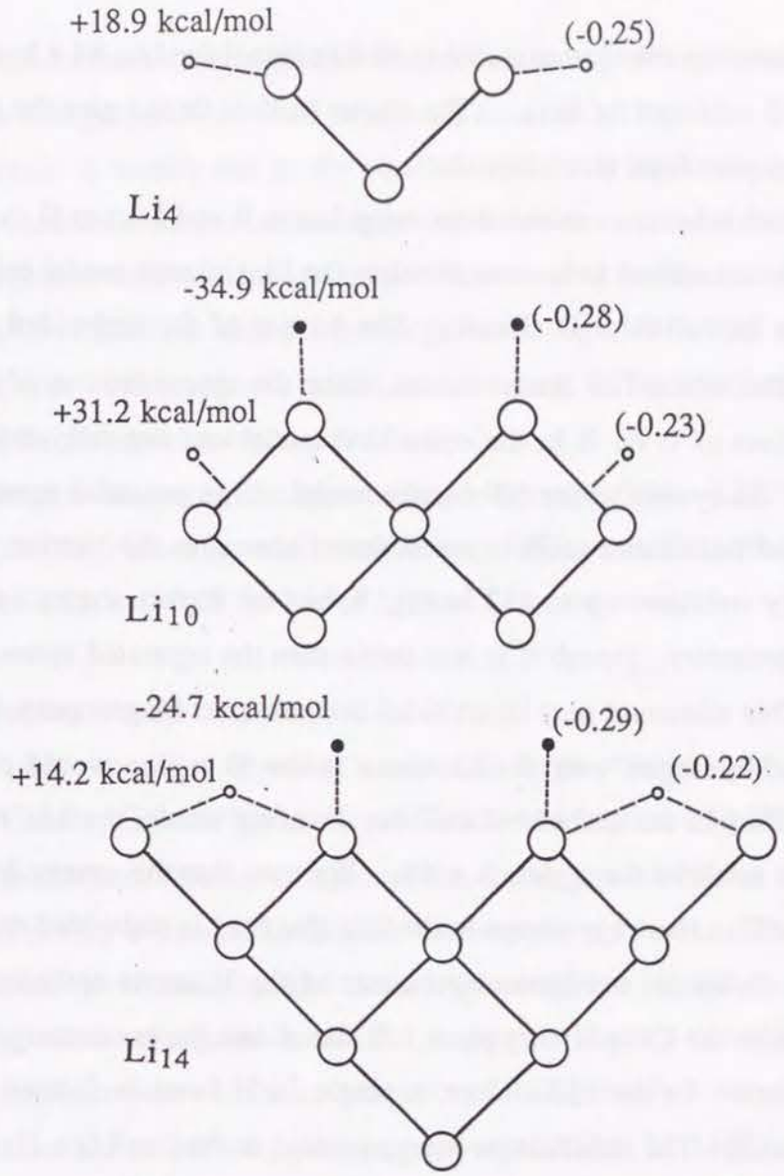

Figure 10. Adsorption site , adsorption energy (stabilization energy relative to $Li_n + H_2$ in kcal / mol) and atomic population of the adsorbed hydrogen. Filled small circles represent the results of the embedded cluster model and open small circles represent the one of the cluster model.

barrier calculated by the cluster model is 40.0 kcal/mol for Li_4, 84.8 kcal/mol for Li_{10}, and 72.3 kcal/mol for Li_{14}. The cluster models do not give the minimum in the reaction path from point 1 to 12.

The embedded cluster calculations using Li_4 as B and Li_{10} as D as shown in Fig. 6 may be considered to have to simulate the Li_{14} cluster model calculations since Li_{14} is the full B $\cup$ D cluster. The barrier of the embedded model is higher than that of the full cluster model, since the approximation of the fixed electronic effect of D on B in the embedded model can not fully describe the relaxation of the system in the full cluster model. The potential curves for the embedded and full-cluster models are different also after the barrier; the latter monotonously stabilizes up to #12 in Fig. 8, but the former shows a minimum near the #9 geometry, though it is less stable than the separated system by 24.7 kcal/mol. This minimum may be artificial because after #9 geometry, the direct interaction of hydrogen with the Li atoms in the D region would occur, but poorly described in the embedded model. In other words, the Li_4 embedded cluster is too small in the region R > #9. We note that the energy for the Li_4 embedded on Li_{10} cluster is always lower than that for Li_4 embedded on Li_6.

Fig. 10 shows the equilibrium geometry of the H atoms optimized for the cluster model on the Cs symmetry plane. It also shows the gross charges on each hydrogen atom. In the Li_4 cluster, a single Li-H bond is formed with the terminal Li atom. The stabilization energy relative to the free $Li_4 + H_2$ system is 18.9 kcal/mol as shown in Fig. 10. The Li_{10} cluster adsorbs hydrogen atom at the three-fold-hollow site and each hydrogen atom makes equivalent three Li-H bonds with Li_3 on the corner. The heat of adsorption is calculated to be 31.2 kcal/mol. The Li_{14} cluster adsorbs the hydrogen atom at the bridge site and each hydrogen makes equivalent two Li-H bonds. The heat of adsorption for this adsorption site is calculated to be 14.2 kcal/mol which is smaller than the adsorption energy on the three-fold hollow site. These results on the adsorption site and the adsorption energy obtained for the cluster model are different from

those obtained from the embedded cluster model; on top adsorption with negative adsorption energy (-34.9 or -24.7 kcal/mol) as show in Fig. 10. We note that this difference is mainly due to the smallness of the B region (only Li_4) in the present embedded cluster model calculation: it can not represent the Li-H bonds in the bridge and three-fold hollow sites. However, we further note that even the Li4 cluster give positive adsorption energy in the region R > #8: at the on top site of #9, it is +9.0 kcal/mol. This is in contrast to the result of the present embedded cluster model calculation.

The atomic charges of the adsorbed hydrogen are -0.25, -0.23, -0.22 for the Li_4, Li_{10} and Li_{14} cluster models, respectively. Those of the embedded cluster models are -0.28 and -0.29 for Li_4 on Li_6 and Li_{10}, respectively.

9. Concluding remarks

We have modified here the moderately large-embedded-cluster (MLEC) model of Grimley, Pisani, Ravenek, and Geurts and applied it to H_2 adsorptions on a lithium surface. We have improved the convergence behavior of the MLEC method by giving a line width to each discrete energy level. The symmetric orthogonalization of basis set and the new convergence algorithm are adopted. The use of semi-orthogonal basis and improved Green's function make the coupling matrix smooth and the convergence of SCF procedure easy.

The calculations of hydrogen adsorption on Li (100) surface are performed by the use of several cluster models and embedded cluster models. In the embedded cluster model, the equilibrium structure of the adsorbed hydrogen is obtained at the on-top position, but this adsorption structure is 24.7 or 34.9 kcal/mol less stable than the isolated system. In the region that the direct interaction between A and D is small, the embedded model simulate rather well the full cluster model (*i.e.*, A $\cup$ B $\cup$ D model). However, outside the region, the embedded cluster model does not well simulate the full cluster model. A reason is clearly that the present MLEC model calculations are too small for

dealing with the D region as a small perturbation to the A + B region. The cluster models, on the other hand, show the three-fold-hollow or bridge site adsorption which are 14.2 and 31.2 kcal/mol more stable than the isolated system.

The criticism of the present result is rather difficult. If the results of the embedded cluster model should reproduce those of the full-cluster model, the results shown in Fig. 9 is by no means favorable to the embedded cluster model. On the other hand, if the D region of the embedded cluster model should be considered as representing a boundary of the bulk metal instead of an outer part of the larger cluster, the present result shown in Fig. 9 is difficult to evaluate since there are no experimental estimation on the potential surface for the dissociative adsorption of H_2 on a Li surface, especially between #1 and #9.

For doing the embedded cluster model calculations, we have to calculate the B $\cup$ D cluster, which is Li_{10} or Li_{14} in the present calculations. For studying catalytic activity of a metal surface, we have to deal with transition metals, and doing *ab-inito* calculations for even an M_n cluster (n =10-20) is still a very hard job. Therefore, though the calculational labour has made somewhat smaller by the present modification of the MLEC model, a full application of this model to transition metal surface is still difficult at present. Further, accounts of electron correlations are very important for dealing with such systems.[10]

Acknowledgements

The calculations have been carried out with FACOM M-780 computer at the Data Processing Center of Kyoto University and HITAC M-680H computer at the Institute for Molecular Science. The authors thank the IMS computer center for the grants of computing time. Part of this study has been supported by a Grant-in-Aid for Scientific Research from the Japanese Ministry of Education, Science, and Culture.

Reference

[1] H. O. Beckmann and J. Koutecky, Surf. Sci. **120**, 127 (1982).

[2] G. Pacchioni, J. Koutecky and H. O. Beckmann, Surf. Sci. **144**, 602 (1982).

[3] K. Przybylski, J. Koutecky, V. B. Koutecky, P. von Rague-Schleyer, and M. F. Guest, J. Chem. Phys. **94**, 5533 (1991).

[4] D. Post and E. J. Baerends, Surf. Sci. **109**, 167 (1981).

[5] K. Hermann and P. S. Bagus, Phys. Rev. B**17**, 4082 (1978).

[6] B. K. Rao, P. Jena and M. Mannien, Phys. Rev. Lett. **53**, 2300 (1984).

[7] A. K. Ray and A. S. Hira, Phys. Rev. B**37**, 9943 (1988).

[8] A. S. Hira and A. K. Ray, Phys. Rev. B**40**, 3507 (1989).

[9] H. Nakatsuji, J. Chem. Phys. **87**, 4995 (1987); H. Nakatsuji, H. Nakai, and Y. Fukunishi, J. Chem. Phys. **95**, 640 (1991).

[10] H. Nakatsuji and H. Nakai, Chem. Phys. Letters., **174**, 283 (1990).

[11] T. B. Grimley and C. Pisani, J. Phys. C**7**, 2831 (1974).

[12] T. B. Grimley and E. E. Mola, J. Phys. C**9**, 3437 (1976).

[13] C. Pisani, Phys. Rev. B**17**, 3143 (1978).

[14] C. Pisani, R. Dovesi and P. Carosso, Phys. Rev. B**20**, 5345 (1979).

[15] C. Pisani and F. Ricca, Surf. Sci. , **92**, 481 (1980).

[16] C. Pisani, R. Dovesi, and P, Ugliengo, Phys. Status Solidi B**116**, 249 (1983);**116**, 547 (1983).

[17] C. Pisani, R. Dovesi, R. Nada, and S. Tamiro, Surf. Sci., **216**, 489 (1989).

[18] M. Causa, R. Dovesi, C. Pisani, R. Colle, and A. Fortunelli, Phys. Rev. B**36**, 891 (1987).

[19] R. Dovesi, C. Pisani, and C. Roetti, Int. J. Quantum. Chem. **17**, 517 (1980).

[20] W. Ravenek and F. M. M. Geurts, J. Chem. Phys. **84**, 1613 (1986).

[21] O. Gunnarsen and H. Hjelmberg, Phys. Scr. **11**, 97 (1975).

[22] O. Gunnarsen, H. Hjelmberg and B. I. Lundqvist, Surf. Sci, **63**, 348 (1977).

[23] R. Colle, A. Fortunelli, and O. Salvetti, J. Chem. Phys. **80**, 2654 (1984).

[24] R. A. van Santen and L. H. Toneman, Int. J. Quamtum. Chem. Suppl. **2**, 83 (1977).

[25] J. Bernholc and S. T. Pantelides, Phys. Rev. B**18**, 1780 (1978).

[26] J. Bernholc, N. O. Lipari and S. T. Pantelides, Phys. Rev. B**21**, 3545 (1980).

[27] J. E. Inglesfield, J. Phys. C**14**, 3795 (1981).

[28] J. E. Inglesfield and G. A. Benesh, Phys. Rev. B**37**, 6682 (1988).

[29] G. A. Baraff and M. Schluter, Phys. Rev. B**19**, 4965 (1979).

[30] G. A. Baraff, M. Schluter and G. Allan, Phys. Rev. B**27**, 1010 (1983).

[31] G. A. Baraff and M. Schluter, J. Phys. C**19**, 4383 (1986).

[32] U. Lindefelt and A. Zunger, Phys. Rev. B**24**, 5913 (1981).

[33] A. R. Williams, P. J. Feibelman and N. D. Lang, Phys. Rev. B**26**, 5433 (1982).

[34] J. L. Whitten and T. A. Pakkanen, Phys. Rev. B**21**, 4357 (1980).

[35] P. Cremaschi and J. L. Whitten, Phys. Rev. Lett, **46**, 1242 (1981).

[36] P. Cremaschi and J. L. Whitten, Surf. Sci., **112**, 343 (1981); **149**, 273 (1985).

[37] P. Cremaschi and J. L. Whitten, Chem. Phys. Lett, **111**, 215 (1984).

[38] P. V. Madhaven and J. L. Whitten, Surf. Sci., **112**, 38 (1981).

[39] P. V. Madhaven and J. L. Whitten, J. Chem. Phys., **77**, 2673 (1982).

[40] C. R. Fischer and J. L. Whitten, Phys. Rev. Lett, **49**, 344 (1982).

[41] C. R. Fischer and J. L. Whitten, Phys. Rev. B**30**, 6821 (1984).

[42] J. P. Muscat and D. M. Newns, Surf. Sci, **89**, 282 (1979); **105**, 570 (1981).

[43] J. P. Muscat and D. M. Newns, Phys. Rev. B**27**, 2025 (1979).

[44] J. P. Muscat, Surf. Sci., **99**, 609 (1980);**110**,85 (1981); **110**, 389 (1981); **118**, 321 (1982); **148**, 237 (1984).

[45] B. R. Brooks, P. Saxe, W. D. Laidig and M. Dupuis, Program Library No. 481, Computer Center of the Institute for Molecular Science (1981).

PART II

Cluster model study on the GaAs epitaxial crystal growth by arsenic molecular beam

Chapter1

Cluster model study on GaAs epitaxial crystal growth by As_2 molecular beam. I. As_2 adsorption on GaAs surface

Abstract

We study chemisorptions of As_2 cluster on a flat GaAs (100) surface and at the step site of this surface with the Hartree-Fock geometry optimization method followed by the energy calculation with the second order Møller-Plesset purterbation method. On the flat surface, the activation energies for both molecular and dissociative adsorptions are high and the molecular adsorption is more favorable than the dissociative one, so that the As_2 cluster is hardly adsorbed and dissociated. At the step site, on the other hand, the dissociative adsorption occurs smoothly: the dissociative adsorption becomes more favorable than the molecular one and the activation energy for the molecular adsorption is only 9.6 kcal/mol. Therefore, the As_2 cluster arriving at the step site is easily adsorbed and dissociated and thus one As layer is added on a Ga surface. We explain the mechanism of this reaction and the difference in the reactivity between the flat surface and the step site.

1. Introduction

Gallium arsenide, an artificial material which does not exist in nature, is a typical compound semiconductor and shows many nice behaviors. Because of the difference between the vapor pressures of gallium and arsenic, the GaAs crystal is difficult to produce and it is made by a special technique, namely by the so called epitaxial method. In molecular beam epitaxial (MBE) growth, gallium atomic beam and arsenic cluster beam composed of As_4 or As_2 are irradiated onto a GaAs surface which is kept at about 600 K in a vacuum chamber, and Ga and As atomic layers grow alternatively. Though the surface morphology has been observed by LEED, RHEED, photoemission and so on, it was difficult to identify the species existing on the surface and to clarify the mechanism of the crystal growth.

Arthur, Foxon, Joys and others studied the reaction mechanisms of the MBE by the reaction rate theory and showed that the mechanisms of the adsorption of the As_2 and As_4 clusters are different to each other [1-3]. In the case of the As_2 beam, the As_2 cluster migrates on the Ga-stabilized surface terminated by Ga atoms and shows the dissociative adsorption there. Thus, the As layer grows with making an As-island region on a Ga surface. The sticking coefficient for the As_2 cluster is close to unity so that even a single As_2 molecule can react. On the other hand, the sticking coefficient for As_4 is smaller than 0.5 and the reaction is more complicated than the As_2 adsorption.

The crystal growth in the metal-organic MBE has been studied theoretically using small cluster models, but there are very few reports on the growth mechanism in the MBE and about the difference due to the size of cluster included in the beam [4-9]. Though Foxon and Joys [2,3] proposed the reaction mechanism of the MBE, they adopted several assumptions on the reaction rate and therefore the explicit geometry of the adsorbate, the reaction path, and the reason of the smooth epitaxial growth are remained to be clarified.

We study the mechanism of the GaAs crystal growth in the As_2 beam epitaxy by ab-initio theoretical method with using the cluster model. In this study, the

adsorption and the dissociative reaction of a single As_2 are studied. We simulate the Ga-stabilized GaAs (100) surface by the $Ga_8As_8H_{18}$ cluster and its step site by the $Ga_8As_{10}H_{20}$ cluster. In Section 2, the method of calculations is briefly explained. In Section 3, the reaction of the As_2 cluster on a flat GaAs surface is studied. The equilibrium structure and transition state are given and the reaction mechanism is explained qualitatively using the orbital correlation diagram. In Section 4, the adsorption of As_2 on a step site is studied similarly to Section 3 and the adsorption mechanisms on the flat surface and at the step site are compared. Conclusions are given in the last section.

2. Computational method

We use the Hartree-Fock (HF) method followed by the second-order Møller-Plesset purterbation (MP2) method. The HF and MP2 calculations are performed with the use of the program HONDO7 [10]. Fig 1 shows the $Ga_8As_8H_{18}$ and $Ga_8As_{10}H_{20}$ clusters which simulate the GaAs(100) surface and its step site, respectively. We assume that the As_2 molecule approaches the cluster and reacts with it as shown in Fig 1. The lattice constant of the Ga and As atoms located in the crystal lattice is 5.654 Å [11]. The H atoms cover the artificial dangling bonds of the Ga_8As_8 and Ga_8As_{10} clusters. Covalent bonding crystal is often simulated by the cluster model whose dangling bonds are covered by hydrogen atoms [12-14]. The Ga-H and As-H bond lengths are fixed to the values of 1.663 and 1.511 Å which are the bond lengths in the free GaH and AsH_3 molecules, respectively [15].

The Gaussian basis sets for the Ga and As atoms at the reaction center are (3s3p)/[2s2p] double zeta contracted Gaussian type orbitals (CGTO's) and for the other atoms are the (3s3p)/[1s1p] minimal basis sets and the Ne cores are replaced by the effective core potential [16]. For H atom, STO-3G basis is used [17]. The double zeta basis sets are used for the two As atoms of the As_2 cluster and the three Ga atoms located on the surface of the cluster: they are indicated by the asterisks in Fig 1.

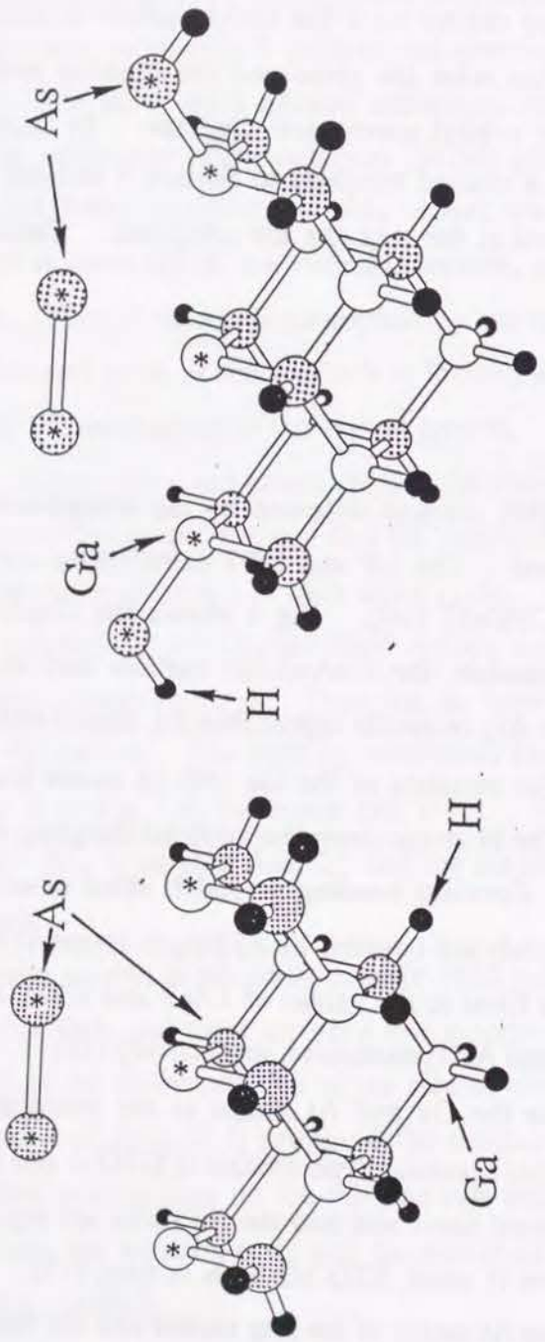

Figure 1. $Ga_8As_8H_{18}$ and $Ga_8As_{10}H_{20}$ clusters interacting with As_2. The atoms indicated by the asterisks are treated with the double zeta basis and the others are with minimal basis.

Other As, Ga and H atoms are treated with the minimal basis sets. For the $Ga_8As_{10}H_{20}$ cluster, two further As atoms which are located on the surface are treated with the double zeta basis.

3. Adsorption of As_2 on a flat GaAs surface

We show in Fig 2 the reaction path optimized by the HF calculations with assuming C_{2v} symmetry. The values in parentheses are the electronic charges of the two As atoms. Table I gives the geometries of the approaching As_2 whose accuracy is within 0.1 Å. Only the two As atoms of the approaching As_2 cluster are optimized with the $Ga_8As_8H_{18}$ cluster fixed. We show the calculated potential curve along the reaction path in Fig 3. The dashed line represents the result of the HF method and the solid line the MP2 method. From points 1 to 8, the horizontal axis stands for the Ga-As distance, that is the distance from the As of the As_2 cluster and the surface Ga of the $Ga_8As_8H_{18}$ cluster, and from points 8 to 14, the axis stands for the As-As distance of the adsorbing As_2 cluster.

The potential curve has two minimum points 7 and 14 and two maximum points 3 and 11: passing though the initial barrier at point 3, As_2 reaches the molecular adsorption at point 7 and then going beyond the barrier at point 11 , it is dissociatively adsorbed at point 14. At point 1, the optimized As-As bond length and the force constant are 2.14 Å and 456 cm^{-1} which are almost equal to the experimental values of the free As_2 of 2.10 Å and 430 cm^{-1}, respectively. The barrier height at point 3 is 23.5 kcal/mol and the As-As distance becomes a bit longer. After passing this barrier, the As atoms become slightly negatively charged and the As_2 is adsorbed keeping the As-As length almost constant. The molecular adsorption is found at point 7 with the adsorption energy of 29.7 kcal/mol: the Ga-As length is 2.55 Å and the As-As length is 2.4 Å , slightly longer than that of the free As_2, and the As net charge is -0.11. These results are similar to the result of the previous study on the $GaAs_2$ system [18]: the Ga-As and As-As lengths were reported to be 2.85 and 2.2 Å,

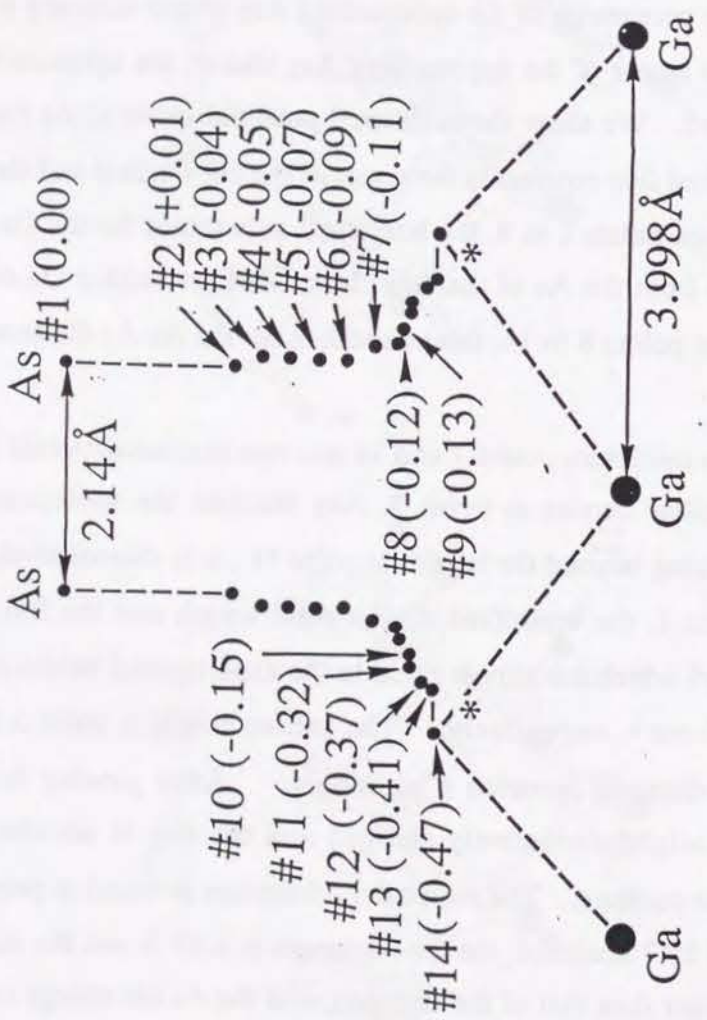

Figure 2. Reaction path for the As_2 adsorption on a GaAs(100) flat surface. This reaction path keeps the C_{2v} symmetry. Values in parentheses shows the gross charge of the adsorbed As atom. Two asterisks indicate the positions of the As atoms in the GaAs crystal lattice without surface relaxation.

Table I
Geometries of As_2 along the reaction path shown in Fig 2.

Position		Distance (Å) R_{As-As}	R_{Ga-As}[a]
1		2.14	5.11
2		2.14	3.66
3	(barrier)	2.30	3.45
4		2.30	3.21
5		2.30	2.98
6		2.30	2.75
7	(minimum)	2.40	2.55
8		2.50	2.38
9		2.70	2.41
10		3.00	2.42
11	(barrier)	3.20	2.48
12		3.50	2.51
13		3.60	2.48
14	(minimum)	4.40	2.78

[a] Distance to the nearest Ga atom.

respectively, and the stabilization energy relative to the Ga + As_2 system to be 30.3 kcal/mol. This result indicates the locality of the interaction between As_2 and the surface in the molecular adsorption state.

Beyond this point, the As-As length becomes longer indicating that the As-As bond is broken by the adsorption and the As atoms reach the second barrier at point 11. The As atoms are suddenly charged at this point; the charge of -0.15 at point 10 becomes the value of -0.32 at point 11. The energy barrier is 10.2 kcal/mol higher than the free system and 39.9 kcal/mol higher than the molecular adsorption state. Finally, the dissociative adsorption occurs at point 14 with the adsorption energy of 19.9 kcal/mol. There, the optimized As-As distance is 4.40 Å which is slightly longer than that in the GaAs crystal which is indicated by the asterisks in Fig 2. The optimized As-Ga distance on the surface is 2.78Å which is slightly shorter than 2.827 Å, the experimental AsGa distance for the crystal. The charge of these As atoms -0.47 is similar to the value -0.48 which is the average for the inner eight As atoms in the cluster. Since the dissociative adsorption state necessary for the crystal growth is less stable than the molecular adsorption state, the crystal growth is hard to occur and we expect that the molecularly adsorbed As_2 cluster migrates on the surface.

The mechanisms of the molecular and dissociative adsorptions are qualitatively explained by the orbital correlation diagrams shown in Figs 4 and 5. Fig 4 is for the first stage of the reaction from the free system at point 1 to the molecular adsorption at point 7, and Fig 5 is for the second stage of the reaction from the molecular adsorption at point 7 to the dissociative adsorption at point 14. Orbitals playing a role in the reaction are the highest occupied molecular orbital (HOMO), lowest unoccupied molecular orbital (LUMO) and their neighboring orbitals. The surface dangling bonds are localized on the three surface Ga atoms. We therefor show only three surface Ga atoms in Figs 4 and 5.

First, the origin of the initial energy barrier and the nature of the interaction in the molecular adsorption are explained with referring to Fig. 4. The orbitals of the free As_2 and the free GaAs cluster are displayed in the left and right hand sides,

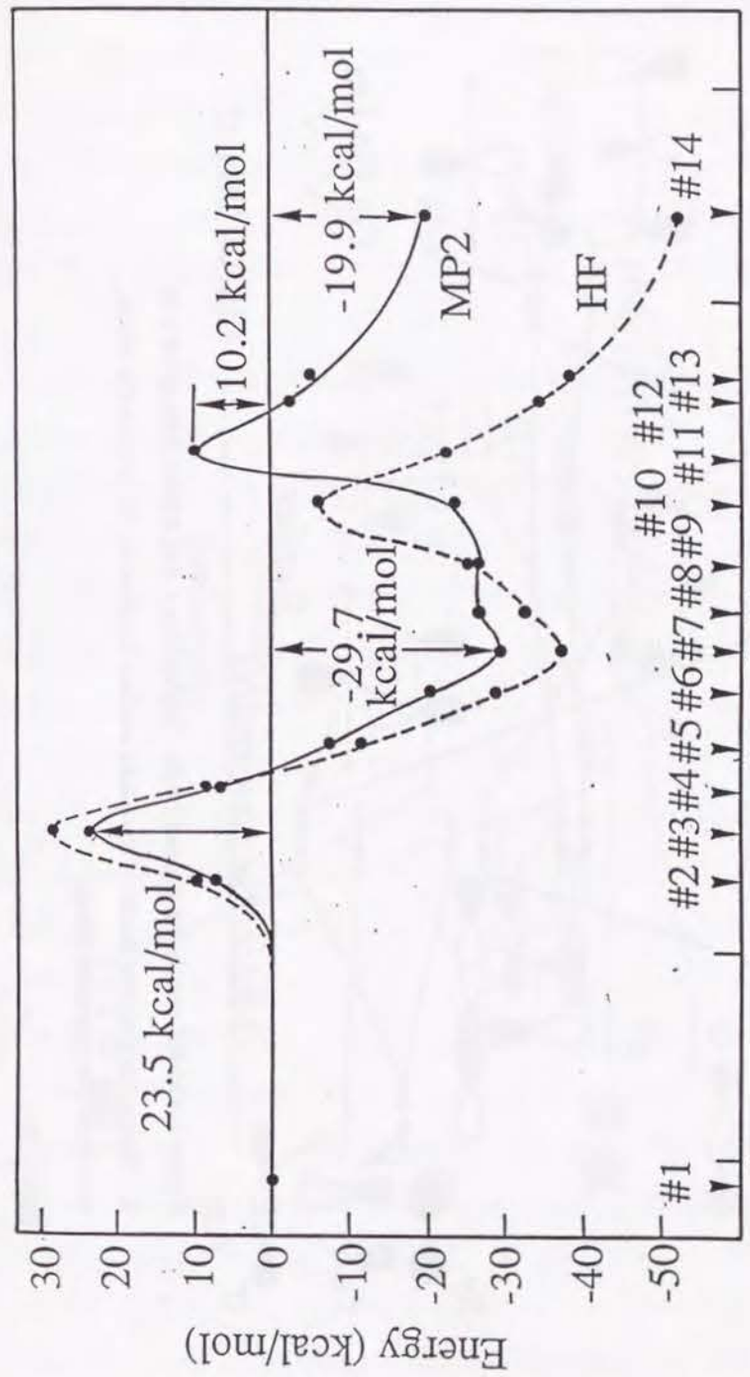

Figure 3. Potential curves for the As_2 adsorption on a GaAs(100) surface. The solid line represents the result of the MP2 method and the broken line the HF method. From point 1 to 8, the coordinate shows the Ga-As distance and from 8 to 14, it shows the As-As distance.

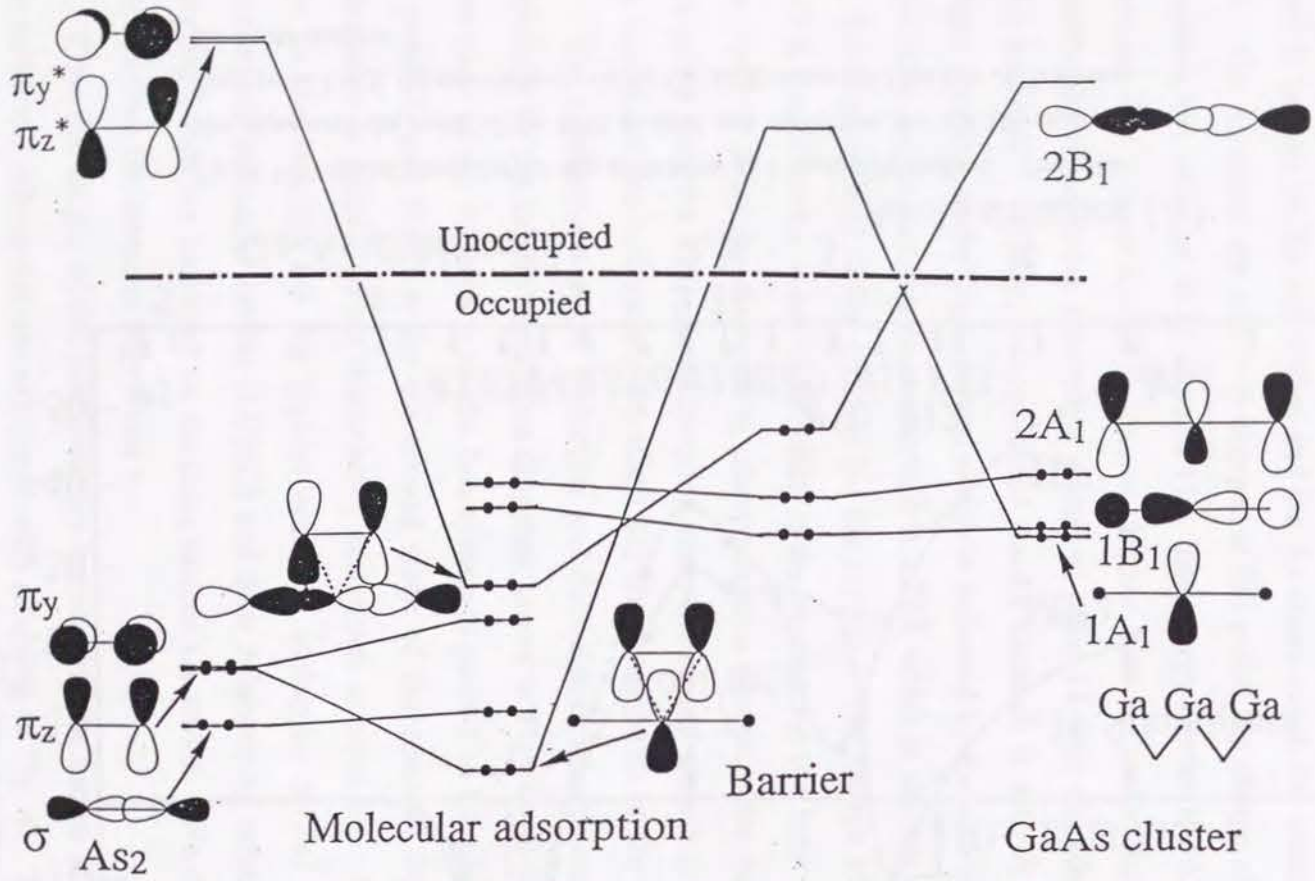

Figure 4. Orbital correlation diagram of the $Ga_8As_8H_{18}$ + As_2 system from point 1 to 8. Since the dangling bonds of the GaAs surface localize on the surface Ga atoms, only three Ga atoms are shown.

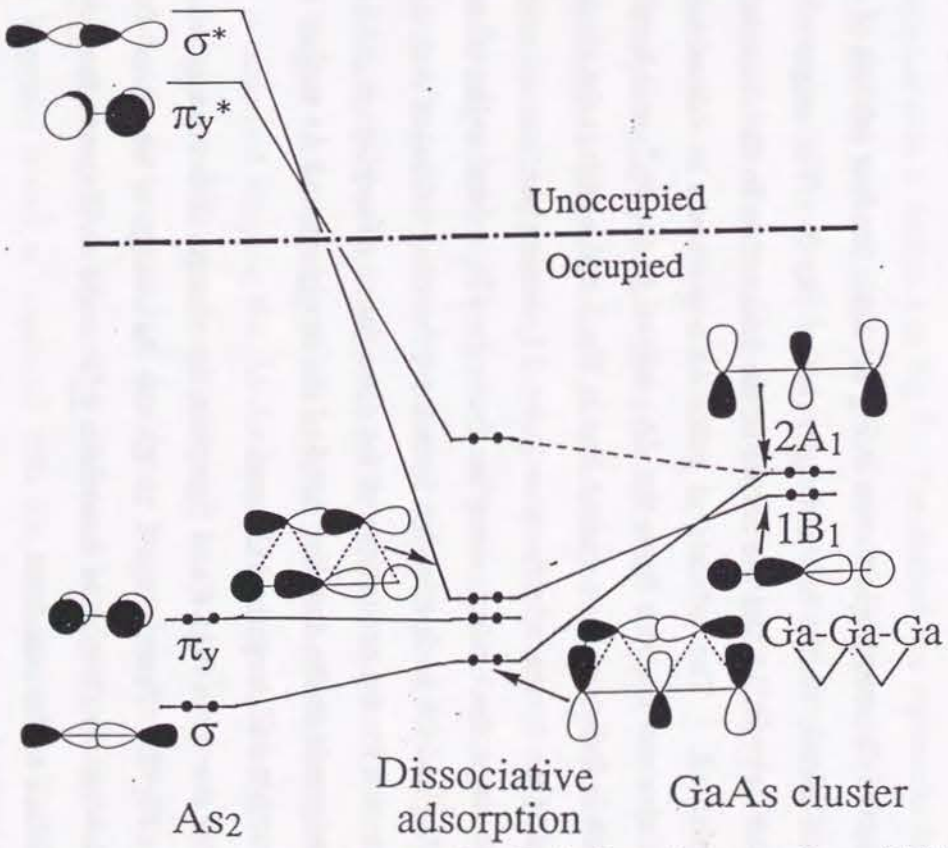

Figure 5. Orbital correlation diagram of the $Ga_8As_8H_{18}$ + As_2 system from point 8 to 14. Only these orbitals which do not have full participation in Fig 4 are shown. The broken line represents a charge transfer from the surface to As_2.

respectively, and the orbitals at "barrier" and "molecular adsorption" represent the orbitals at points 3 and 7, respectively. The approach of the As_2 cluster to the Ga surface leads to the electron excitation from the $1A_1$ orbital to the $2B_1$ orbital of the GaAs cluster. This is the excitation within the surface dangling bonds and causes the energy barrier to the molecular adsorption at point 3. Next step is a electron donation from the $2B_1$ orbital to the π_z^* anti-bonding orbital of As_2 and the back donation from the π_z bonding orbital of As_2 to the $1A_1$ orbital. This step creates the two bonding orbitals which give an attractive interaction for the molecular adsorption at point 7. The As-As bonding orbitals of As_2 remain and keep the As-As bond length constant.

The second stage of the reaction is shown in Fig 5. Only the four orbitals of As_2 and GaAs cluster are shown on the left and right side of Fig 5. The origin of the second energy barrier at point 11 and the nature of the interaction in the dissociative adsorption are explained. The orbitals at point 14 are shown as "dissociative adsorption". The electron transfer from the $2A_1$ orbital to the π_y^* anti-bonding orbital of As_2, which is indicated by a dashed line in Fig 5 and which is the electron transfer from the surface to the adsorbate at point 11, causes the second energy barrier. At the last stage, the electron donation from the $1B_1$ orbital to the σ^* anti-bonding orbital of As_2 and the back donation from the σ bonding orbital of As_2 to the $2A_1$ orbital are important for the occurrence of the dissociative adsorption at point 14. The π_y^* orbital corresponds to the dangling bond of the newly created As surface and it does not interact with the underground Ga atoms.

The mechanisms shown in Figs 4 and 5 explain the change of the charge on the As atoms shown in Fig 2. From point 1 to 10, the As charge is less than -0.11. From point 11 to 14, when As_2 begins to dissociate, it becomes -0.47 due to the charge transfer from the surface to the adsorbate.

4. Adsorption of As_2 at a step site of the GaAs surface

The step site of the Ga-stabilized GaAs(100) surface is simulated by the $Ga_8As_{10}H_{20}$ cluster shown in Fig 1. Two As atoms which represent the As atoms at the step site are added at the edge of the $Ga_8As_8H_{18}$ cluster dealt with in the preceding section. We show in Fig 6 the reaction path optimized by the HF calculations with assuming C_{2v} symmetry. The values in parentheses are the electronic charges of the two As atoms. Table II gives the geometries of the approaching As, and the accuracy is within 0.1 Å. Only the two As atoms of the approaching As_2 cluster are optimized with the $Ga_8As_{10}H_{20}$ cluster fixed. The optimized reaction path is almost the same as the one given in section 3 for the flat surface. The calculated potential curve along the reaction path is depicted in Fig 7. The dashed line represents the result of the HF method and the solid line the MP2 method. From points 1 to 9, the horizontal axis stands for the Ga-As distance, that is the distance from the As of the As_2 cluster to the surface Ga of the $Ga_8As_{10}H_{20}$ cluster, and from point 9 to 14, the axis stands for the As-As distance of adsorbing As_2 cluster.

The potential curve is roughly similar to the one given in section 3, that is, it has two minimum at points 8 and 14 and two maximum at points 3 and 9: after passing the barrier at point 3, As_2 reaches the molecular adsorption state at point 8, and then it is dissociatively adsorbed at point 14. At point 1, the As_2 cluster has the same bond length as in Section 3. The first barrier height at point 3 is only 9.6 kcal/mol, which is almost one half of the barrier for the flat surface and the As-As distance becomes a little longer. After passing this barrier, the As atoms become slightly charged and the As_2 is adsorbed keeping the As-As length constant. The molecular adsorption is found at point 9 with the adsorption energy of 49.2 kcal/mol: the Ga-As length is 2.50 Å and the As-As length is 2.36 Å, slightly longer than the free As_2, and the charge of the As atom is only -0.03. The calculated activation energy for the desorption is 58.8 kcal/mol which is compared with the experimental value of 45 kcal/mol [1]. This result is similar to the result of the previous study on the $GaAs_2$ system [18] and the molecular adsorption discussed in Section 3. It indicates the locality of the interaction between As_2 and the surface in the molecular adsorption state.

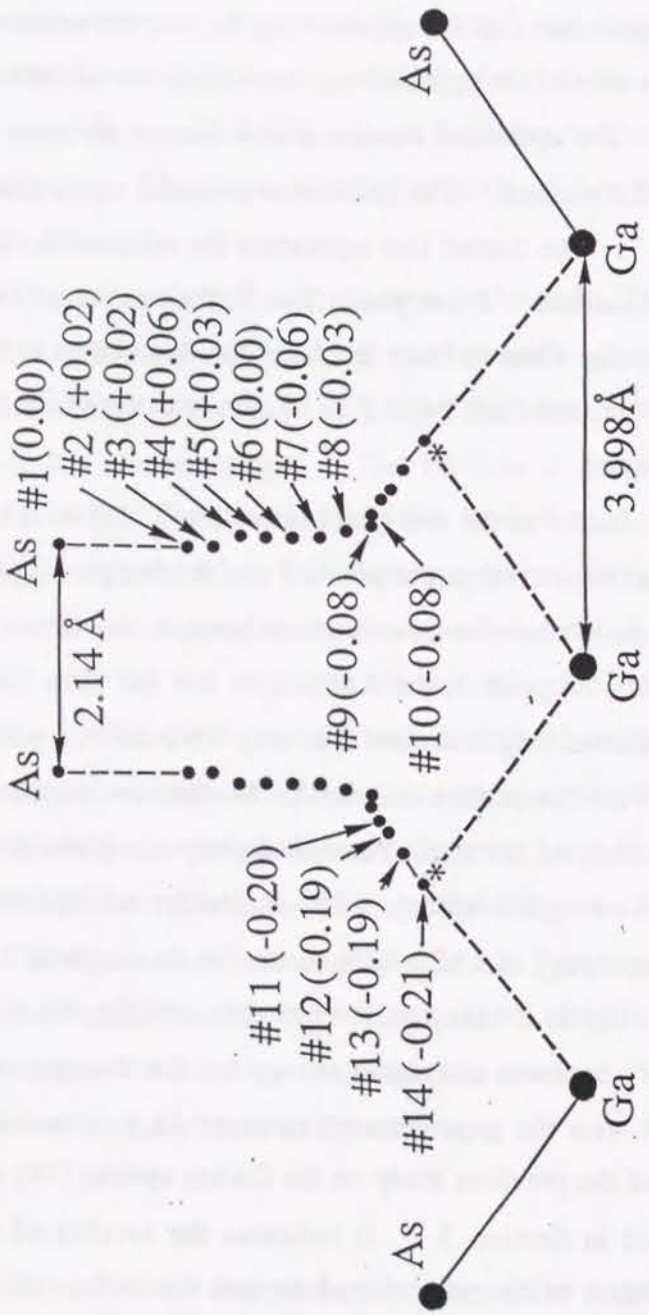

Figure 6. Reaction path for the As_2 adsorption at the step site of a GaAs(100) surface. This reaction path keeps the C_{2v} symmetry. Values in palentheses shows the gross charge of the adsorbed As atom. Two asterisks indicate the positions of the As atoms in the GaAs crystal lattice without surface relaxation.

Table II
Geometries of As_2 along the reaction path shown in Fig 6.

Position		Distance (Å) R_{As-As}	R_{Ga-As}[a]
1		2.14	5.11
2		2.14	3.90
3	(barrier)	2.14	3.66
4		2.30	3.45
5		2.30	3.21
6		2.30	2.98
7		2.30	2.75
8	(minimum)	2.40	2.55
9	(barrier)	2.50	2.36
10		2.70	2.41
11		3.00	2.42
12		3.20	2.45
13		3.60	2.48
14	(minimum)	4.20	2.58

[a] Distance to the nearest Ga atom

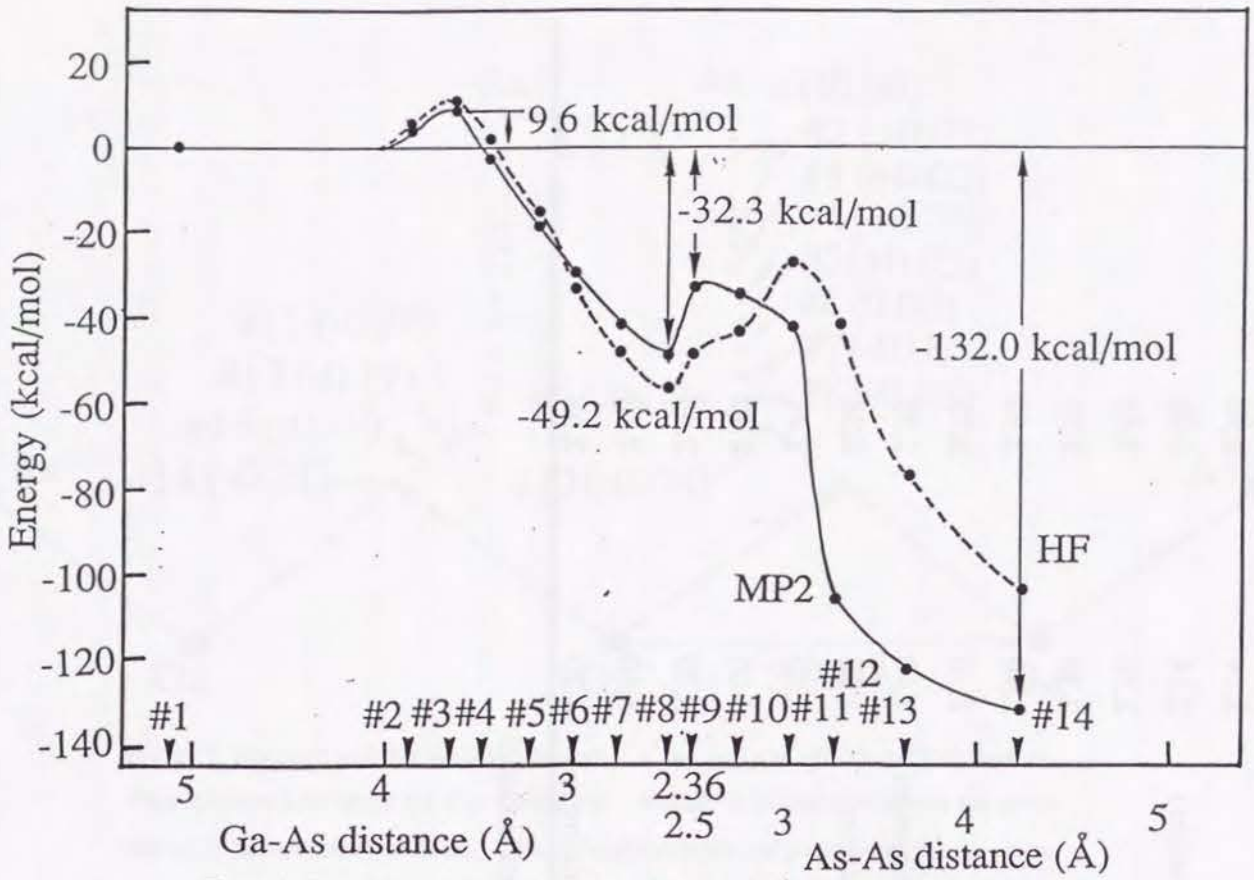

Figure 7. Potential curve for the As_2 adsorption on a GaAs surface. The solid line represents the result of the MP2 method and the broken line the HF method. From point 1 to 9, the coordinate shows the Ga-As distance and from 9 to 14, it shows the As-As distance.

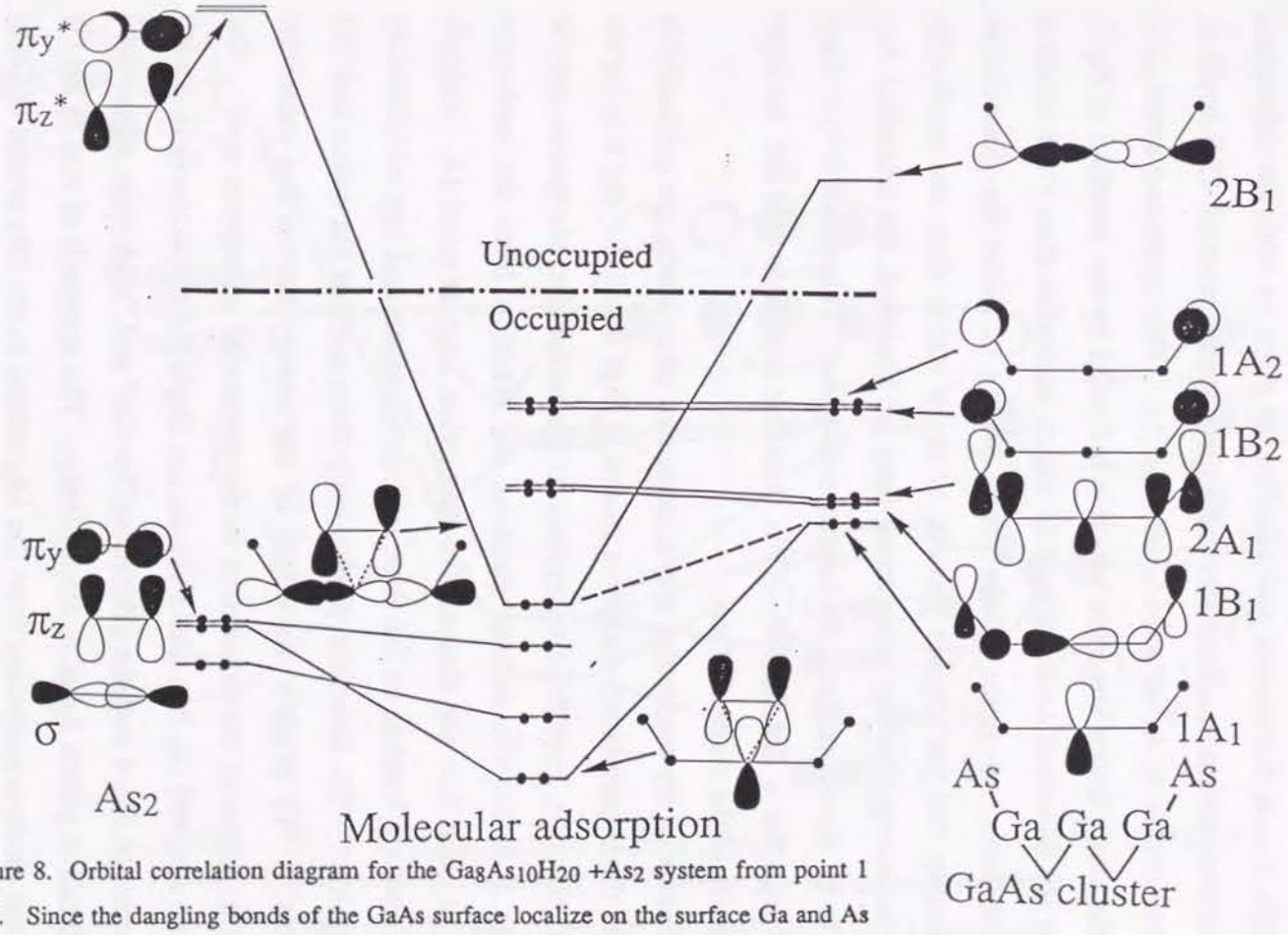

Figure 8. Orbital correlation diagram for the $Ga_8As_{10}H_{20}$ +As_2 system from point 1 to 8. Since the dangling bonds of the GaAs surface localize on the surface Ga and As atoms, only these atoms are shown. The broken line represents an excitation of surface dangling bond.

After passing the molecular adsorption state, the As-As length becomes longer indicating that the As-As bond is broken by the adsorption, and the As atoms reach the second barrier at point 9. The As atoms are rapidly charged near this point; the charge is -0.08 at point 9 and -0.20 at point 11. The energy barrier is 32.3 kcal/mol lower than the free system and 16.9 kcal/mol higher than the molecular adsorption state. Finally, the As_2 is dissociated and adsorbed at point 14 with the adsorption energy 132.0 kcal/mol which overestimates the experimental value of 45.9 kcal/mol for a complete monolayer of As on a GaAs surface [1]. This optimized structure is very similar to the GaAs lattice structure which is indicated by the asterisks in Fig 6, but the charge of the adsorbed As atom is -0.21 which is smaller than -0.48 which is the charge of the inner As atoms of the GaAs cluster. Since the dissociative adsorption necessary for the crystal growth is more stable than the molecular adsorption and the energy barrier is no more than 17 kcal/mol, the adsorbed As_2 cluster is likely to be dissociated and the crystal will grow. This result is in a sharp contrast to the result for a flat surface. We therefore conclude that the As layer grows at the step site of the GaAs surface.

The mechanisms of the molecular and dissociative adsorptions are qualitatively explained by the orbital correlation diagrams shown in Figs 8 and 9. Fig 8 is for the first stage of the reaction from the free system to the molecular adsorption state at point 8, and Fig 9 is for the second stage of the reaction from the molecular adsorption state at point 8 to the dissociative adsorption state at point 14. Orbitals important in the reaction localize on the three surface Ga atoms and two additional As atoms at the step site. We therefore display only three surface Ga atoms and two surface As atoms. We explain the origin of the energy barrier for molecular adsorption and the nature of the interaction in the molecular adsorption state. The orbitals of the free As_2 and the free GaAs cluster are displayed respectively in the left and right hand sides of Fig 4 and the orbitals at "barrier" and "molecular adsorption" represent the orbitals at points 3 and 8, respectively. The approach of As_2 to the Ga surface leads to the electron excitation from the $1A_1$ orbital to the $2B_1$ orbital of GaAs

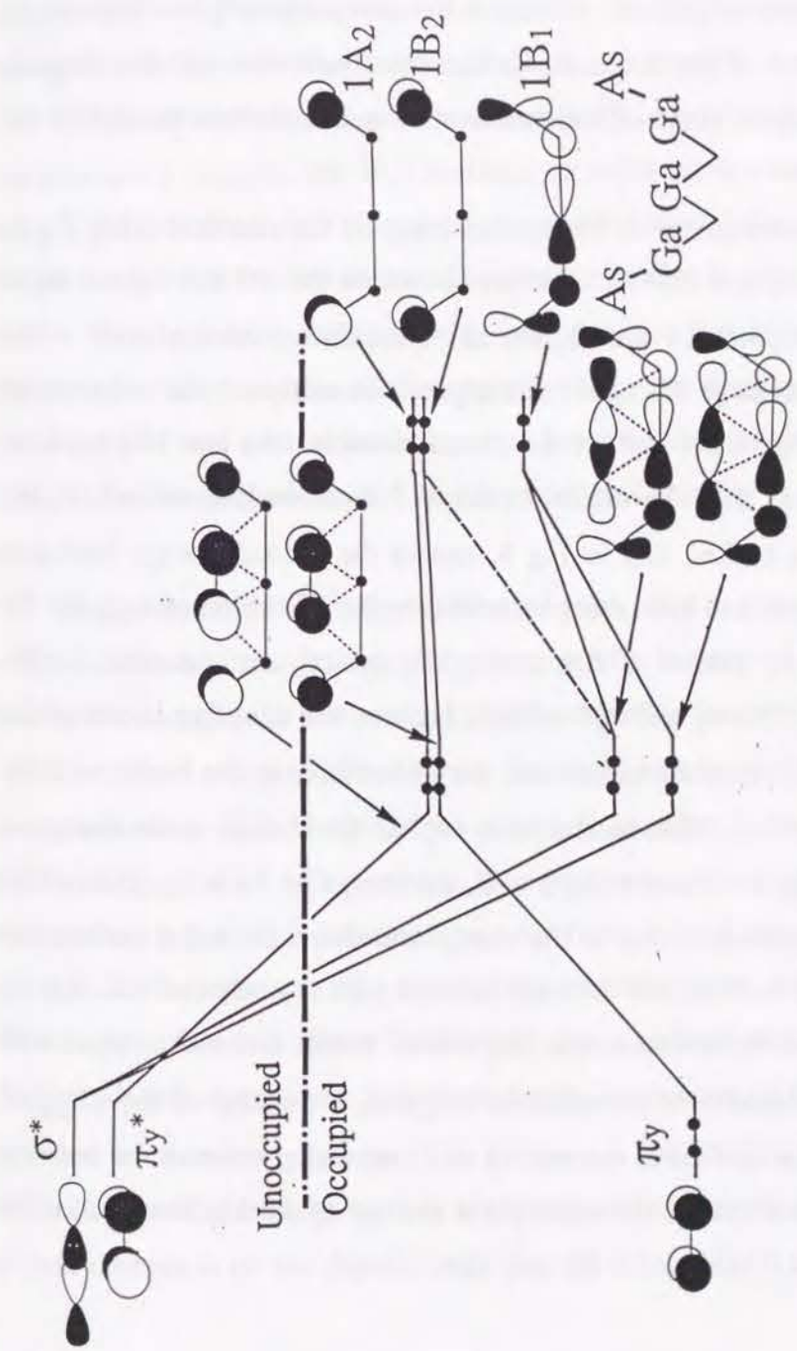

Dissociative adsorption

As_2

Figure 9. Orbital correlation diagram for the $Ga_8As_{10}H_{20}$ + As_2 system from point 9 to 14. Only these orbitals which do not have full participation in Fig 8 are shown. The broken line shows a charge transfer from the surface to As_2.

cluster which is indicated by the broken line in Fig 8. This excitation causes the first energy barrier at point 3. The next step is an electron donation from the $2B_1$ orbital to the π_z^* anti-bonding orbital of As_2 and the back donation from the π_z bonding orbital of As_2 to the $1A_1$ orbital. This step creates the two bonding orbitals which give an attractive interaction at point 8. Two As atoms representing the step site do not take part in this stage of the reaction, so that the mechanism of this stage is essentially equal to the same stage of the reaction on a flat surface studied in the previous section.

We next study the mechanism in the second stage of the reaction using Fig 9. Only the six orbitals of As_2 and GaAs cluster are shown on the left and right sides of Fig 6. The orbitals at point 14 are shown as "dissociative adsorption". The difference from the second stage discussed in the previous section is the existence of the two orbitals belonging to the surface As atoms, namely $1A_2$ and $1B_2$ orbitals. The electron transfer from the $1B_2$ orbital to the π_y^* anti-bonding orbital of As_2 which is indicated by the broken line in Fig 9, causes the second energy barrier at point 9. The electron donation from the $1A_2$ orbital to the σ^* orbital of As_2 and the back donation from the π_y orbital of As_2 to the $1B_2$ orbital are important for the dissociative adsorption. The π_y and π_y^* orbitals become the dangling bonds of the newly created As surface, but at the same time, they contribute to the bonds with the neighboring surface As atoms. This mechanisms explain the change of the charge on the As atoms shown in Fig 6. From point 1 to 8, the charge of As is less than -0.06. At point 9 to 14, it becomes -0.21 due to the charge transfer. On a flat surface, the π_y bonding orbital of As_2 is filled and does not interact with any other orbital, but the electron donation from the π_y orbital to the $1B_2$ orbital occurs and makes bond with neighboring As atoms. Because of this electron donation, the charge of the adsorbed As atoms of -0.48 on a flat surface is reduced to -0.21 on a step site and the bonding with the surface As atoms makes the adsorption energy of 19 kcal/mol on a flat surface to the value of 132.0 kcal/mol.at the step site

5. Conclusion

The As_2 cluster beamed on a Ga-stabilized GaAs surface is molecularly adsorbed and migrates on a flat surface, and then it is dissociated at a step site, giving a new As layer growing on the Ga surface. The calculated energy barrier for the As_2 adsorption is 23.5 kcal/mol on a flat surface and 9.6 kcal/mol at a step site, and the energy barrier for the dissociative adsorption at a step site is 16.9 kcal/mol.

The molecular adsorption state at a step site is similar to that on a flat surface and the adsorption energies are 29.7 kcal/mol on a flat surface and 49.2 kcal/mol at a step site. The adsorbed As_2 cluster is almost neutral and the As-As length is slightly longer than that of a free As_2. The energy barrier for the molecular adsorption is due to the orbital reorganization within the dangling bonds of the Ga surface. At the molecular adsorption, the electron transfer from the dangling bond of the surface to the As_2 π^* orbital and the back donation from the As_2 π orbital to the dangling bond break the π bonding of the As_2 and make a bond between the As_2 and the surface Ga atom.

The geometry of the dissociative adsorption state at a step site is similar to that on a flat surface and shows a good agreement with the crystal lattice structure, but the adsorption energy on a flat surface, 49.2 kcal/mol is much different from the value of 132.0 kcal/mol at a step site showing that the dissociative adsorption at a step site is more favorable. The charge of the adsorbed As atom is -0.48 on a flat surface and -0.21 at a step site. The energy barrier between the molecular and dissociative adsorptions is due to the electron transfer from the dangling bond of the surface Ga atom to the As_2 cluster. At the dissociative adsorption, the electron transfers from the dangling bond to the σ^* orbital of As_2 and from the σ orbital of As_2 to the dangling bond of the surface work to break the σ bond of the As_2 and make a bond between the As atom and the surface Ga atom. The bonding between the adsorbed As atom and the neighboring As atom at the step site makes the adsorption energy and the atomic charges to be site-dependent .

Acknowledgements

The calculations were carried out with the FACOM M-1800 computer at the Data Processing Center of Kyoto University and the HITAC M-680H at the Institute for Molecular Science. The authors thank the IMS computer center for the grants of computing time. Part of this study has been supported by the Grant-in-Aid for Scientific Research from the Japanese Ministry of Education, Science, and Culture.

Referrence

[1] J. R. Arthur, Surf. Sci. , 43 (1974) 449.

[2] C. T. Foxon, M. R. Boudry and B. A. Joyce, Surf. Sci.,44 (1974) 69.

[3] C. T. Foxon and B. A. Joyce, Surf. Sci.,50 (1975) 434,*ibid* , 64(1977) 293.

[4] A. A. Bonapasta, M. R. Bruni, A. Lapiccirella, P. Nota, G. Scavia and N. Tomassini, Surf. Sci. , 204 (1988) 273.

[5] M. Tsuda, S. Oikawa, M. Morishita and M. Mashita, Jpn. J. Appl. Phys., 26.(1987) L564

[6] A. Doi, Y. Aoyagi and S. Namba, Appl. Phys. Lett. , 48(1986) 1787; 49 (1986) 785.

[7] T. Ohno, Phys. Rev. B44 (1991) 6306 .

[8] R. M. Graves and G. E. Scuseria, J. Chem. Phys., 95 (1991) 6602.

[9] K. Balasubramanian, J. Chem. Phys., 87(1987) 3518.

[10] M. Dupuis, J. D. Watts, H. O. Villar and G. H. B. Hurst, Program Libraly No. 1501, Computer Center of the Institute for Molecular Science, (1987).

[11] K. H. Hellwege, W. Pies, A. Weiss: Crystal Structure Data of Inorganic Compounds, Landolt-Börnstein, New Series, Group III, Vol. 7, (Springer-Verlag, Berlin, 1979).

[12] L. C. Snyder and Z. Wasserman, Surf. Sci., 71(1978) 407; 77 (1987) 52.

[13] A. C. Kenton and M. W. Ribarsky, Phys. Rev. B23 (1981) 2897.

[14] K. Hermann and P. S. Bagus, Phys. Rev. B20 (1979) 1603.

[15] J. H. Callomon, E. Hirota, K. Kuchitsu, W. J. Lafferty, A. G. Maki, and C. S. Pote: Structure Data of Free Polyatomic Molecules, Landolt-Börnstein, New Series, Group II, Vol. 7, (Springer-Verlag, Berlin, 1976).

[16] W. R. Wadt and P. J. Hay, J. Chem. Phys., 82 (1985) 284.

[17] W. J. Hehre, R. F. Stewart and J. A. Pople, J. Chem. Phys., 51 (1969) 2567.

[18] K. Balasubramanian, J. Chem. Phys., 86 (1987) 3410.

Chapter 2

Cluster model study on GaAs epitaxial crystal growth by As_2 molecular beam. II. Mechanism involving $GaAs_2$ intermediate cluster.

Abstract

The mechanisms of the GaAs epitaxial crystal growth by Ga atomic and As_2 molecular beams on Ga-stabilized and As-stabilized GaAs(100) surfaces are studied with the use of the cluster model and the Hartree-Fock method. We propose the mechanism involving the formation of the $GaAs_2$ cluster as an intermediate. When the As_2 beam is irradiated on the surface, the $GaAs_2$ cluster is generated from As_2 and free Ga atom without energy barrier. This $GaAs_2$ is adsorbed on the As-stabilized surface and gives a new Ga-layer on the surface and the As_2 remains to be molecularly adsorbed on the new Ga layer without an activation energy. On the other hand, the adsorption of this $GaAs_2$ on the Ga-stabilized surface gives a new As layer and the remaining Ga atom migrates on the surface to make a new Ga layer. The mechanism involving the dissociative adsorption of As_2 studied previously and the presently proposed mechanism involving the $GaAs_2$ intermediate cluster are compared and it is concluded that the present mechanism is more favorable than the previous one. We summarize the overall reaction mechanism of the GaAs epitaxial crystal growth by the Ga atomic and As_2 molecular beams.

1. Introduction

The mechanism of GaAs crystal growth in molecular beam epitaxy (MBE) has been studied extensively by both experimental and theoretical methods. Arthur, Foxon, Joys and others investigated the adsorption mechanisms of the As_2 and As_4 clusters on the GaAs surface [1-3]. The mechanism of the As_2 adsorption they proposed is as follows: the As_2 molecule reaches the GaAs surface and is adsorbed and migrates as a precursor species. This precursor dissociates into two As atoms at an active Ga site, making the Ga-As bond with the surface Ga atom and the crystal grows. However, since this argument is based on the reaction rate theory and since this reaction has not been observed explicitly by an experimental technique, the details of the actual crystal growth mechanism are not yet known. In particular, we have to clarify what is the precursor species and the role of the active Ga site. If the molecularly adsorbed As_2 does not arrive at the active Ga site, it may be desorbed from the surface as As_2 or As_4 cluster.

The crystal growth mechanism in the metal-organic MBE (MOMBE) has been studied theoretically using small cluster models, but there are very few reports about the growth mechanism of the GaAs crystal in the MBE [4-9]. In our previous report, the reactions of the As_2 beam on the Ga-stabilized GaAs(100) surface have been studied by the cluster model combined with the *ab-initio* method [10]. It was clarified that the As_2 molecule irradiated on the surface is molecularly adsorbed on a flat surface and at the step site with the energy barriers of 23.5 kcal/mol and 9.6 kcal/mol, respectively, and migrates on the surface.

As_2 (beam) + Ga (surface) → As_2 (adsorbed) + Ga (surface)

The dissociative adsorption does not occur on a flat surface but occurs on a step site with the energy barrier of 16.9 kcal/mol and with an appreciable stabilization energy.

As_2 (adsorbed) → 2 As (surface)

In MBE, the GaAs surface is heated up at about 600 K for generating free Ga atom on the surface whose life time is about 0.1 second and it is said that this species

plays an important role in the crystal growth, though the actual reaction of the free Ga atom and its product remain to be clarified. In the present study, we examine the role of the free Ga atom in the crystal growth mechanism, assuming the following reaction steps.

(step 1) The As_2 beam reaches on the surface, reacts with the free Ga atom on the surface and gives a $GaAs_2$ cluster.

$$Ga + As_2 \rightarrow GaAs_2$$

(step 2) The $GaAs_2$ cluster thus generated reacts with the GaAs surface and leads to the crystal growth. There are two possibilities: the Ga site of the $GaAs_2$ cluster reacts with the As-stabilized surface or the As site of the $GaAs_2$ cluster reacts with the Ga-stabilized surface.

$$GaAs_2 + As\ (surface) \rightarrow reaction \rightarrow new\ GaAs\ surface$$

or

$$GaAs_2 + Ga\ (surface) \rightarrow reaction \rightarrow new\ GaAs\ surface$$

In the following section, we explain the details of the computational method. In Section 3, the reaction of As_2 with free Ga atom (step 1) is examined and in Sections 4 and 5, the above two reactions in step 2 are studied. Throughout the calculations, the GaAs surface is simulated by the small cluster model.

2. Computational method

Fig 1 shows $Ga_5As_4H_{11}$ and $Ga_8As_8H_{18}$ clusters which simulate the As-stabilized and Ga-stabilized GaAs (100) surfaces, respectively. The $GaAs_2$ molecule approaches and reacts with the cluster in two alternative ways shown in Fig 1, which are discussed in Sections 4 and 5, respectively. The Ga and As atoms are located at the crystal lattice whose lattice constant is 5.654 Å [11]. The H atoms cap the artificial dangling bonds of the Ga_5As_4 and Ga_8As_8 clusters except for the surfaces. The covalent bonding crystal has often been simulated by the cluster model whose dangling bonds are capped by hydrogen atoms [12-14]. The Ga-H and As-H lengths are fixed to 1.663 and 1.511 Å, respectively, which are the bond lengths of the free GaH and AsH_3

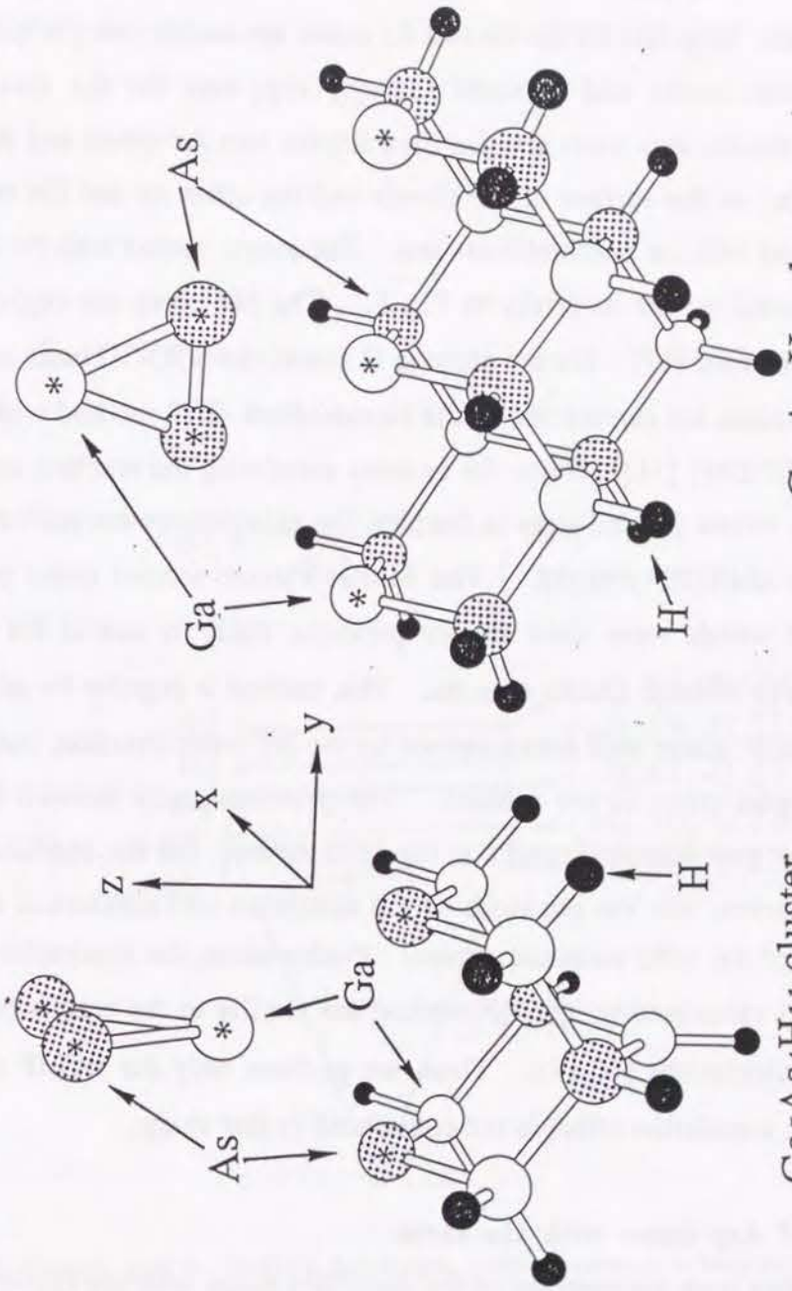

Figure 1. $Ga_5As_4H_{11}$ and $Ga_8As_8H_{18}$ clusters interacting with $GaAs_2$. The atoms indicated by the asterisks are treated with the double zeta basis and the others are with minimal basis.

molecules, respectively [15].

The Gaussian basis sets for the Ga and As atoms are double zeta (3s3p)/[2s2p] sets for the important atoms and minimal (3s3p)/[1s1p] sets for the less important atoms[17]; the double zeta basis sets are used for the two As atoms and for the three Ga atoms located on the surface of the cluster and the other As and Ga atoms of the cluster are treated with the minimal basis sets. The atoms treated with the double zeta basis are indicated by the asterisks in Fig 1. The Ne cores are replaced by the effective core potential [17]. For the capping H atoms, the STO-3G basis is used [18].

All calculations are carried out by the Hartree-Fock (HF) method with the use of the program HONDO7 [16]. Since the systems simulating the reaction steps 1 and 2 include $GaAs_2$ whose ground state is doublet, the calculations are performed by the Roothaan open-shell HF method. The Møller-Plesset second order perturbation (MP2) method which were used in our previous study is useful for estimating correlation energy of large cluster systems. This method is popular for calculating of closed-shell singlet states well approximated by the HF wave function, but the use for doublet and triplet states is not general. The previous study showed that the HF method does not give identical results as the MP2 method, but the implications of the HF potential curves, like the positions of the minimum and maximum, are roughly equal to those of the MP2 potential curves. Furthermore, the results for the $GaAs_2$ cluster and As_2 calculated by the HF method are similar to the results of the multi-reference CI calculations [10,19]. Then, we perform only the ROHF method and further electron correlation effect is not considered in this study.

3. Reaction of As_2 beam with Ga atom

We calculate here the reaction of the $As_2(^1\Sigma^+)$ beam with the $Ga(^2P)$ atom as a beam or on the surface using the double zeta basis set for the Ga and As atoms. The reaction path, which is assumed to keep the C_{2v} symmetry, and the Mulliken gross charge of the Ga and As atoms are shown in Fig 2. At point 1, the As-As bond length

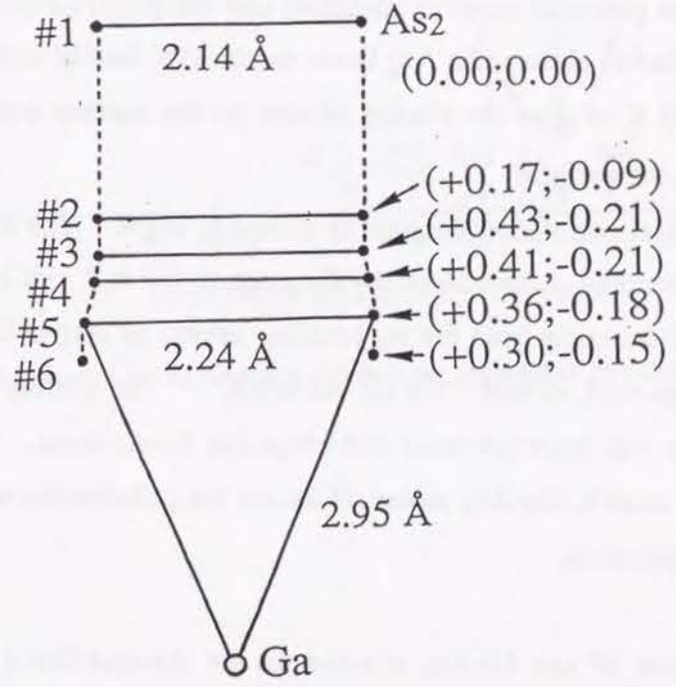

Figure 2. Reaction path for the Ga + As_2 system, which is assumed to keep the C_{2v} symmetry. The values in the left and right-hand sides in the parentheses show the gross charges of the Ga and As atoms, respectively.

is kept to 2.14 Å which is the optimized value for the free As_2 molecule. The potential curve along the reaction path is shown in Fig 3. The As_2 cluster approaches the Ga atom without energy barrier and reaches the equilibrium at point 5. The calculated heat of formation of the $GaAs_2$ cluster is 18.9 kcal/mol. The optimized As-As length is 2.24 Å, which is slightly longer than 2.14 Å of the free As_2, and the optimized Ga-As length is 2.95 Å. These values are very similar to the values reported by Balasubramanian: the As-As length 2.2 Å, the Ga-As length 2.85 Å, and the heat of formation, 30.3 kcal/mol [19]. At point 5, the charges of the Ga and As atoms are +0.36 and -0.18, respectively; 0.36 electron is transferred from Ga atom to As_2.

Since the potential curve is attractive and the potential minimum is deep enough to keep the $GaAs_2$ cluster, the As_2 beam reacts with the Ga atom on the GaAs surface heated at 600 K to give the $GaAs_2$ cluster on the surface and this cluster does not dissociate on the surface.

The orbital correlation diagram is shown in Fig 4. The electron donation from the singly occupied p_y orbital of the Ga atom to the π_z^* anti-bonding orbital of As_2 and the back donation from the π_z bonding orbital of As_2 to the p_z orbital of the Ga atom are important to make the Ga-As bond. The doubly occupied π_x bonding orbital of the As_2 does not react and keeps the As-As bond. The electron donation from the Ga atom to the As_2 molecule causes the polarization of the $GaAs_2$ cluster as the reaction proceeds.

4. Adsorption of the $GaAs_2$ cluster on an As-stabilized GaAs surface

The approach of the $GaAs_2$ cluster onto the As-stabilized GaAs surface is simulated by the cluster model shown on the left-hand side of Fig 1. Fig 5 shows the different view of the reaction path and the electronic charges of the Ga and two As atoms. Throughout the reaction, the system is kept in C_{2v} symmetry and only the Ga and As atoms belonging to the $GaAs_2$ cluster are optimized with the $Ga_5As_4H_{11}$ cluster fixed. The geometry of the optimized reaction path is shown in Table I: the

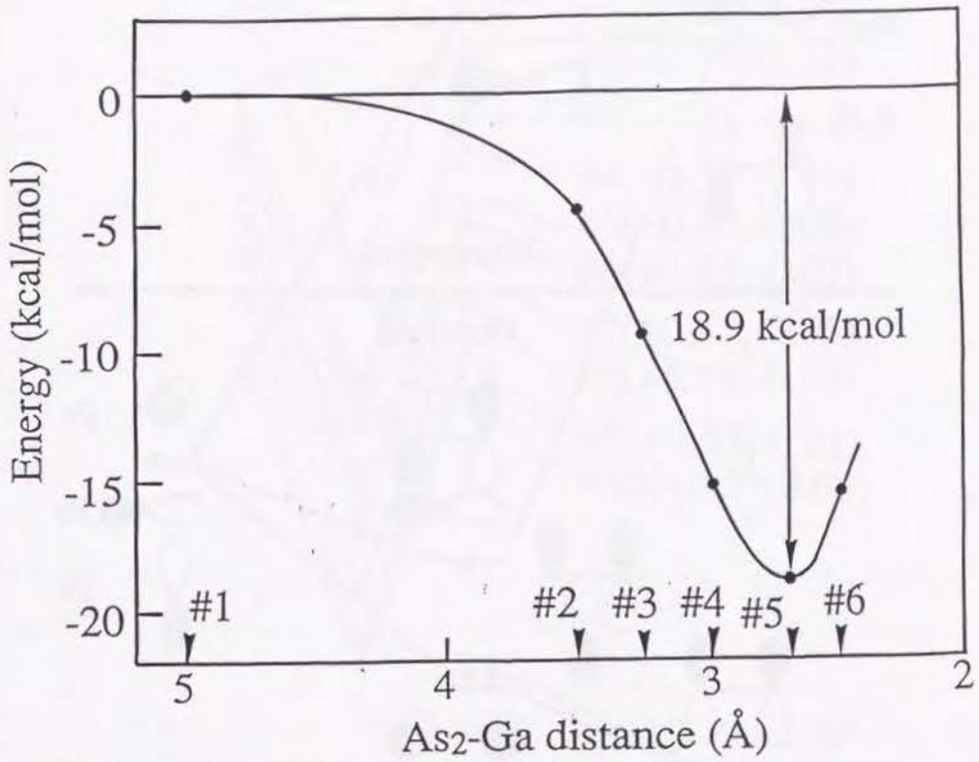

Figure 3. Potential curve for the Ga + As_2 system along the reaction path shown in Fig 2.

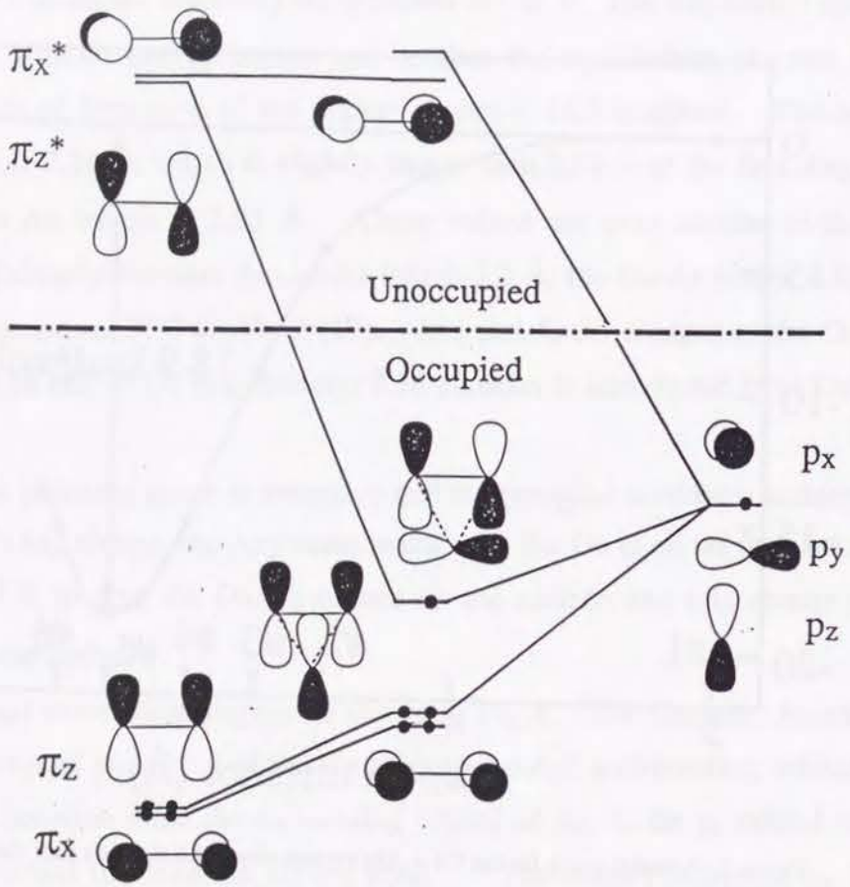

Figure 4. Orbital correlation diagram for the Ga +As_2 system .

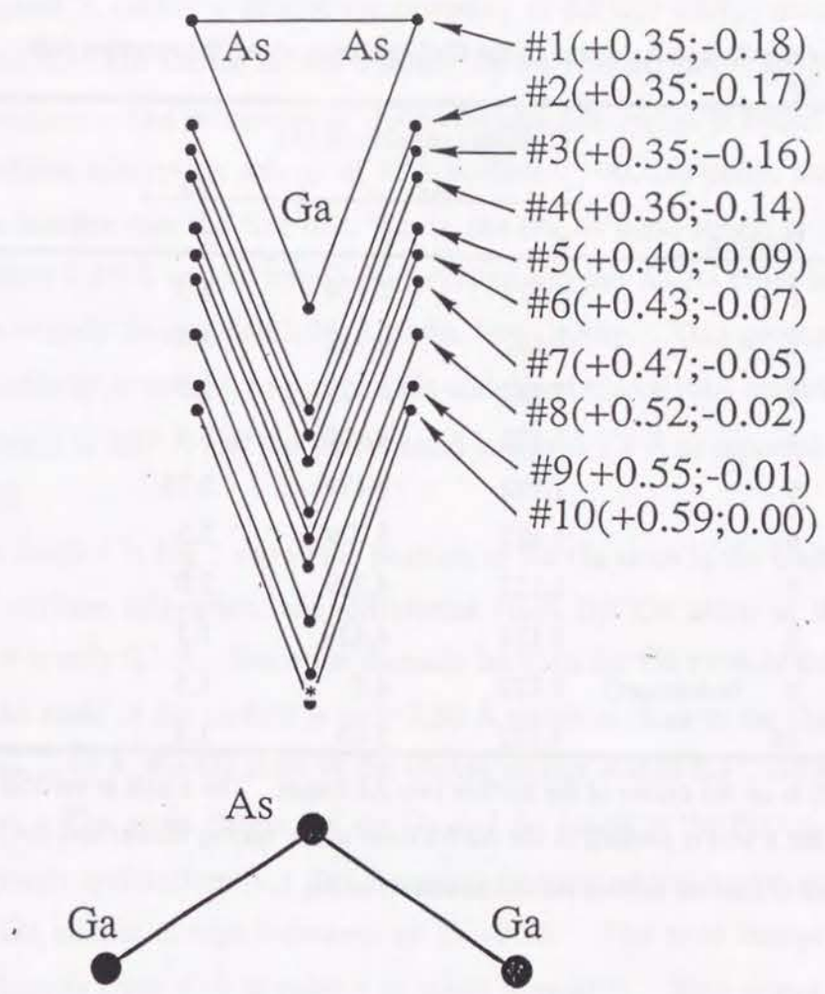

Figure 5. Reaction path for the $GaAs_2$ adsorption on a As-stabilized GaAs(100) surface with keeping the C_{2v} symmetry. The values in the left and right-hand sides of the parentheses are the charges of the Ga and As atoms, respectively. The asterisk indicates the position of the Ga atom in the GaAs crystal lattice without surface relaxation.

Table I
Geometries of the Ga and As atoms of the $GaAs_2$ cluster along the reaction path shown in Fig 5.[a]

	Cartesian coordinate (Å)		
	As		Ga
Position	x	z	z
1	1.122	7.729	5.0
2	1.122	6.729	4.0
3	1.122	6.229	3.5
4	1.122	5.729	3.0
5	1.122	5.479	2.75
6	1.122	5.229	2.5
7	1.122	4.729	2.0
8	1.122	4.429	1.7
9 (minimum)	1.122	4.0	1.5
10	1.122	3.65	1.3

[a] Point (0,0,0) is on the center of the surface two As atoms. The z axis is vertical to the surface , the x axis is pararell to the As-As bond of the $GaAs_2$ cluster and the y axis is pararell to the two surface As atoms shown in Fig 1.

accuracy is within 0.1 Å. The potential curve along the path is shown in Fig 6.

At point 1, $GaAs_2$ is kept at the geometry of the free $GaAs_2$ molecule optimized in Section 3. The $GaAs_2$ cluster approaches the surface and is adsorbed without an energy barrier. The minimum of the molecular adsorption is found at point 9 with the calculated adsorption energy of 68.8 kcal/mol. At this point, the $GaAs_2$ cluster becomes smaller than the free one, that is, the Ga-As bond length is 2.55 Å which is shorter than 2.95 Å of the free $GaAs_2$ cluster and the As-As bond length is 2.22 Å which is slightly longer than 2.24 Å of the free $GaAs_2$. This geometry is similar to the molecularly adsorbed As_2 on the Ga-stabilized GaAs(100) surface for which the Ga-As length is 2.55 Å and the As-As bond length is 2.4 Å as reported in our previous study [10].

The asterisk in Fig 5 shows the position of the Ga atom in the GaAs crystal lattice without surface relaxation: the difference from the Ga atom at the equilibrium position 9 is only 0.1 Å. Since the distance between the Ga atom of the $GaAs_2$ cluster and the As atom of the surface is only 2.50 Å which is close to the Ga-As distance in the crystal, 2.45 Å, the Ga atom of the $GaAs_2$ cluster makes the bond with the surface As atoms. The gross charges of the Ga and As atoms in the $GaAs_2$ cluster change monotonously and uniformly. The As atoms become neutral as the reaction proceeds and the Ga atomic charge increases up to +0.55. The total charge of the $GaAs_2$ cluster changes from +0.0 at point 1 to +0.53 at point 9. This shows the occurrence of the electron donation from $GaAs_2$ to the surface in the course of the adsorption.

The $GaAs_2$ cluster is adsorbed on the GaAs surface without energy barrier. The Ga-As bond of the $GaAs_2$ cluster becomes weak and the Ga atom is put onto the lattice site of the GaAs crystal : the two As atoms of the $GaAs_2$ cluster become molecularly adsorbed As_2 on the surface. Namely, the $GaAs_2$ adsorption gives a new Ga surface on the As-stabilized surface and a molecularly adsorbed As_2 species.

$GaAs_2 + As\ (surface) \rightarrow Ga\ (surface) + As_2\ (adsorbed)$

This reaction has no energy barrier and therefore this mechanism is more favorable than the direct adsorption of As_2 whose energy barrier is 23.5 kcal/mol for a flat

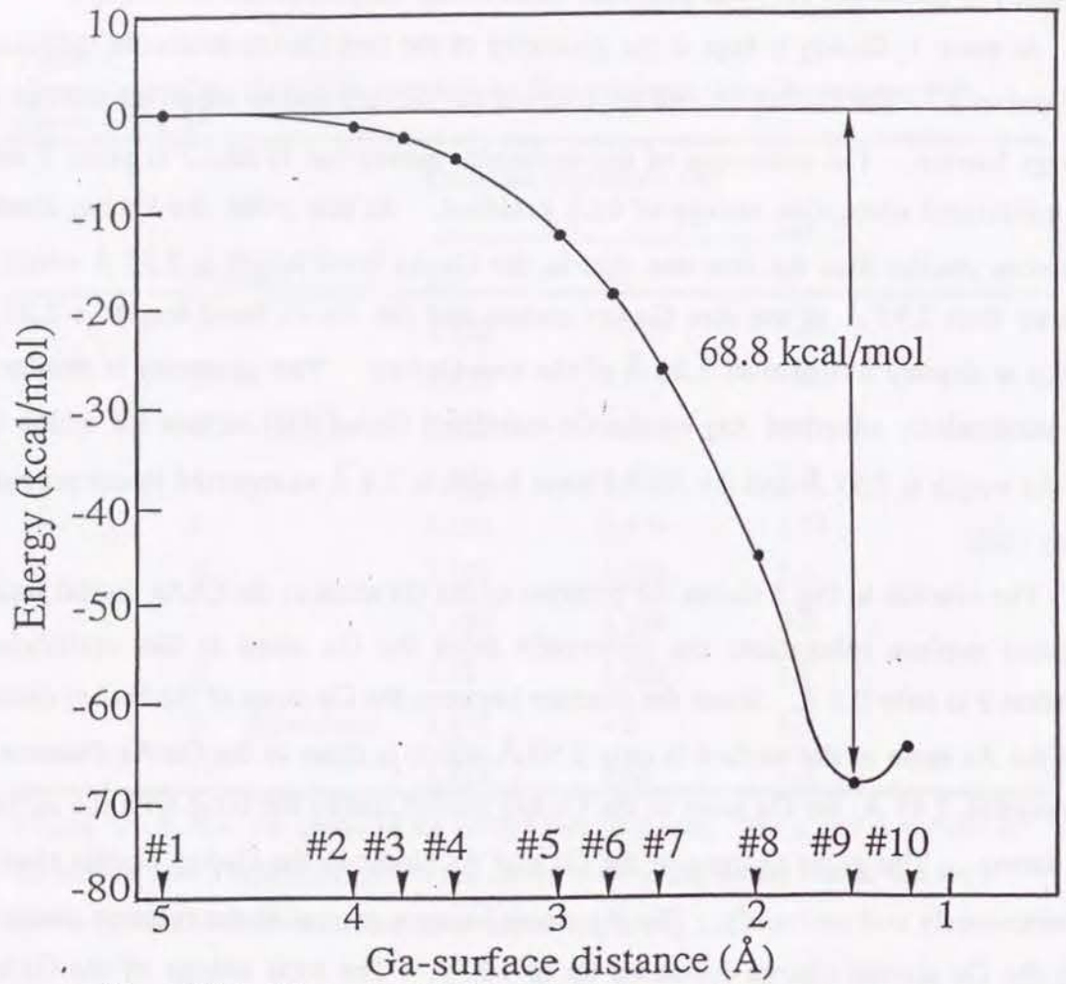

Figure 6. Potential curve for the $GaAs_2$ adsorption on a As-stabilized GaAs surface along the reaction path shown in Fig 5.

GaAs surface and 9.6 kcal/mol for a step site as shown in the previous paper [10]. Through the formation of the intermediate $GaAs_2$ cluster, the As_2 beam gives molecular adsorption of As_2 without activation energy. Furthermore, as shown in the previous paper [10], this molecularly adsorbed As_2 on a Ga surface is dissociated with 16.9 kcal/mol at its step site: thus a new As surface is generated again on the Ga surface, and the reaction cycle is closed.

As_2 (adsorbed) + Ga (surface) → As (surface)

This cyclic generation of the similar As (surface) as in the above equation is an essential aspect of the crystal growth.

The adsorption mechanism of the $GaAs_2$ cluster is qualitatively explained by the orbital correlation diagram shown in Fig 7. Orbitals playing a role in the reaction are the highest occupied molecular orbital (HOMO) , lowest unoccupied molecular orbital (LUMO) and their neighboring orbitals which correspond to the dangling bonds localized on the two surface As atoms. Only two surface As atoms and the orbitals localized on them are displayed in Fig 7. The electron donation from the A_1 orbital of the $GaAs_2$ cluster to the LUMO of the GaAs surface facilitates the adsorption and makes the Ga-As bond of the $GaAs_2$ cluster weak, causing the total charge of the adsorbed $GaAs_2$ cluster to increase from +0.0 to +0.53. The other B_1 and A_2 orbitals of the $GaAs_2$ cluster are not active in this reaction and keep the Ga-As and As-As bond of the $GaAs_2$ cluster. The occupied orbitals, B_2, A_2, B_1, and A_1 orbitals of the surface are also not activated. The electron donation from $GaAs_2$ to the surface occurs smoothly, so that this reaction does not require any activation energy. The gross charge of the As atom of the adsorbed $GaAs_2$ cluster is -0.01 which is similar to the values of the molecularly adsorbed As_2 which are previously reported to be -0.11 for the adsorption on a flat Ga-stabilized surface and -0.03 for the adsorption on a step site of the GaAs crystal [10].

5. Adsorption of the $GaAs_2$ cluster on a Ga-stabilized GaAs surface

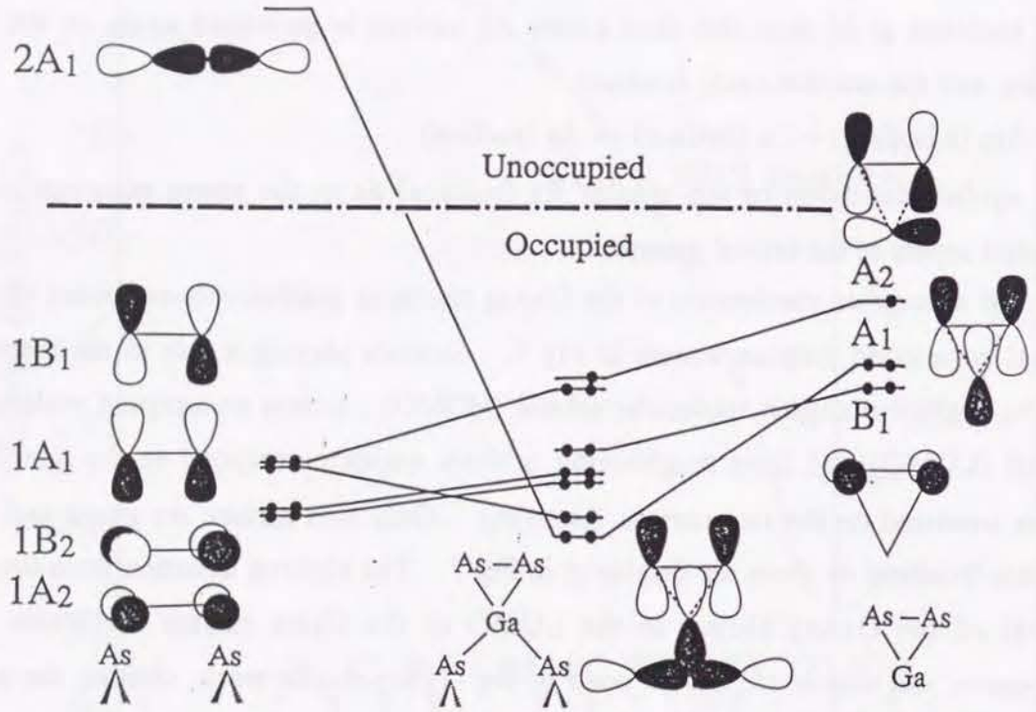

Figure 7. Orbital correlation diagram for the reaction of the $Ga_5As_4H_{11}$ + $GaAs_2$ system. Since the orbitals of the $Ga_5As_4H_{11}$ cluster localize on the surface As atoms, only the two As atoms are displayed.

The As-stabilized GaAs(100) surface is simulated by the $Ga_8As_8H_{18}$ cluster shown on the right-hand side of Fig 1. Throughout the reaction, the system is kept to C_{2v} symmetry and only the Ga and As atoms belonging to the $GaAs_2$ cluster are optimized with the $Ga_8As_8H_{18}$ cluster fixed. Fig 8 and Table II show the optimized reaction path : the accuracy is within 0.1 Å. The gross charges of the Ga and As atoms of the $GaAs_2$ cluster are shown at the left and right-hand sides, respectively, in the parentheses of Fig 8. The calculated potential curve along the path is shown in Fig 9.

The potential curve has two minima at points 8 and 12 and two maxima at points 4 and 9 : passing through the initial barrier at point 4, the $GaAs_2$ reaches the molecular adsorption state at point 8 and then going over the barrier at point 9 , it is dissociatively adsorbed at point 12. At point 1, the $GaAs_2$ cluster is kept to the geometry of the free $GaAs_2$ molecule. The $GaAs_2$ cluster is let to approach the surface horizontally and reach the first transition state at point 4 whose energy barrier is 4.8 kcal/mol. The molecular adsorption is found at point 8 with the adsorption energy of 48.4 kcal/mol. At this point, the As-As length is 2.4 Å, slightly longer than 2.24 Å of the free As_2, and the charges of the Ga and As atoms are +0.46 and -0.43, respectively. Beyond this point, the system reaches the second transition state at point 9: the energy barrier from the molecular adsorption state is only 3.3 kcal/mol. Finally, the As-As bond is dissociated completely and are adsorbed at point 12 with the adsorption energy of 86.8 kcal/mol. The optimized structure at point 12 is not identical with the GaAs lattice structure at point 12 which is indicated by the asterisks in Fig 6. The charges of the adsorbed Ga and As atoms are +0.46 and -0.66, respectively, and the latter is smaller than -0.48, the charge of the inner As atom of the crystal.

We show in Fig 10 the dissociatively adsorbed $GaAs_2$ cluster at point 12 on the left-hand side and the Ga adsorption site on a GaAs surface on the right-hand side. Since the Ga atom is adsorbed at the bridge site of the As-stabilized surface, the alignment of the As atoms along the y-axis gives the Ga adsorption site. On the other

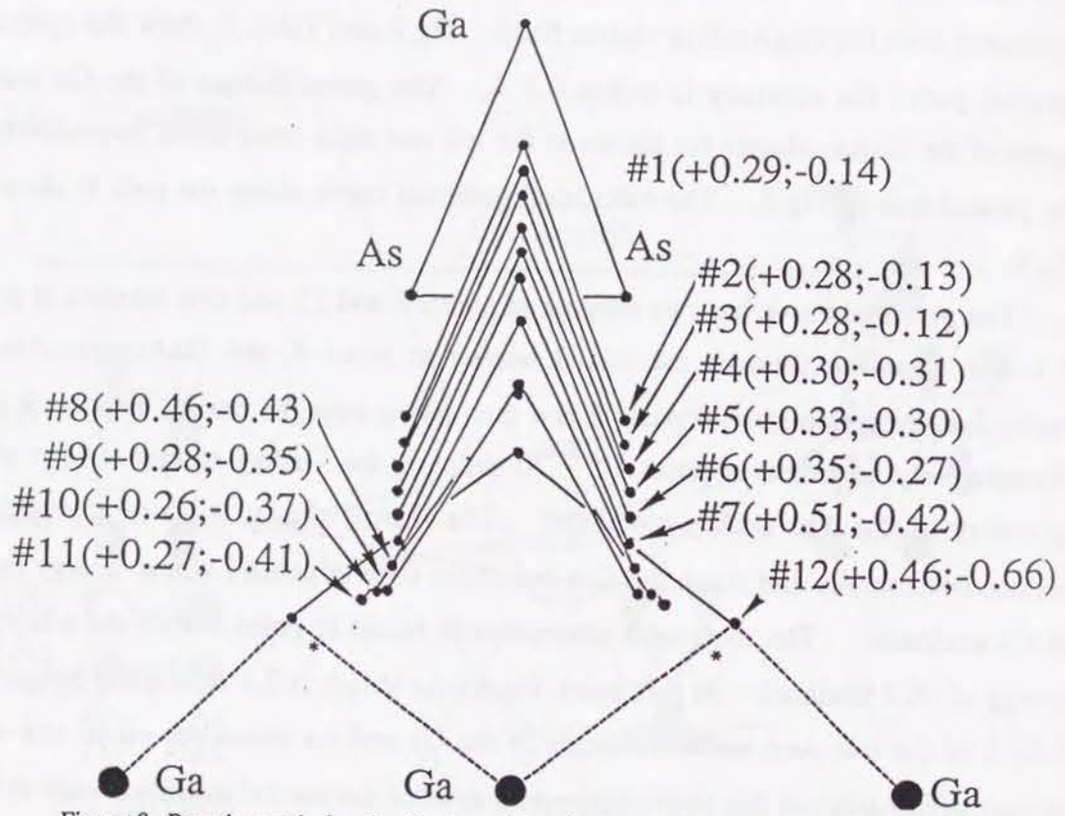

Figure 8. Reaction path for the $GaAs_2$ adsorption on a Ga-stabilized GaAs(100) surface with keeping the C_{2v} symmetry. The values in the left and right-hand sides of the parentheses are the charges of the Ga and As atoms, respectively. The two asterisks indicate the positions of the As atom in the GaAs crystal lattice without surface relaxation.

Table II
Geometries of the Ga and As atoms of the $GaAs_2$ cluster along the reaction path shown in Fig 8.[a]

		Cartesian coordinate (Å)		
		As		Ga
Position		y	z	z
1		1.122	5.0	7.729
2		1.122	3.75	6.479
3		1.122	3.5	6.229
4	(maximum)	1.15	3.25	5.979
5		1.15	3.0	5.729
6		1.15	2.75	5.479
7		1.15	2.5	5.229
8	(minimum)	1.2	2.25	4.77
9	(maximum)	1.25	2.0	4.12
10		1.35	2.0	4.1
11		1.5	1.9	4.0
12	(minimum)	2.2	1.7	3.429

[a] Point (0,0,0) is on the surface center Ga atom. The z axis is vertical to the surface and the y axis is pararell to the As-As bond of the $GaAs_2$ cluster shown in Fig 1.

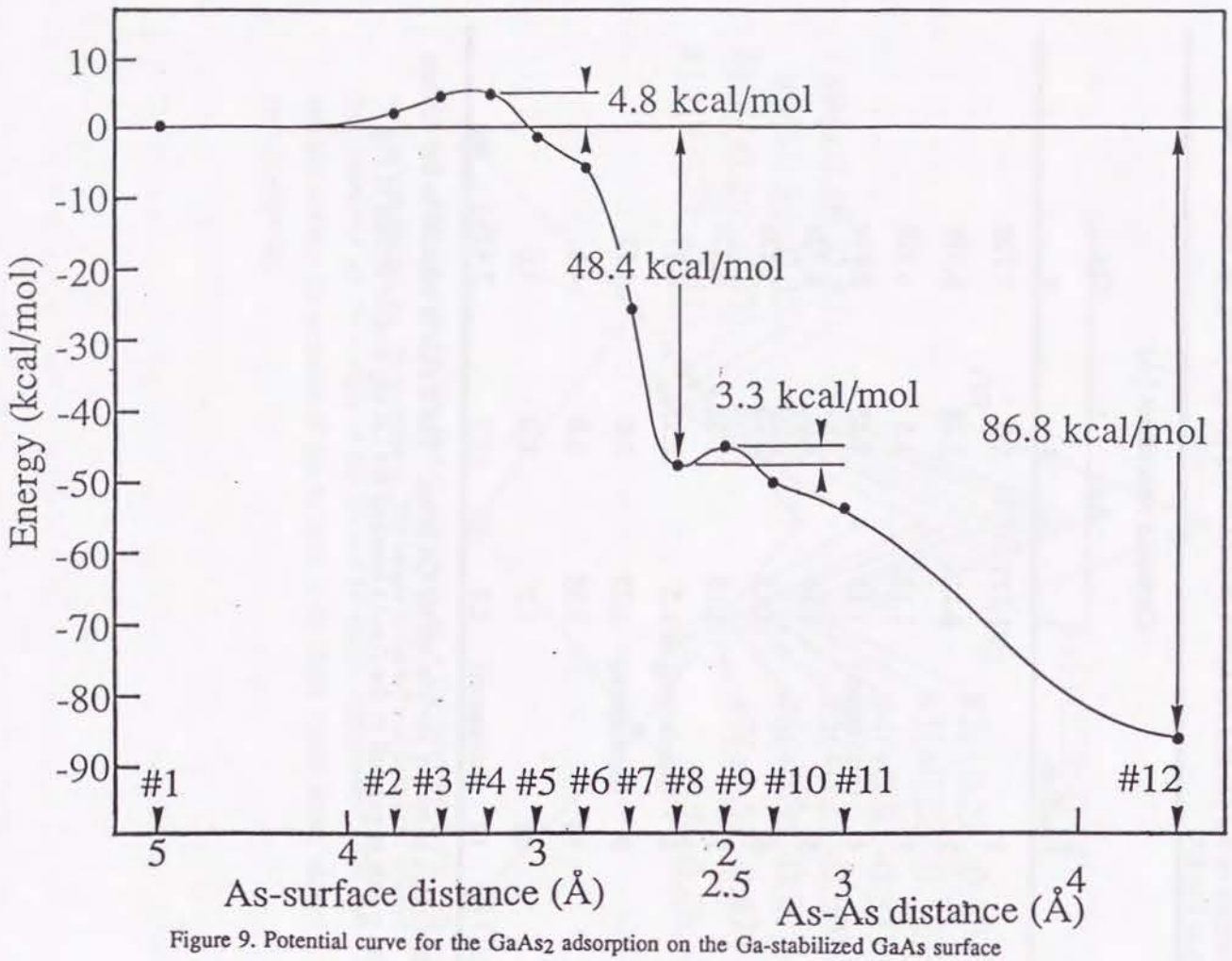

Figure 9. Potential curve for the $GaAs_2$ adsorption on the Ga-stabilized GaAs surface along the reaction path shown in Fig 8.

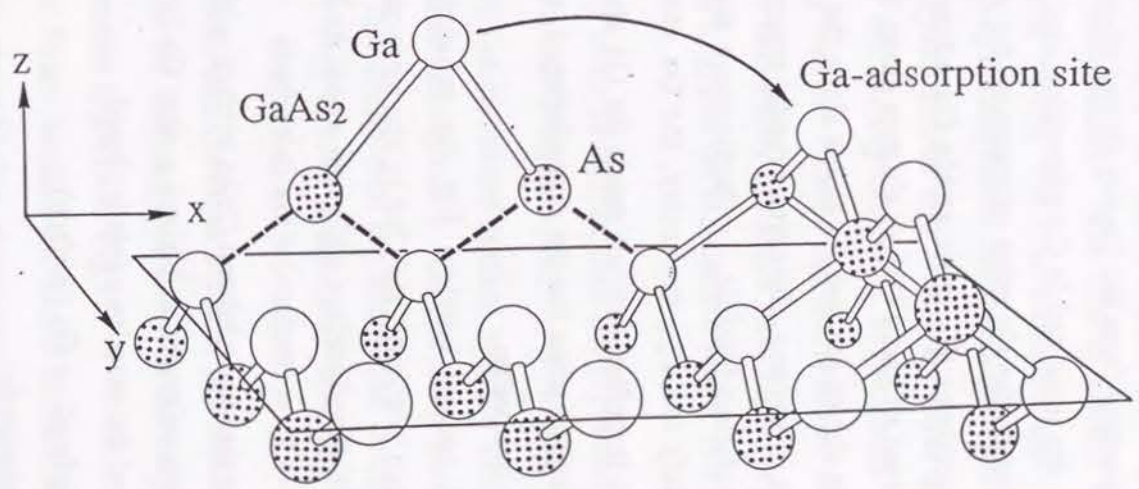

Figure 10. Adsorbed $GaAs_2$ cluster (left-hand side) and Ga-adsorption site (rigth-hand side) on a GaAs surface. The filled and empty circles represent As and Ga atoms, respectively. The adsorbed $GaAs_2$ is located at the optimized geometry (point 12) of Figure 8 and the arrow represents a migration path of the Ga atom.

hand, the alignment of the As atoms along the x-axis does not give the Ga adsorption site. Comparing Fig 10 with the $Ga_8As_8H_{18}$ cluster shown in Fig 1, it is shown that the $Ga_8As_8H_{18}$ cluster is too small as a surface to give the Ga adsorption site. Since the adsorbed As atoms originating from the $GaAs_2$ cluster aligns along the x-axis, the Ga atom on them is not at the most stable Ga-adsorption site. Therefore, after the adsorption of the $GaAs_2$ cluster, the Ga atom migrates on the surface as indicated by an arrow in Fig 10 and occupies the most stable Ga adsorption site. Another possibility is the coadsorptions of many $GaAs_2$ clusters along the y-axis and the shift of the Ga atom at the bridge site of the two As atoms along the x-axis, giving another empty Ga site opposite to it. Anyway, the cluster model representing this reaction is too large to make the calculation feasible. Furthermore since the present model cluster is restricted to satisfy the C_{2v} symmetry, the Ga atom of $GaAs_2$ must be located on the C_2 axis and therefore can not reach the Ga site of the GaAs crystal lattice. The calculated energy barrier for the dissociation, i. e. 3.3 kcal/mol, would therefore be larger than the true value.

Since the calculated energy barriers for the molecular and dissociative adsorptions are less than five kcal/mol, the $GaAs_2$ cluster would be easily adsorbed and dissociated on the Ga-stabilized surface and gives a new As layer.

$GaAs_2$ + Ga (surface) → 2 As (surface) + Ga (adsorbed)

The Ga atom is adsorbed on the As-stabilized GaAs surface without activation energy [4]. The adsorbed Ga atom migrates and gives a new Ga layer: the Ga-stabilized surface is again generated and the reaction cycle is closed.

Ga (adsorbed) + As (surface) → Ga (surface)

Thus, the crystal grows continuously.

6. Conclusion and remarks

The activation energies calculated here are less than 5 kcal/mol and the reactions examined are all allowed. Without the restriction of the C_{2v} symmetry, we may expect lower activation energies, but the orbital correlation diagram indicates the

preference of the C_{2v} symmetry. We therefore expect that the relaxation of the C_{2v} restriction would not change much the calculated results.

We propose in this paper the GaAs crystal growth mechanism involving the $GaAs_2$ cluster as an intermediate. The cluster $GaAs_2$ is easily formed from As_2 molecular and Ga atomic beams, and it is stable enough on a heated GaAs surface. The reaction of the $GaAs_2$ cluster on the As-stabilized surface occurs easily and the Ga atom is put into the crystal lattice and a new Ga layer grows on the As-stabilized surface. The As_2 of the $GaAs_2$ cluster is molecularly adsorbed on this new Ga surface without energy barrier. Likewise, the reaction of the $GaAs_2$ cluster on the Ga-stabilized surface occurs easily too and a new As layer grows on the Ga-stabilized surface. The Ga atom migrates on the surface and a new Ga layer grows on the As-stabilized surface.

This mechanism is more favorable than the previously studied direct adsorption mechanism of As_2 on a GaAs surface [10]. Previously, we have shown that As_2 is hardly adsorbed on the Ga-stabilized surface and the dissociative adsorption is less stable than the molecular adsorption. On the other hand, at the step site, the As_2 molecular adsorption can occur with the activation energy of 9.6 kcal/mol and the molecularly adsorbed As_2 cluster dissociates with the activation energy of 16.9 kcal/mol.

Based on the present and previous studies, the mechanism of the GaAs crystal growth using the Ga atomic and As_2 molecular beams may be summarized as follows and a qualitative illustration is given in Fig 11.

(1) The As_2 molecular beam reaches the GaAs surface and reacts with the free Ga atom or atomic beam to create $GaAs_2$ cluster without activation energy. This species is stable on the surface.

Ga + As_2 → $GaAs_2$ (activation energy = 0 kcal/mol)

(2) The $GaAs_2$ cluster is molecularly adsorbed on the As-stabilized surface without energy barrier and a new Ga layer grows: the Ga atom of the $GaAs_2$ is put onto the crystal lattice and the As_2 of the $GaAs_2$ is molecularly adsorbed on it.

$GaAs_2$ + As (surface) → As_2 (adsorbed) + Ga (surface)

(activation energy = 0 kcal/mol)

(3) The $GaAs_2$ cluster is molecularly adsorbed on the Ga-stabilized surface with the energy barrier of 4.8 kcal/mol and a new As layer grows. The Ga atom of the $GaAs_2$ migrates on the surface and is adsorbed on the As-stabilized surface.

$GaAs_2$ + Ga (surface) → 2 As (surface) + Ga (adsorbed)

Ga (adsorbed) + As (surface) → Ga (surface)

(activation energy = 4.8 kcal/mol)

(4) On the other hand, the direct adsorption path also exists, though it is less favorable than the above ones. Namely the As_2 cluster of the beam is molecularly adsorbed directly on the flat surface or at the step site of the Ga-stabilized surface with the activation energy of 23.5 kcal/mol or 9.6 kcal/mol, respectively.

As_2 + Ga (surface) → As_2 (adsorbed) + Ga (surface)

(activation energy = 9.6 kcal/mol for step site, 23.5 kcal/mol for flat surface)

(5) The molecularly adsorbed As_2 given in the steps (2) and (4) dissociates thermally with the activation energy of 16.9 kcal/mol, and a new As layer grows on the Ga-stabilized surface.

As_2 (adsorbed) → 2 As (surface) (activation energy = 16.9 kcal/mol)

This step is the rate-determining step in the crystal growth reactions.

The reaction cycles (1) → (2) → (5) and (1) → (3) are closed, giving new As-stabilized and Ga-stabilized GaAs surfaces, respectively. Since the previous study showed that the Ga atom is adsorbed on the As stabilized GaAs surface without energy barrier and gives a new Ga layer on the surface [4], the reaction cycle (4) → (5) and the following Ga beam radiation is also closed and gives the As-stabilized and Ga-stabilized GaAs surface alternatively. However, the last cycle is less favorable because it involves the step (4). In conclusion, we propose the reaction cycles (1) → (2) → (5) and (1) → (3) as the crystal growth mechanism of the GaAs crystal.

Finally, it must be noted that the reaction steps examined in the present and previous studies represent only one possibility for the reactions on the GaAs surface

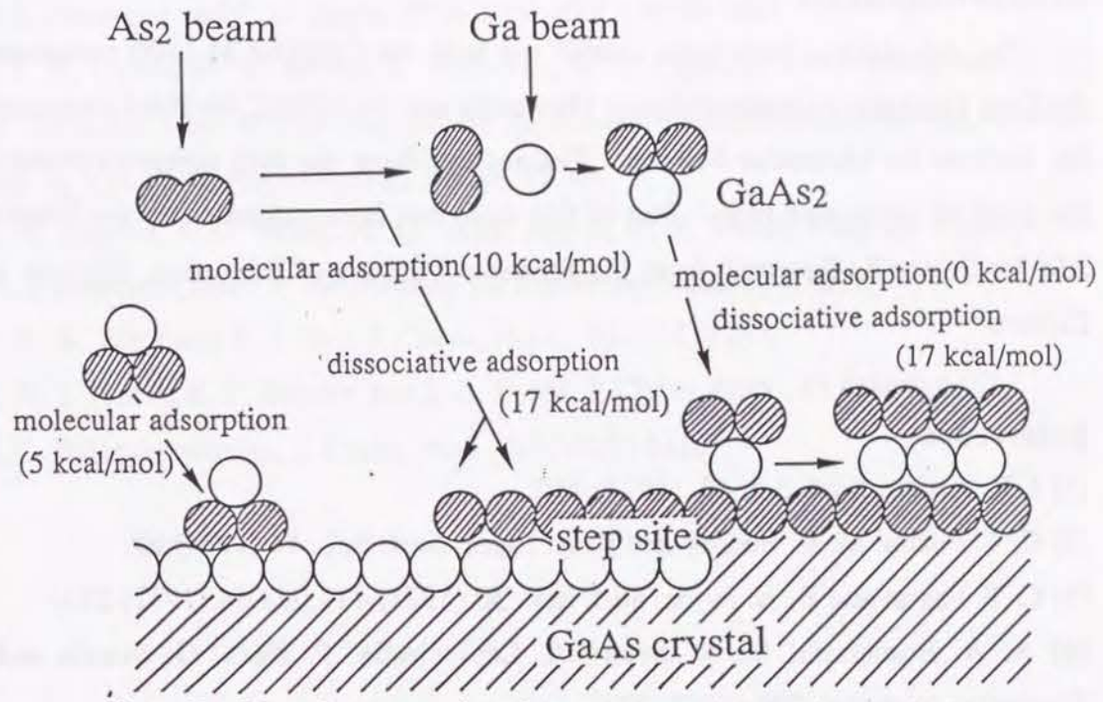

Figure 11. Schematic representation of the crystal growth mechanisms by the As_2 beam epitaxy method. Only the most probable reactions are displayed. The hatched and empty circles represent As and Ga atoms, respectively. The value in the parentheses shows the energy barrier for each reaction.

and another reactions may also be assumed; e.g. coadsorption is not examined in this study. However, the coadsorption of two As_4 clusters is believed to occur when the As_4 cluster beam is irradiated on the GaAs surface This is the subject of our forth coming article.

Acknowledgements

The calculations have been carried out with the FACOM M-1800 computer at the Data Processing Center of Kyoto University and the HITAC M-680H computer at the Institute for Molecular Science. The authors thank the IMS computer center for the grant of computing time. Part of this study has been supported by the Grant-in-Aid for Scientific Research from the Japanese Ministry of Education, Science, and Culture.

Referrence

[1] J. R. Arthur, Surf. Sci. 43, (1974) 449.

[2] C. T. Foxon, M. R. Boudry and B. A. Joyce, Surf. Sci. 44 (1974) 69.

[3] C. T. Foxon and B. A. Joyce, Surf. Sci. 50 (1975) 434,*ibid* 64 (1977) 293.

[4] A. A. Bonapasta, M. R. Bruni, A. Lapiccirella, P. Nota, G. Scavia and N. Tomassini, Surf. Sci. 204 (1988) 273.

[5] M. Tsuda, S. Oikawa, M. Morishita and M. Mashita, Jpn. J. Appl. Phys., 26.(1987) L564.

[6] A. Doi, Y. Aoyagi and S. Namba, Appl. Phys. Lett. 48.(1986) 1787; 49 (1986) 785.

[7] T. Ohno, Phys. Rev. B44, (1991) 6306.

[8] R. M. Graves and G. E. Scuseria, J. Chem. Phys., 95 (1991) 6602.

[9] K. Balasubramanian, J. Chem. Phys., 87 (1987) 3518.

[10] Y. Fukunishi and H. Nakatsuji, Surf. Sci., submitted.

[11] K. H. Hellwege, W. Pies, A. Weiss: Crystal Structure Data of Inorganic Compounds, Landolt-Börnstein, New Series, Group III, Vol. 7 (Springer-Verlag, Berlin, 1979).

[12] L. C. Snyder and Z. Wasserman, Surf. Sci., 71 (1978) 407; 77 (1987)52.

[13] A. C. Kenton and M. W. Ribarsky, Phys. Rev. B23 (1981) 2897 .

[14] K. Hermann and P. S. Bagus, Phys. Rev. B20 (1979) 1603.

[15] J. H. Callomon, E. Hirota, K. Kuchitsu, W. J. Lafferty, A. G. Maki, and C. S. Pote: Structure Data of Free Polyatomic Molecules, Landolt-Börnstein, New Series, Group II, Vol 7 (Springer-Verlag, Berlin, 1976).

[16] M. Dupuis, J. D. Watts, H. O. Villar and G. H. B. Hurst, Program Libraly No. 1501, Computer Center of the Institute for Molecular Science, (1987).

[17] W. R. Wadt and P. J. Hay, J. Chem. Phys., 82 (1985) 284.

[18] W. J. Hehre, R. F. Stewart and J. A. Pople, J. Chem. Phys., 51 (1969) 2567.

[19] K. Balasubramanian, J. Chem. Phys., 86 (1987) 3410.

Chapter 3

Cluster model study on GaAs epitaxial crystal growth by arsenic molecular beam. III. As4 molecular beam.

Abstract

We study the mechanism of the GaAs epitaxial crystal growth by the As_4 cluster beam on Ga-stabilized GaAs (100) surface using the cluster model and the Hartree-Fock and Møller-Plesset second-order perturbation method. When the As_4 beam is irradiated on the surface, the As_4 cluster is adsorbed at a step site of the GaAs surface and the two adsorbed As_4 clusters give the coadsorption state which gives a new As-layer with releasing an As_4 cluster into vacuum: four atoms of the two As_4 clusters are dissociatively adsorbed on the surface to give a new As-layer and the other four As atoms are released into vacuum as an As_4 cluster. This reaction was experimentally proposed previously and is confirmed here. Furthermore, we suggest a possibility of the reaction by a single As_4 cluster: a single As_4 is adsorbed at a step site, two As atoms of it are dissociatively adsorbed on the surface to give a new As-layer and the other two As atoms are released into vacuum as an As_2 molecule. We summarize the overall reaction mechanism of the GaAs epitaxial crystal growth by the As_4 beam.

1. Introduction

In this series of articles, we investigate the mechanism of GaAs epitaxial crystal growth by ab-initio quantum chemical method based on the cluster model. In the first paper of this series, we have studied the molecular and dissociative adsorption of As_2 on the GaAs surface and the site effect of the surface is clarified [1]. In the second paper, we studied the crystal growth mechanism through the formation of the intermediate $GaAs_2$ cluster [2]. In these studies we assumed to use the As_2 molecular beam, but the reaction mechanism is different, depending on the cluster size in the molecular beam. Actually, much more defects are observed in the GaAs crystal produced by the As_4 beam than in that produced by using the As_2 beam, however it is difficult to explain the causes and the types of the defects [3]. Then, in the present study, we study the mechanism of the epitaxial crystal growth assuming the use of the As_4 cluster beam. We examine the epitaxial growth mechanisms involving single As_4 cluster and two As_4 clusters proposed by experiments [4,5].

It was found that at temperatures 300-450 K As_4 is physically adsorbed with an adsorption energy of 0.38 ± 0.03 eV (8.8 kcal/mol) and the surface migration energy barrier of 0.24 eV (5.5 kcal/mol)[3,4]. At an active Ga site, the molecularly adsorbed species is dissociated and a new As layer grows on the surface. Above the temperature 600 K As_2 is lost from the surface by dissociation from the GaAs surface, but this loss is supplied by the As_4 cluster beam irradiated on the surface. When two As_4 clusters migrating on the surface collide with each other, they may make a coadsorption state. The coadsorption state is decomposed into four dissociatively adsorbed As atoms and an As_4 cluster which is released into vacuum. This mechanism involves two As_4 clusters but one As_4 remains finally, and therefore the sticking coefficient is always less than 0.5.

In addition to the reaction model of Foxon and Joyce derived experimentally, several reaction mechanisms have been proposed for the GaAs crystal growth. For example $(GaAs)_n$ cluster generation as an intermediate in a gas phase was proposed by

Frolov et. al.[6] and the surface reaction of the adsorbed As_4 with a free Ga atom on the surface was proposed by Lays et.al. [7] and Nishijima et.al. [8].

The structures of the As_2, As_4 and small GaAs clusters have been studied by ab-initio molecular orbital method [9-15], but their reactivities have not yet been reported except for the As hydride [16-18].

In this study, we first examine the energetics for the following dissociation combination reactions,

$$As_4\ (gas) \leftrightarrow 2\ As_2\ (gas) \qquad (1)$$

in order to confirm the independence between the mechanism involving the As_4 cluster beam studied here and that involving the As_2 molecular beam previously studied.[1,2] In the previous study [2] we showed that the As_2 cluster reacts with a free Ga atom existing on the surface to give a $GaAs_2$ cluster which is an important intermediate for the crystal growth. We examine here the possibility of the following similar reaction involving the As_4 cluster.

$$As_4\ (gas) + Ga\ (gas) \rightarrow GaAs_4\ (gas) \qquad (2)$$

We then investigate the roles of the As_4 cluster in the following two types of the crystal growth reaction.

(i) The surface reaction involving a single As_4 cluster: an As_4 cluster reaches the Ga-stabilized GaAs surface and is molecularly adsorbed.

$$As_4\ (gas) + Ga\ (surface) \rightarrow As_4\ (adsorbed) + Ga\ (surface) \qquad (3)$$

Then the molecularly adsorbed As_4 is dissociated into two As atoms dissociatively adsorbed on the surface to make a new As layer, and the other two As atoms desorb from the surface as an As_2 molecule.

$$As_4\ (adsorbed) \rightarrow 2\ As\ (surface) + As_2\ (gas) \qquad (4)$$

Two possibilities in these reactions are examined: the As_4 cluster reacts at a flat surface and at a step site.

(ii) The surface reaction involving two As_4 clusters: two As_4 clusters are adsorbed on the Ga-stabilized GaAs surface or the two adsorbed As_4 clusters migrate and form a coadsorption state.

$$2\ As_4\ (adsorbed) \rightarrow 2\ As_4\ (coadsorbed) \qquad (5)$$

Then the two adsorbed As_4 react to form an As_8 cluster, from which four As atoms are dissociatively adsorbed on the surface to make a new As-layer while the other four As atoms form an As_4 cluster and desorb from the surface.

$$2\ As_4\ (coadsorbed) \rightarrow 4\ As\ (surface) + As_4\ (gas) \qquad (6)$$

In the following section, we explain the details of the computational method. In section 3, the dissociation of As_4 into two As_2 (reaction (1)) is studied and in section 4, the reaction of As_4 with a free Ga atom (reaction (2)) is discussed. In sections 5 and 6, the reactions (3) and (4) and in section 7 the reactions (5) and (6) are discussed. In whole calculations, the GaAs surface is simulated by a small cluster model.

2. Computational method

We use the Hartree-Fock method followed by the Møller-Plesset second-order perturbation (MP2) method and the calculations are performed by the use of the program HONDO7 [19].

Fig 1 shows the $Ga_8As_8H_{18}$, $Ga_8As_{10}H_{20}$, and $Ga_8As_3H_{12}$ clusters which simulate the Ga-stabilized GaAs (100) surface, its step site for the adsorption of a single As_4 molecule and the Ga-stabilized GaAs (100) surface for the coadsorption of two As_4 molecules. These clusters are small to represent the surface, but the cluster beam experiments have shown that using the silicon cluster, the cluster size effect converges with respect to the ionization potential and electron affinity, when its size becomes larger than 10 atoms [20,21]. In this sense, the present cluster model is not too small to study the reaction mechanism.

A single As_4 molecule approaches and reacts with the $Ga_8As_8H_{18}$ and $Ga_8As_{10}H_{20}$ clusters which represent a flat and a stepped surface, respectively. Since the present cluster is small and the step edges are closed to each other, the latter model may also represent the ditch effect. These reactions are examined in sections 3 and 4. The reaction of two As_4 molecules with the $Ga_8As_3H_{12}$ cluster is studied in section 5 . The lattice constant of the Ga and As atoms in these clusters are 5.654 Å which is the

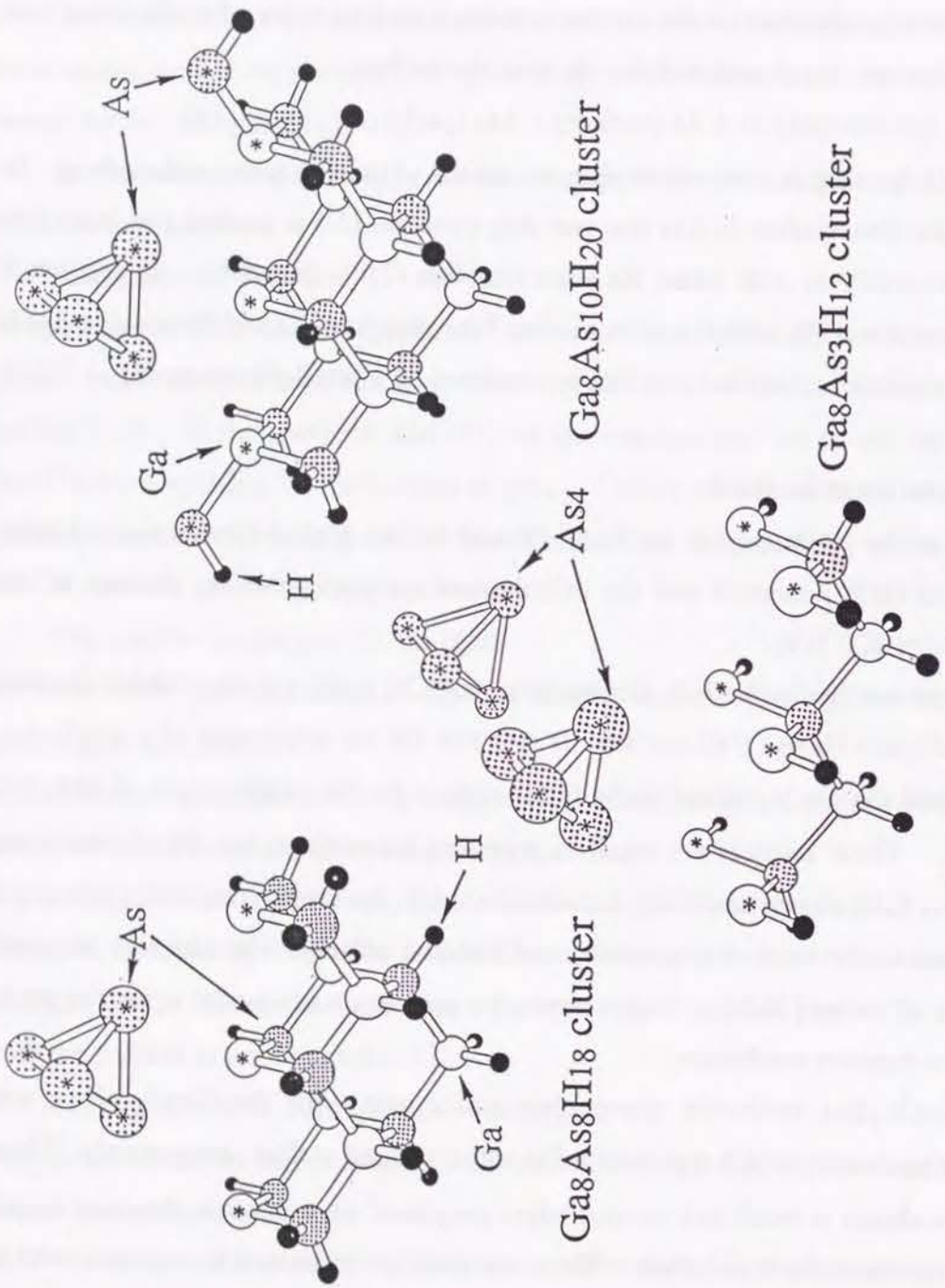

Figure 1. $Ga_8As_8H_{18}$ and $Ga_8As_{10}H_{20}$ clusters interacting with As_4, and $Ga_8As_3H_{12}$ cluster interacting with two As_4 clusters. The atoms marked by the asterisks are treated with the SZP basis and the others are with minimal basis.

value for the crystal [22]. The H atoms cover the artificial dangling bonds of the Ga_8As_8 and Ga_8As_3 clusters. A covalent bonding crystal is often simulated by the cluster model whose dangling bonds are covered by hydrogen atoms [23-25] and our previous study shows the usefulness of this model. The Ga-H and As-H bond lengths are fixed respectively to 1.663 and 1.511 Å which are the bond lengths in free GaH and AsH_3 molecules, respectively [26].

The Gaussian basis sets for the Ga and As atoms at the reaction center are the (3s3p)/[1s1p] minimal basis plus polarization d functions (zeta = 0.293 for As, zeta = 0.207 for Ga atom), and for the other atoms are the (3s3p)/[1s1p] minimal basis sets. For the capping H atoms, the STO-3G basis set is used [27]. The Ne cores of Ga and As atoms are replaced by the effective core potentials [28].

3. Dissociation of As_4 cluster into two As_2 molecules

At first we check the reliability of the basis set. The As_2 and As_4 clusters are optimized for the bond length within the HF method with several basis sets. The As_4 cluster is kept in a Td symmetry. The results are summarized in Table I. SZ stands for (3s3p)/[1s1p] basis, DZ (3s3p)/[2s2p], DZP (3s3p)/[2s2p] plus polarization d functions (zeta = 0.293), and SZP stands for SZ plus polarization d functions. All basis sets give longer bond lengths than the experimental values for both As_2 and As_4; the tendency is remarkable in the minimal basis set. The DZ basis gives the better value, but the heat of formation is not improved against the minimal basis set. The SZP basis gives the best value for the bond length of As_4 and reproduces the experimental heat of formation, though it does not give a good value for the bond length of As_2. Since the As_4 cluster is in Td symmetry, the As-As-As angle is only 60°, and then the polarization d functions are necessary for representing the As-As bond of As_4. These results show that the SZP basis is the best compromise for the present calculation.

The dissociation reaction of As_4 to two As_2 are examined assuming D_{2h} symmetry. Fig 2 shows the schematic reaction path and the explicit reaction path

Table I

Examination of the accuracy of several basis sets.

	SZ	DZ	SZP	DZP	Exptl
As_2 bond length	2.297	2.139	2.22	-	2.1026
As_4 bond length	2.7117	2.5795	2.5654	-	2.435
Heat of formation (kcal/mol) for 2 $As_2 \rightarrow As_4$					
Hartree-Fock	-35.93	-7.94	-60.10	-36.77	-54.1
MP2	-4.93	+3.55	-54.51	-46.38	

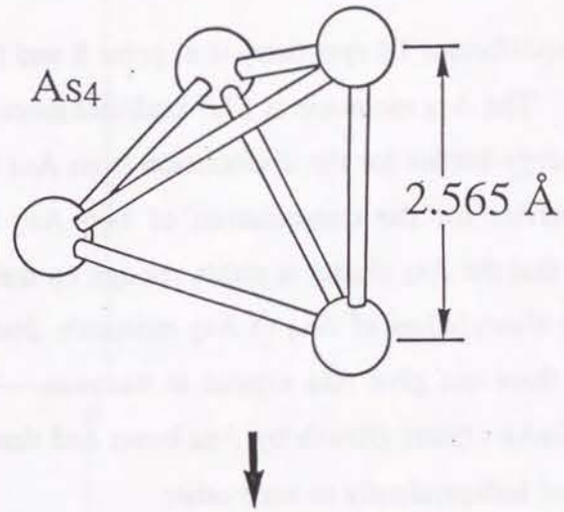

Figure 2. Schematic representation of the dissociative reaction path of As_4 to two As_2. The system is kept in D_{2h} symmetry.

shown in Fig 3 is optimized by the HF calculation whose accuracy is within 0.1 Å. The geometries are summarized in Table II. The potential curve along the path is shown in Fig 4, and the solid and broken lines stand for the results of the HF and MP2 methods, respectively. The potential curves by the MP2 and HF methods are similar to each other but the As-As bond length of the MP2 method is shorter than that of the HF method.

The As_4 cluster at the equilibrium Td symmetry is at point 8 and the two isolated As_2 molecules are at point 1. The As_4 molecule is 67.0 kcal/mol more stable than the two As_2 molecules. The energy barrier for the dissociation from As_4 to As_2 is 140.4 kcal/mol and the energy barrier for the combination of two As_2 to As_4 is 73.4 kcal/mol. This result shows that the As_4 cluster is stable enough on the surface heated at 600K. Furthermore, the dissociation of As_4 to As_2 molecule does not occur in vacuum and the As_2 beam does not give As_4 cluster in vacuum. Therefore, the reaction mechanism of the GaAs crystal growth by As_4 beam and that by As_2 beam previously reported are studied independently to each other.

4. Reaction of As_4 cluster with Ga atom

We first study the reaction between a Ga atom and an As_4 cluster. The As_4 cluster is kept in the Td symmetry and we examine three reaction paths shown in Fig 5 which correspond to the Ga adsorptions on the on-top, bridge and three-fold hollow site of the As_4 cluster. Throughout the reactions, the system is kept in C_3, C_{2v}, and C_3 symmetries, respectively and other lower symmetry paths are not examined. Since this is an open-shell system, the calculations are preformed by the Roothaan open-shell HF method and further electron correlations are not considered. The geometries of all the Ga and As atoms are optimized within the accuracy of 0.1 Å. Fig 6 shows the potential curves along the three paths depicted in Fig 5. At point 1, the As_4 cluster keeps the Td symmetry and the As-As bond length is 2.565 Å which is the value of the free As_4 molecule. Since all the potential curves are repulsive and do not give any bound state, the Ga atom and the As_4 cluster do not react to form

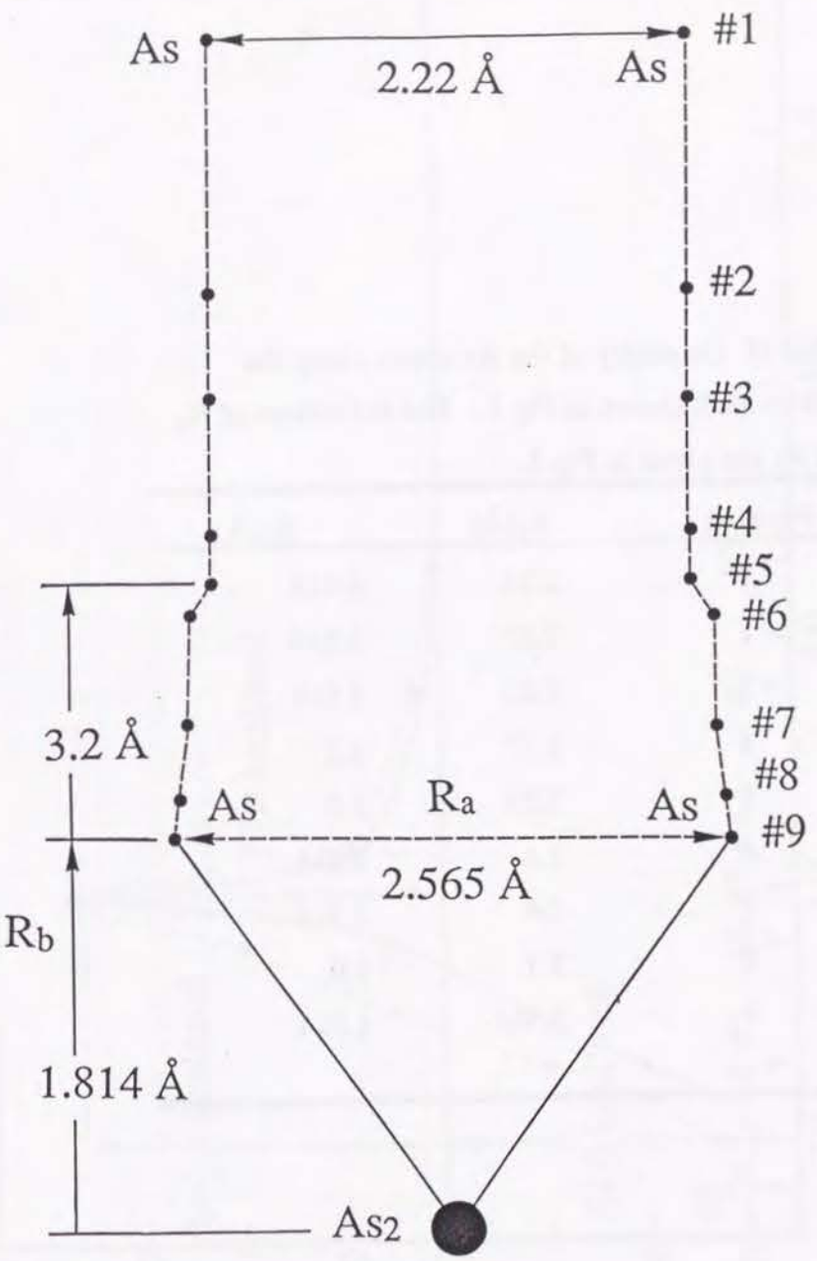

Figure 3. Reaction path for the As_4 dissociation to two As_2 molecules. This reaction path keeps C_{2v} symmetry. R_a stands for the distance between the two As atoms and R_b the distance between the two As_2 molecules.

Table II Geometry of the As atoms along the reaction path shown in Fig 3. The definitions of R_a and R_b are given in Fig 3.

Position	R_a(Å)	R_b(Å)
1	2.22	6.814
2	2.22	4.314
3	2.22	3.814
4	2.22	3.2
5	2.22	3.0
6	2.4	2.814
7	2.4	2.314
8	2.5	2.0
9	2.565	1.814

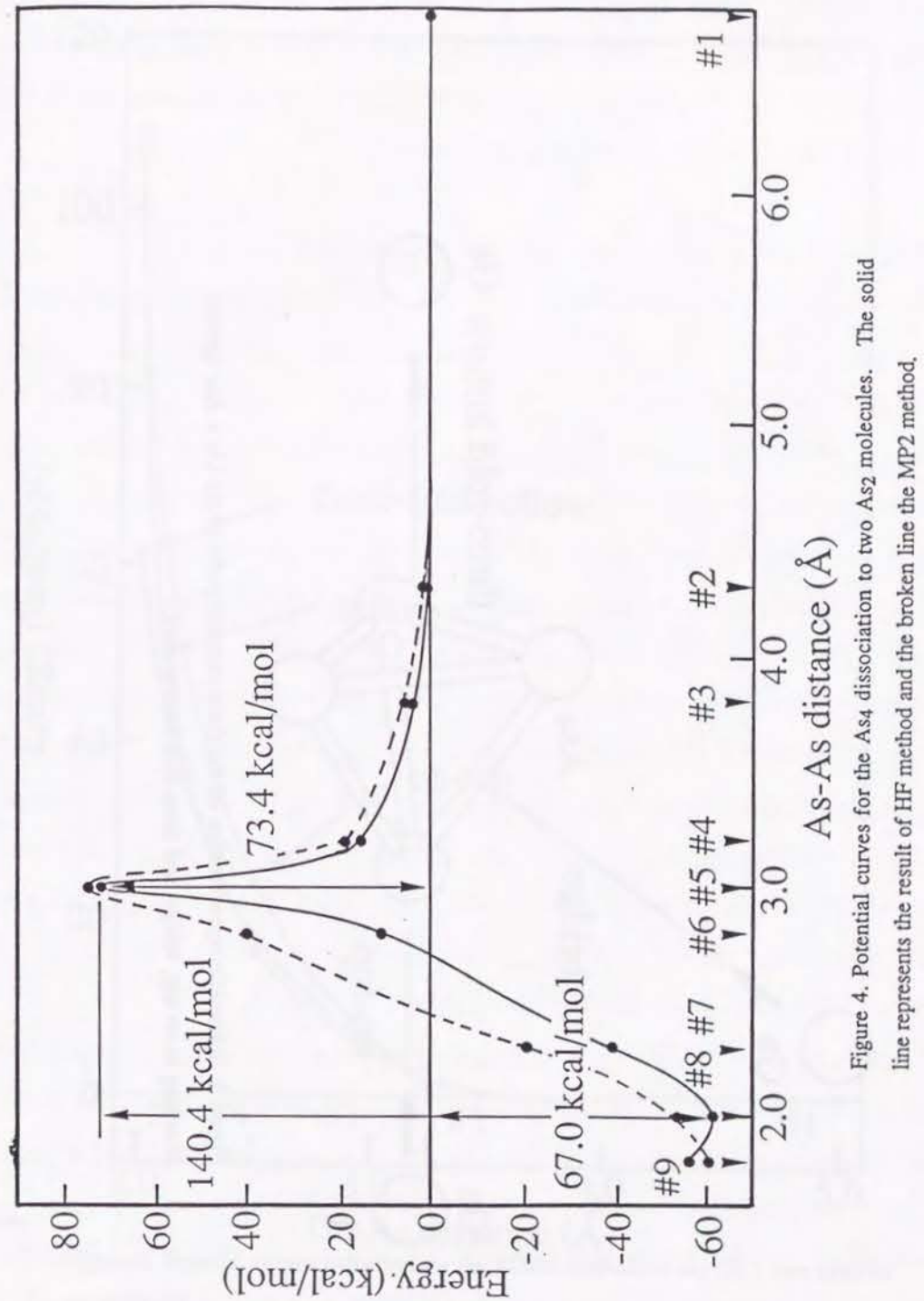

Figure 4. Potential curves for the As4 dissociation to two As2 molecules. The solid line represents the result of HF method and the broken line the MP2 method.

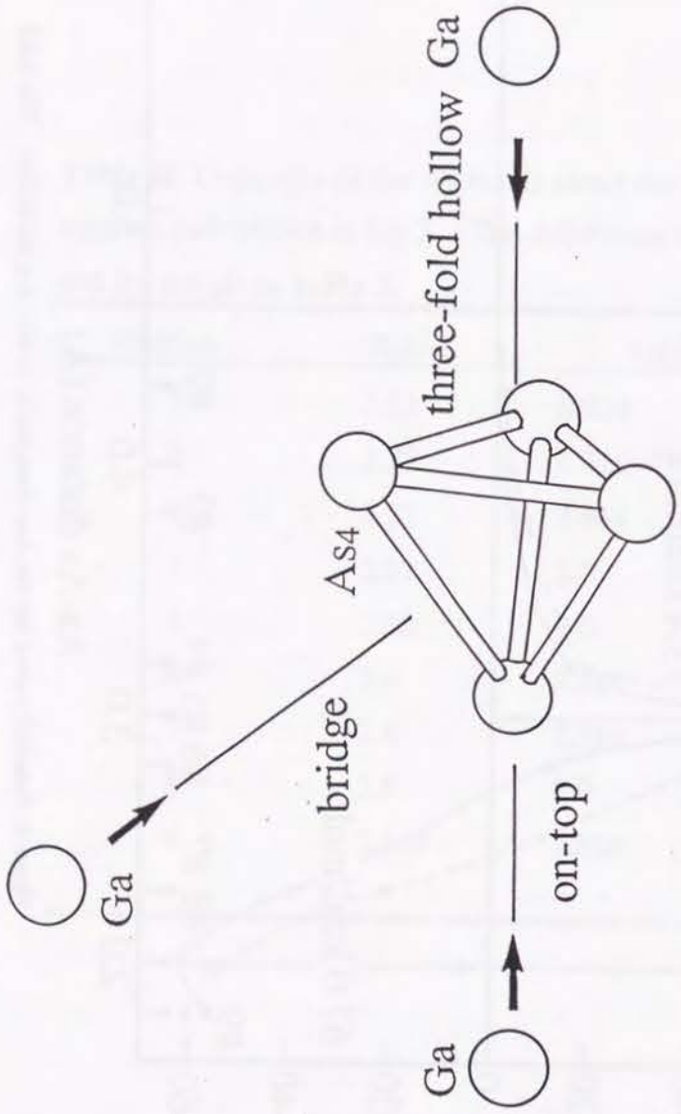

Figure 5. Schematic representation of the three reaction paths of the Ga + As4 system : attacking to on top, bridge, and three-fold hollow sites.

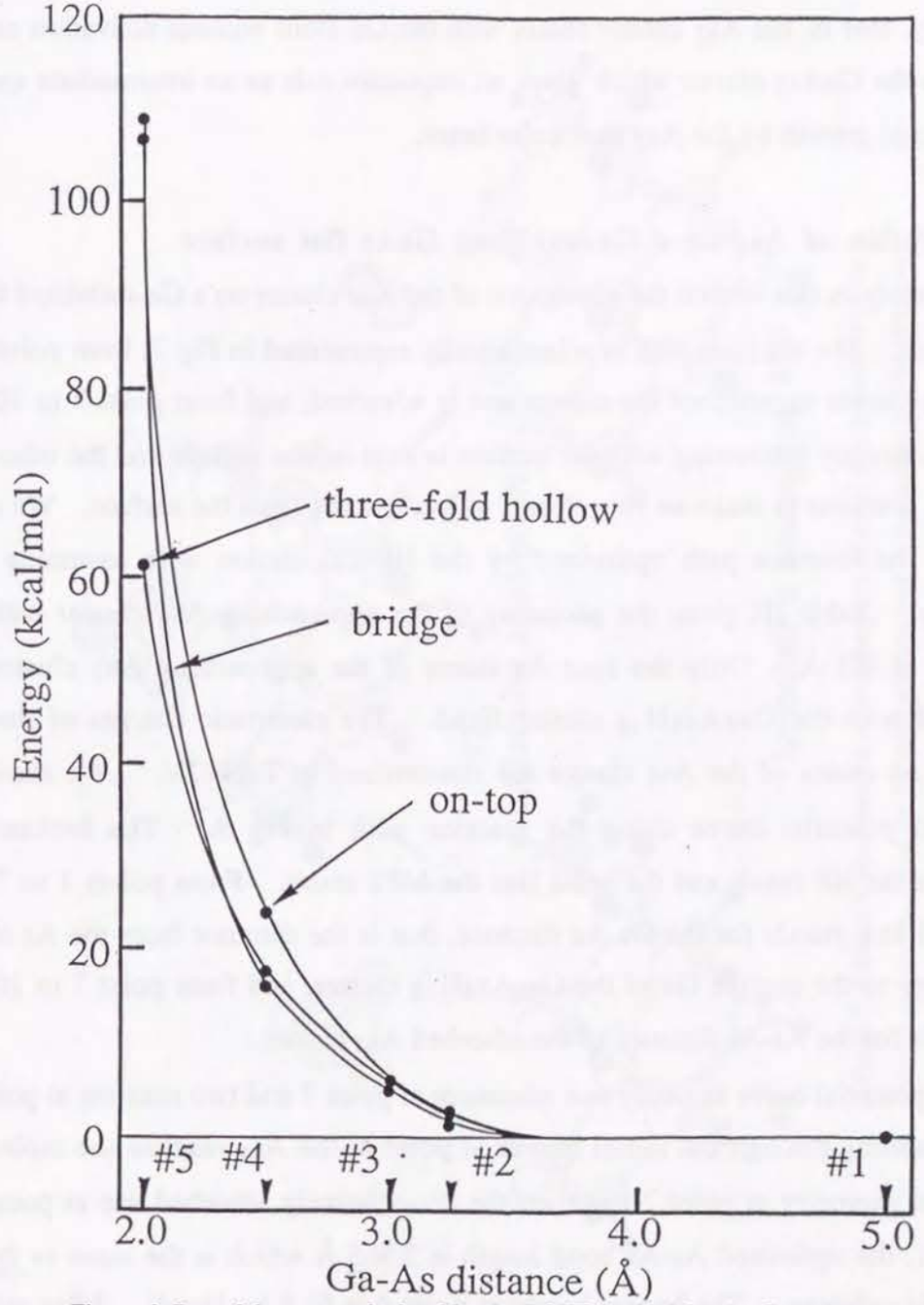

Figure 6. Potential curves calculated by the ROHF method for the Ga + As4 systems shown in Fig 5.

$GaAs_4$ cluster. This result is different from that for the As_2 cluster studied previously, that is, the As_2 cluster reacts with the Ga atom without activation energy and gives the $GaAs_2$ cluster which plays an important role as an intermediate species in the crystal growth by the As_2 molecular beam.

5. Adsorption of As_4 on a Ga-stabilized GaAs flat surface

We study in this section the adsorption of the As_4 cluster on a Ga-stabilized GaAs flat surface. The reaction path is schematically represented in Fig 7: from point 1 to 7 the As_4 cluster approaches the cluster and is adsorbed, and from point 7 to 10 two As atoms directly interacting with the surface is kept on the surface and the other two As atoms combine to make an As_2 cluster which desorbs from the surface. We show in Fig 8 the reaction path optimized by the HF calculation with assuming C_{2v} symmetry. Table III gives the geometry of the approaching As_4 cluster with the accuracy of 0.1 Å. Only the four As atoms of the approaching As_4 cluster are optimized with the $Ga_8As_8H_{18}$ cluster fixed. The electronic charges of the two different As atoms of the As_4 cluster are summarized in Table IV. We show the calculated potential curve along the reaction path in Fig 9. The broken line represents the HF result and the solid line the MP2 result. From points 1 to 7, the horizontal axis stands for the Ga-As distance, that is the distance from the As of the As_4 cluster to the surface Ga of the $Ga_8As_8H_{18}$ cluster, and from point 7 to 10, the axis stands for the As-As distance of the adsorbed As_4 cluster.

The potential curve has only one minimum at point 7 and two maxima at points 4 and 10: passing through the initial barrier at point 4, the As_4 reaches the molecular adsorption geometry at point 7 and then the dissociatively adsorbed one at point 10. At point 1, the optimized As-As bond length is 2.565 Å which is the same as that of the free As_4 cluster. The barrier height at point 4 is 61.5 kcal/mol. After passing this barrier, the As atoms become slightly negatively charged and the As_4 cluster is adsorbed keeping its tetrahedral form. The molecular adsorption corresponds to the geometry at point 7. At the HF level, the molecular adsorption state of As_4 is

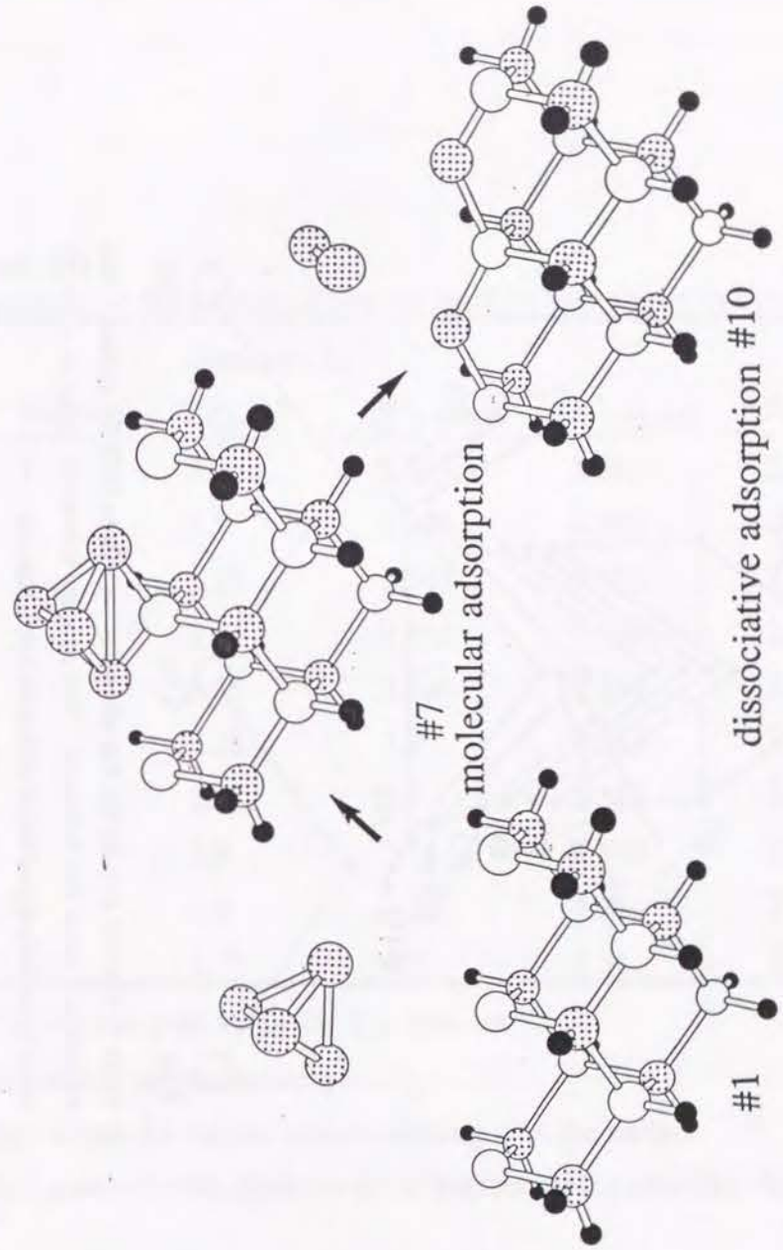

Figure 7. Schematic representation of the adsorption of As_4. As_4 is adsorbed on the cluster and two As atoms are dissociatively adsorbed on the surface and the other two As atoms are released into vacuum as As_2 molecule.

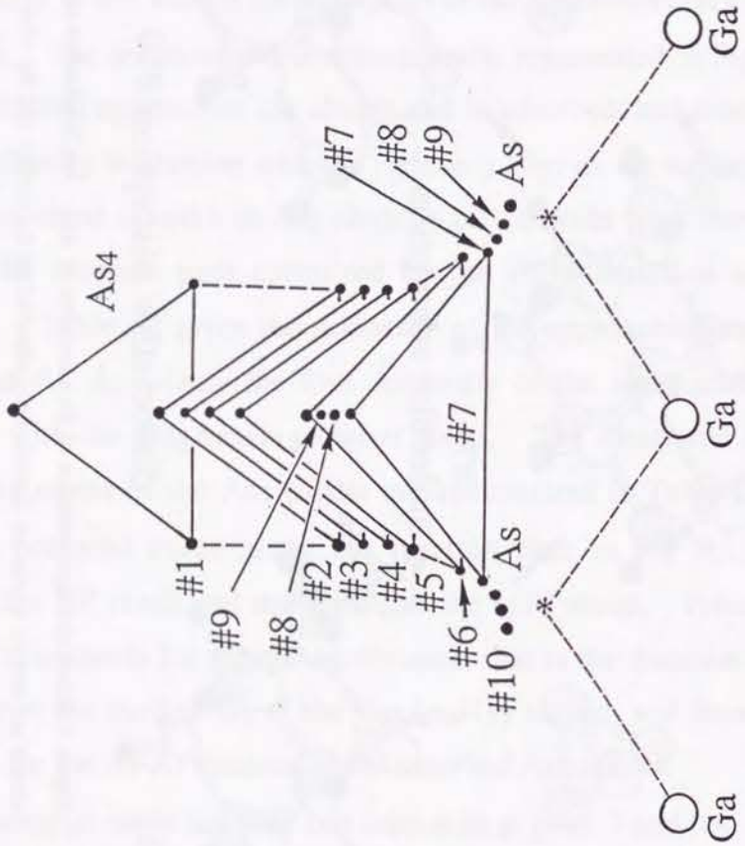

Figure 8. Reaction path for the As4 adsorption on a GaAs (100) flat surface. This reaction path keeps C_{2v} symmetry. Two asterisks indicate the positions of the As atoms in the GaAs crystal lattice without surface relaxation.

Table III
Geometry of the As atom along the reaction path shown in Fig 8[a].

	Distance (Å)			
Position	$R_{Ga\text{-}As}$[b]	$R^{c}_{As1\text{-}As1}$	$R^{d}_{As1\text{-}As2}$	$R_{As2\text{-}As2}$
1	5.0	2.565	2.565	2.565
2	3.5	2.565	2.565	2.565
3	3.25	2.565	2.565	2.565
4	3.0	2.565	2.565	2.565
5	2.75	2.6	2.528	2.56
6	2.25	3.2	2.513	2.50
7	2.0	3.3	2.513	2.44
8	1.9	3.74	2.860	2.40
9	1.8	4.16	2.981	2.30
10	1.77	4.3	5.555	2.22

[a] The reaction path keeps the C_{2v} symmetry.

[b] Distance to the Ga surface.

[c] As1 stands for the As atom contacting with the surface.

[d] As2 stands for the As atom at top position of the adsorbed As_4 cluster.

Table IV
Mulliken gross charges of the As atoms of the As_4 cluster along the reaction path shown in Fig 8.

	$Ga_8As_8H_{18}$ cluster		$Ga_8As_{10}H_{20}$ cluster	
Position	As^1	As^2	As^1	As^2
1	+0.04	-0.04	+0.01	-0.01
2	+0.06	-0.07	+0.02	-0.00
3	+0.07	-0.07	+0.04	+0.07
4	+0.04	-0.01	+0.04	+0.07
5	+0.03	-0.03	+0.03	+0.06
6	-0.12	-0.08	-0.18	+0.04
7	-0.20	-0.05	-0.22	+0.07
8	-0.26	-0.06	-0.25	+0.12
9	-0.37	-0.07	-0.30	+0.12
10	-0.56	0.00	-0.24	0.00

[1] As atoms directly contacting with the surface.

[2] Other As atoms which are finally released into vacuum.

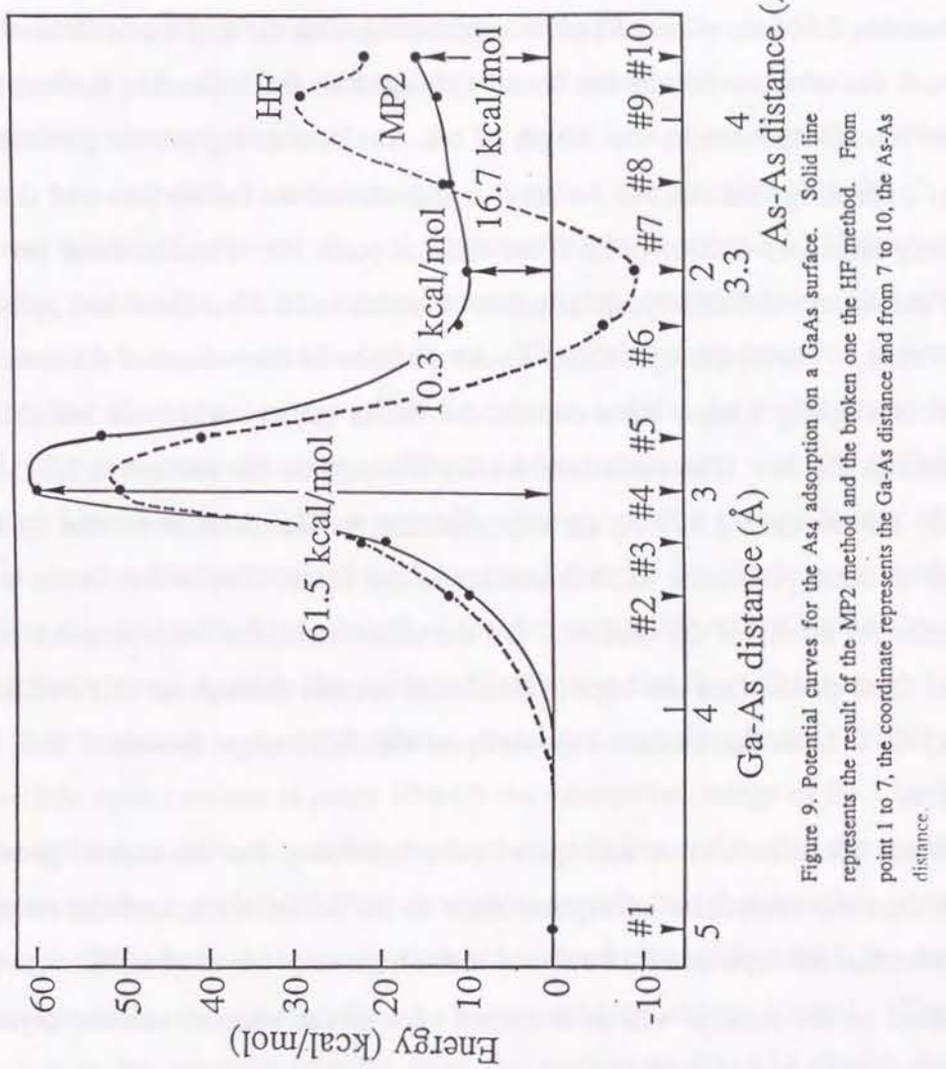

Figure 9. Potential curves for the As_4 adsorption on a GaAs surface. Solid line represents the result of the MP2 method and the broken one the HF method. From point 1 to 7, the coordinate represents the Ga-As distance and from 7 to 10, the As-As distance.

calculated to be stable relative to the initial state, but the consideration of the electron correlation reveals that the molecular adsorption energy is -10.3 kcal/mol, and therefore less stable than the initial state. The geometry is shown in Fig 8: the Ga-As length is 2.0 Å and the As-As length close to the surface is 3.3 Å, longer than that of the free As_4 2.565 Å. Two As atoms contacting with the surface become charged to -0.20 and the other two As atoms become charged to -0.05: the As_4 is charged by -0.5. As the reaction proceeds, the length of the As_2 contacting on the surface becomes longer indicating that this As-As bond is dissociated on the surface and their charges suddenly increase, -0.20 at point 7 but -0.56 at point 10. Finally, these two As atoms reach the dissociated adsorption at point 10 which is 16.7 kcal/mol less stable than the initial state. There, the optimized As-As distance of the adsorbed As atoms is 4.3 Å which is slightly longer than that in the GaAs crystal which is indicated by the asterisks in Fig 8. The optimized As-Ga distance on the surface is 2.71 Å which is slightly shorter than 2.827 Å, the experimental As-Ga distance for the crystal. The charge of these As atoms -0.56 is similar to the value -0.48 which is the average for the inner As atoms of the cluster. On the other hand, the other two As atoms more distant from the surface are kept to be almost neutral throughout this reaction. They are repelled from the surface especially at the final stage (points 9 and 10) of the reaction.

Since the dissociative adsorption state necessary for the crystal growth is less stable than the molecular adsorption state or the initial state, and the energy barrier for molecular adsorption 61.5 kcal/mol is too high to get over at 600K, the As_4 cluster irradiated on the surface will be desorbed back to the vacuum and the crystal growth is hard to occur in this mechanism.

6. Adsorption of As_4 at a step site of a GaAs surface

The step site of the Ga-stabilized GaAs(100) surface is simulated by the $Ga_8As_{10}H_{20}$ cluster shown in Fig 1. Two As atoms which represent two As atoms at the step site are added at the edge of the $Ga_8As_8H_{18}$ cluster dealt with in the preceding

section. We use the same reaction path as that calculated in section 5. The electronic charges of the four As atoms along the path are summarized in the right-hand side of Table IV. The calculated potential surface along the reaction path is shown in Fig 10. The broken line represents the result of the HF method and the solid line the MP2. The horizontal axis in Fig 10 is defined in the same way as in the previous section.

The potential curve has two minima at points 7 and 10 and two maxima at points 3 and 9: passing through the initial barrier at point 3, As_4 reaches the molecular adsorption state at point 7 and then going beyond the barrier at point 9, it is dissociatively adsorbed at point 10. The barrier height at point 3 is 33.6 kcal/mol. After passing this barrier, the As atoms become slightly negatively charged and the adsorbed As_4 is almost in a tetrahedral form. The molecular adsorption is found at point 7 with the adsorption energy of 20.5 kcal/mol and the As atoms are suddenly charged around this point: the charge of the As atoms contacting with the surface is -0.03 at point 5 but becomes -0.22 at point 7. The calculated energy barrier of 33.6 kcal/mol is about a half of that of 61.5 kcal/mol for the flat surface of section 5. After passing this point, the As-As length of the As_2 contacting on the surface becomes longer and the cluster reaches the second barrier at point 9. The energy barrier height is 18.0 kcal/mol higher than the molecular adsorption state. Finally, the dissociative adsorption occurs at point 10 with the adsorption energy of 94.4 kcal/mol. Though the HF calculation shows that the final state is less stable than the molecular adsorption state, the correlated MP2 calculation reveals that the reaction proceeds. Throughout the reaction, the charge of the As atoms contacting with the surface changes dramatically, though the other As atoms are kept almost neutral. The first barrier is due to the electron transfer from the surface to the As_4 cluster and the second one is due to the dissociation of the adsorbed As_4 cluster. The charge of the adsorbed As atom is almost equal to the charge of the surface As atom of -0.21 in our previous study [1]. The calculated molecular adsorption energy of 20.5 kcal/mol is larger than the experimental value of 8.8 kcal/mol [4].

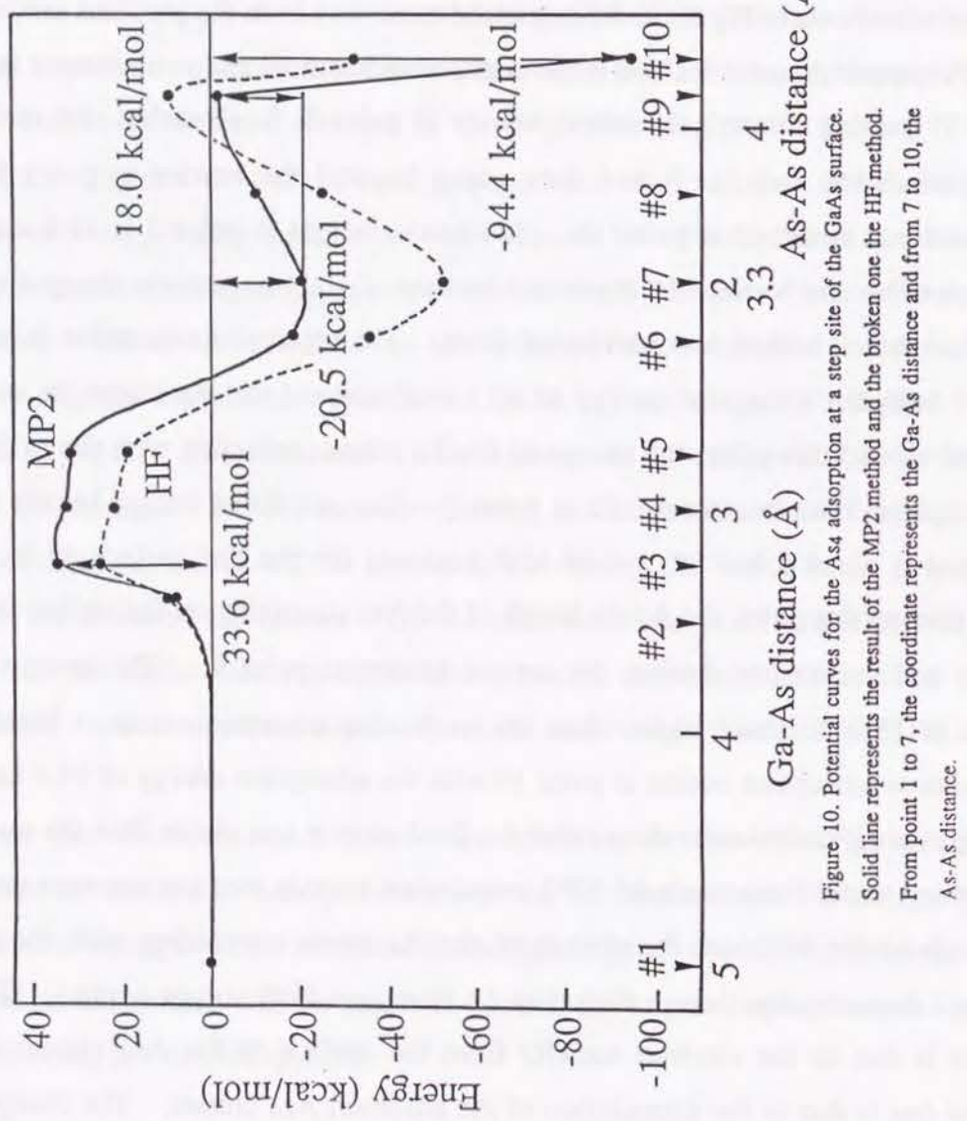

Figure 10. Potential curves for the As4 adsorption at a step site of the GaAs surface. Solid line represents the result of the MP2 method and the broken one the HF method. From point 1 to 7, the coordinate represents the Ga-As distance and from 7 to 10, the As-As distance.

Since the dissociative adsorption necessary for the crystal growth occurs more easily than the molecular adsorption and the energy barrier is about 30 kcal/mol, the As_4 cluster is likely to be adsorbed and dissociated at the step site of the GaAs surface. This result is in sharp contrast to the result for a flat surface. We therefore suggest that by the As_4 molecular beam, the As layer could grow at a step site of the GaAs surface with desorbing out As_2 from the surface.

7. Coadsorption of two As_4 on a Ga-stabilized GaAs surface

We finally study the possibility of coadsorption of two As_4 clusters on a Ga-stabilized GaAs surface. The Ga-stabilized GaAs(100) flat surface is simulated by the $Ga_8As_3H_{12}$ cluster shown in Fig 1. The reaction path is explained in Fig 11, that is, from point 1 to 2 the two As_4 clusters are coadsorbed on the GaAs surface, from 2 to 4, two As_4 clusters coadsorbed molecularly on the GaAs surface couple, and from point 4 to 6 the four As atoms directly interacting with the surface are adsorbed on the surface and at the same time, the other four As atoms rearrange to make an As_4 cluster which desorbs out from the surface. We explain the reaction path in more detail using Fig 12: from point 2 to 3, the As atoms contacting directly with the surface are fixed at the molecularly adsorbed position (i.e. point 7 in Fig 7) calculated in section 5; and from point 4 to 6 they are fixed at the dissociatively adsorbed position (i.e. point 10 in Fig 7) calculated in section 5. The other four As atoms are optimized by the HF calculation within the accuracy of 0.1 Å by assuming C_{2v} symmetry with the $Ga_8As_3H_{12}$ cluster fixed. Geometries and the electronic charges of these As atoms along the reaction path are summarized in Tables V and VI, respectively, and the calculated potential curve is shown in Fig 13. The dashed line represents the result of the HF method and the solid line that of the MP2 method. From point 1 to 4, the horizontal axis stands for the As-As distance, that is the distance between the As atoms indicated by the filled circles in Fig 11, and from point 4 to 6, the axis stands for the Ga-As distance, that is the distance from the As atom of the desorbing As_4 molecule to the surface Ga atom.

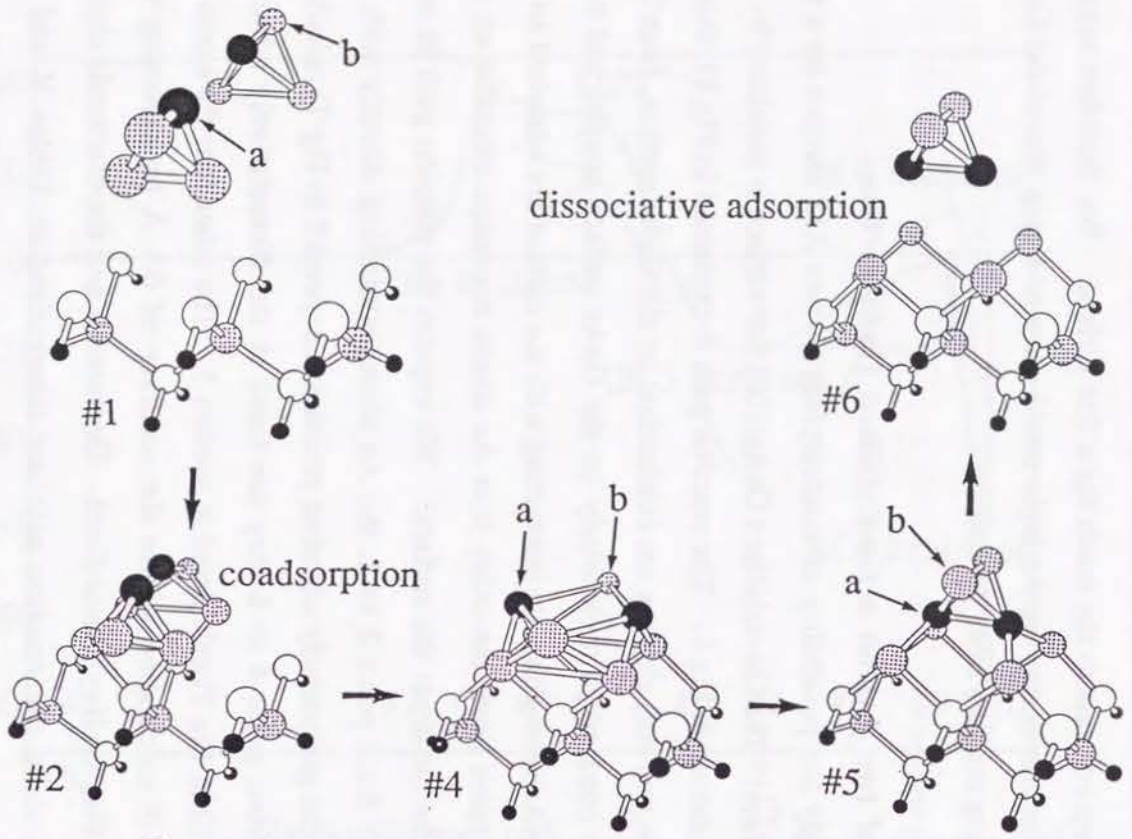

Figure 11. Schematic representation of the dissociation of the coadsored two As_4 clusters. From the two As_4 coadsorbed on the cluster, four As atoms are dissociatively adsorbed on the surface and the other four As atoms are released into vacuum as an As_4 cluster. Filled circle is given to distingush the two As atoms.

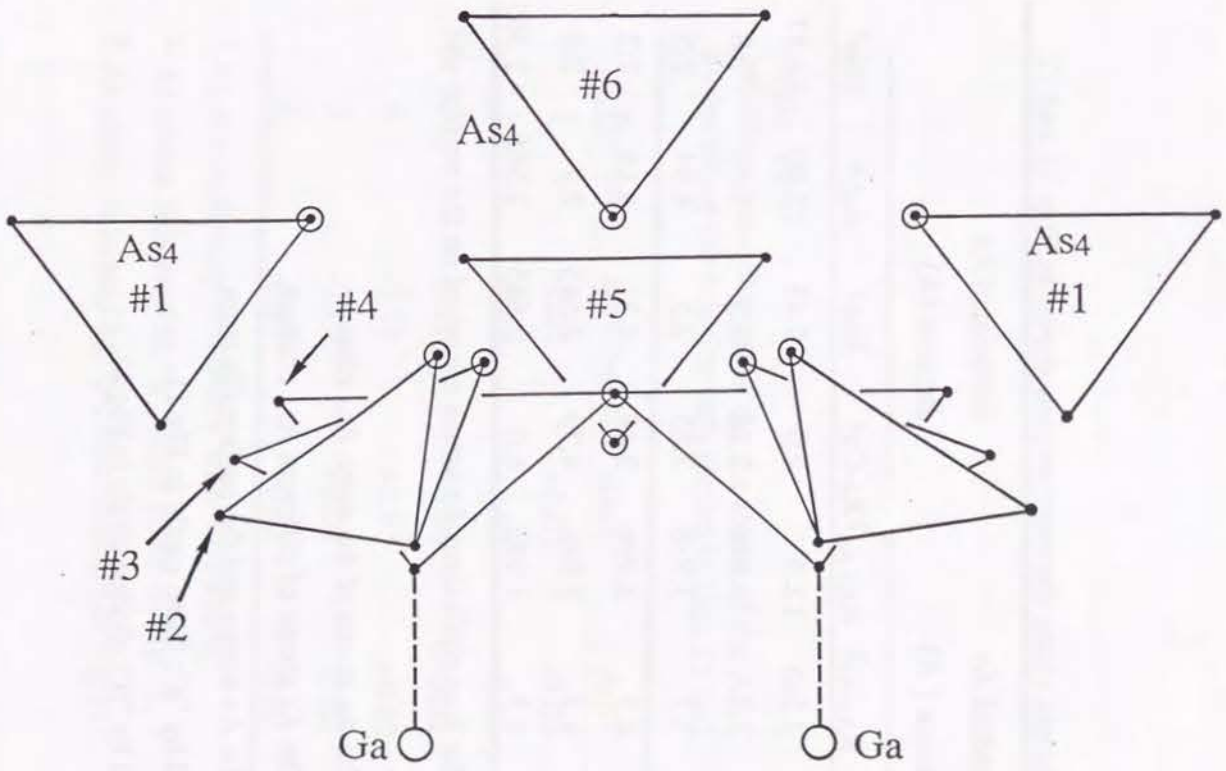

Figure 12. Reaction path for the coadsorption of two As_4 clusters on a GaAs (100) surface. This reaction path keeps C_{2v} symmetry. Double circles stand for the same As atom.

Table V

Geometry of the As atoms along the reaction path shown in Figs 11 and 12.

	adsorbed As distance (Å)			dissociated As distance (Å)			
Position	R_{Ga-As}[1]	R_{As-As}[2]	R_{As-As}[3]	Ra-Ga[4]	Raa[5]	Rab[6]	Rbb[7]
1	5.0	2.565	12.0	7.0	9.43	12.00	14.57
2	2.0	3.3	3.998	2.28	3.5	5.66	7.8
3	2.0	3.3	3.998	2.85	2.5	4.94	7.5
4	1.77	4.3	3.998	3.48	4.3	4.19	7.2
5	1.77	4.3	3.998	4.79	2.565	2.7	2.6
6	1.77	4.3	3.998	6.0	2.565	2.565	2.565

[1] Distance between the four equivalent As atoms adsorbed on the surface and the surface Ga atom.

[2] Distance between the As atoms of the same As_4 cluster.

[3] Distance between the As atoms of different As_4 clusters.

[4] Distance between the As atoms and the surface Ga atom.

[5] As atoms indicated by "a"; filled circle in Fig 11.

[6] As atoms indicated by "b"; shaded circle in Fig 11.

Table VI

Mulliken gross charges of the As atoms of the As_4 cluster along the reaction path shown in Figs 11 and 12.

Position	adsorbed As[1]	Asa[2]	Asb[3]
1	-0.02	+0.03	-0.00
2	-0.18	+0.03	-0.01
3	-0.22	+0.06	-0.02
4	-0.21	+0.05	+0.02
5	-0.19	+0.04	-0.04
6	-0.18	+0.02	-0.02

[1] As atoms directly contacting with the surface.

[2] As atoms indicated by "a", filled circle in Fig 11.

[3] As atoms indicated by "b", shaded circle in Fig 11.

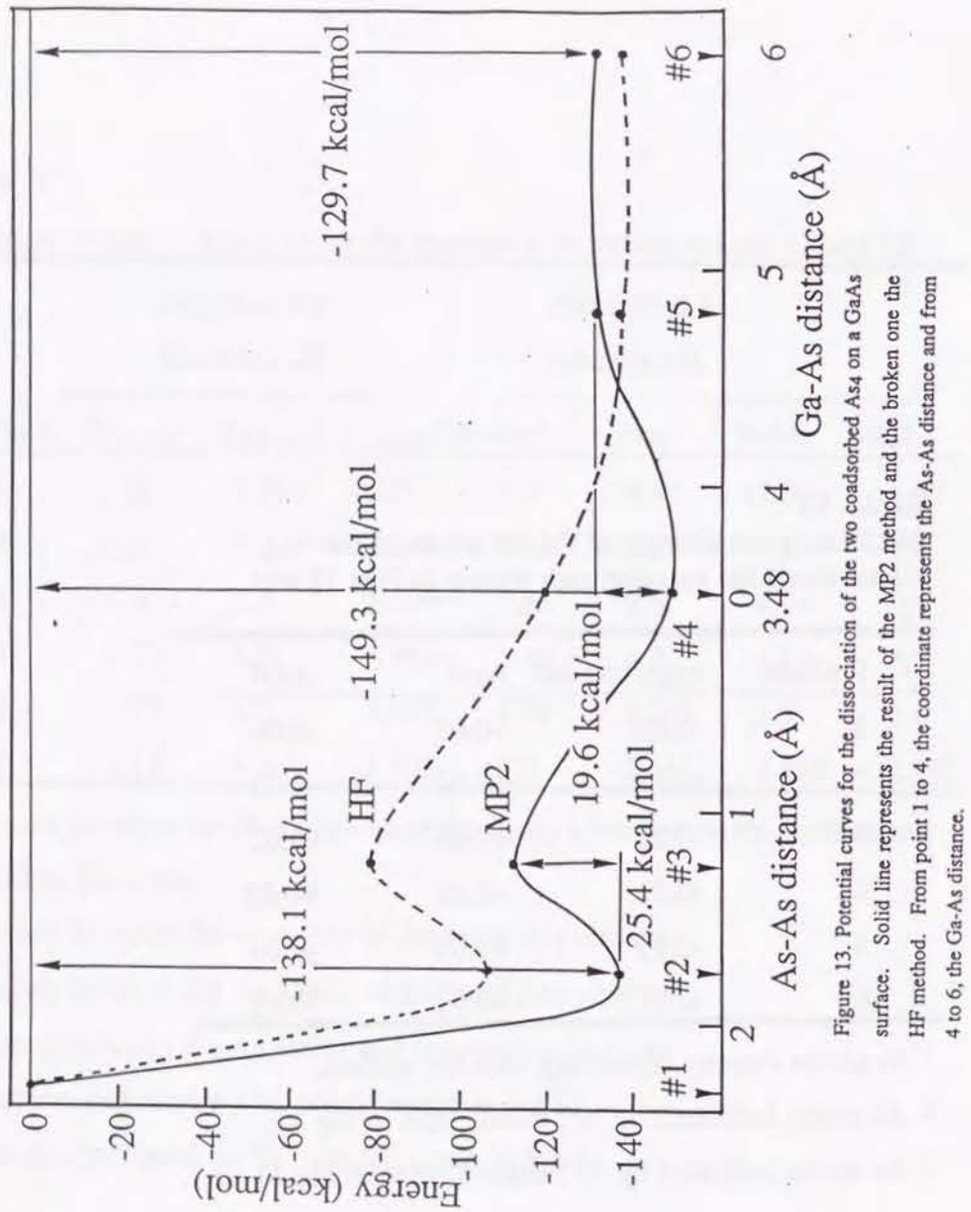

Figure 13. Potential curves for the dissociation of the two coadsorbed As_4 on a GaAs surface. Solid line represents the result of the MP2 method and the broken one the HF method. From point 1 to 4, the coordinate represents the As-As distance and from 4 to 6, the Ga-As distance.

The potential curve has two minima at points 2 and 4, and two maxima at points 3 and 6: As_4 is molecularly coadsored at point 2 and then dissociatively adsorbed at point 6. At point 1, the optimized As-As bond length is 2.565 Å which is the same as that of a free As_4 molecule. The molecular adsorption at point 2 occurs with the adsorption energy of 138.1 kcal/mol and then the As_4 cluster collapses with the barrier of 19.6 kcal/mol indicating that the two As_4 clusters receive repulsive forces to each other. Four As atoms contacting with the surface are charged to -0.18 and the other four As atoms are charged to only +0.03 and -0.01. Beyond this point, two As_4 clusters come closer to each other and the four As atoms on top of the As_4 cluster combine at point 4 with the energy barrier of 25.4 kcal/mol. Finally, the As atoms reach the dissociative adsorption state at point 6 which is 129.7 kcal/mol more stable than the initial state and 8.4 kcal/mol less stable than the coadsorption state. There, four As atoms combine and desorb as a As_4 cluster from the surface and the other four As atoms are adsorbed on the Ga stabilized surface. Throughout the reaction, the change of the charges of the As atoms is very monotonous and kept almost constant; the charge of the adsorbed As is kept in the range of -0.18 ~ -0.22 and that of the desorbed As is almost neutral, -0.04 ~ +0.06. The charge of the adsorbed As at point 6, -0.18 is similar to the value -0.24 of the adsorbed As atom at the step site in section 5. The MP2 result shows a minimum at point 4. Since the actual surface is heated up to 600K, the As atoms would be able to reach points 5 and 6. However since the minimum lies at near point 4, there would be a large possibility of finding As_4 molecule around there.

Pairwise adsorption of two As_4 clusters will scarcely occur because of the repulsive interaction between two As_4 clusters. If the molecularly adsorbed As_4 clusters could migrate on the surface and meet together, they would form a coadsorption state and react. The adsorption energy of 129.7 kcal/mol is obtained from the results of sections 3, 5, and 6. Namely, the reaction ,

$2\ As_4\ (gas) \rightarrow As_4(gas) + 4\ As\ (adsorbed\ on\ surface)$

is constructed from the following three reaction steps.

(step 1) One As_4 is adsorbed on a flat surface and dissociated into two As atoms on the surface and the As_2 molecule is released into vacuum.

As_4 (gas) → 2As (surface) + As_2 (gas)

This reaction is simulated in section 5 and the reaction energy is given as -16.7 kcal/mol.

(step 2) Another As_4 is adsorbed on the surface near the previously adsorbed two As atoms. This corresponds to the adsorption at a step site simulated in section 6 and the reaction formula is the same as that given in step 1. The reaction energy is calculated as 94.4 kcal/mol.

(step 3) The released two As_2 clusters react and give an As_4 cluster.

As_2 (gas) + As_2 (gas) → As_4 (gas)

This step is simulated in section 2 and the reaction energy is calculated as 54 kcal/mol. Summation of the energies of the three steps gives 131.7 kcal/mol which is almost equal to to the reaction energy of 129.7 kcal/mol in this section.

The adsorption energy of a single As_4 cluster is -10.3 kcal/mol on a flat surface or +20.5 kcal/mol at a step site as calculated in sections 5 and 6, respectively. The adsorption energy for the coadsorption, 138.1 kcal/mol is remarkably large in comparison with these values showing the stabilization by the coadsorption. We now apply the discussion similar to the above one to the molecular adsorption. The coadsorption

2 As_4 (gas) → 2 As_4 (coadsorbed)

is divided into the following two reaction steps.

(step 1) Two As_4 are adsorbed apart by a long distance on the surface with the adsorption energy of 20.5 kcal/mol at a step site as discussed in section 6.

2 As_4 (gas) → 2 As_4 (adsorbed)

(step 2) They approach to each other by a migration on the surface, interact and become into the coadsorption state.

2 As_4 (adsorbed) → 2 As_4 (coadsorbed)

Since the sum of the molecular adsorption energy in step 1 and the energy change by the coupling in step 2 is equal to the coadsorption energy of 138 kcal/mol given in this section, the energy change by the coupling is estimated to be about 100 kcal/mol.

This reaction path is fixed to C_{2v} symmetry, though the movement of the As atom from point 3 to 4 requires a lower symmetry of at least C_2 symmetry. Therefore, the exact transition state is not necessarily at point 4 and a higher barrier is expected. However, the potential curve is smooth and the barrier is not so sensitive to the geometrical change. Therefore the energy barrier of 25.4 kcal/mol is somewhat reliable.

This result shows that when the adsorbed As_4 migrates on the surface, the coupling of two As_4 is preferable and the energy barrier for the reaction

2 As_4 (coadsorbed) → As_4 (gas) + 4 As (adsorbed)

is only 25.4 kcal/mol. We therefore conclude that this reaction occurs and a new As-layer grows on the surface with desorbing the As_4 molecule.

8. Concluding remarks

At a step site of the Ga-stabilized surface, the As_4 cluster shows molecular adsorption and the two adsorbed As_4 clusters give the coadsorption state which gives a new As-layer with releasing an As_4 cluster into vacuum. Furthermore, we suggest the possibility of the reaction involving only a single As_4 cluster. These energy profiles are summarized as follows and a qualitative representation is given in Fig 14.

(1) The As_4 cluster of the beam is molecularly adsorbed at a step site of the Ga-stabilized GaAs surface with the energy barrier of 30.3 kcal/mol. This is the rate-determing step in the crystal growth.

As_4 (gas) + Ga (surface) → As_4 (adsorbed) + Ga (surface) (30.3 kcal/mol)

(2) Two As_4 clusters adsorbed on the Ga-stabilized GaAs surface may migrate and collide together giving the coadsorption state.

2 As_4 (gas) + Ga (surface) → 2 As_4 (coadsorbed) + Ga (surface)

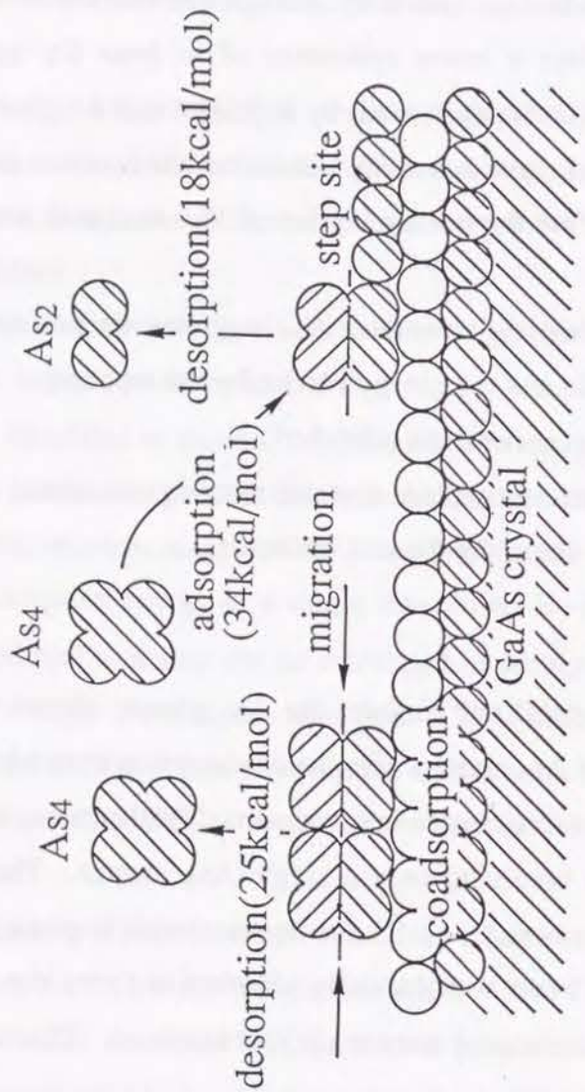

Figure 14. Schematic representation of the GaAs epitaxial crystal growth by the As4 cluster beam.

(3) The coadsorbed As_4 clusters are reconstructed to give the four As atoms dissociatively adsorbed on the surface to make a new As-layer and the other four As atoms make an As_4 cluster and desorb from the surface with the energy barrier of 25.4 kcal/mol.

2 As_4 (coadsorbed) → As_4 (gas) + 4 As (surface) (25.4 kcal/mol)

The energy barrier for the reaction involving only a single As_4 cluster is 18.0 kcal/mol as discussed in Sec 6. This energy barrier is lower than that of Sec 7, 25.4 kcal/mol and the sticking coefficient of this reaction (=0.5) is consistent with that of the experimental value which is less than 0.5. Then we suggest the following reaction step could occur.

(4) The molecularly adsorbed As_4 given above is dissociated thermally and a new As layer grows on the Ga-stabilized surface with the energy barrier of 18.0 kcal/mol.

As_4 (adsorbed) → As_2 (gas) + 2 As (surface) (18.0 kcal/mol)

We thus have confirmed the reaction involving two As_4 clusters, steps 2 and 3 which were experimentally proposed previously. Furthermore, we can very roughly estimate the magnitude of the reaction probability from the calculated reaction barrier: Namely the reaction involving a single As_4 cluster would occur more easily than the one involving two As_4 clusters, but the rate-determing step is the molecular adsorption step (1) in the crystal growth. In the previous paper Bonapasta et al. showed that the Ga atom is adsorbed on a As-stabilized surface without energy barrier [16]. Then the irradiation of the As_4 cluster and Ga atom beams make the As and Ga layer alternatively and the GaAs crystal grows. It must be noted finally that the reaction steps examined in this study are only a part of the possible reactions on the surface and another reaction can be assumed.

Acknowledgements

The calculations have been carried out with the FACOM M-1800 computer at the Data Processing Center of Kyoto University and the HITAC M-680H at the Institute for Molecular Science. The authors thank the IMS computer center for the

grants of computing time. Part of this study has been supported by the Grant-in-Aid for Scientific Research from the Japanese Ministry of Education, Science, and Culture.

Referrence

[1] Y. Fukunishi and H. Nakatsuji, Surf. Sci., 291, (1993) 271.

[2] Y. Fukunishi and H. Nakatsuji, Surf. Sci., 291 (1993) 281.

[3] H. Kunzel and K. Ploog, Appl. Phys. Lett., 37, (1980) 416.

[4] J. R. Arthur, Surf. Sci. 43, (1974) 449.

[5] C. T. Foxon, M. R. Boudry and B. A. Joyce, Surf. Sci. 44 (1974) 69.; C. T. Foxon and B. A. Joyce, *ibid* , 50 (1975) 434; *ibid* , 64 (1977) 293.

[6] I. A. Frolov, P. B. Baldyrevskii, B. L. Druy and E. B. Sokolor, Inorg. Mater., 13, (1977) 632.

[7] M R. Lays and H. Veenvliet, J. Cryst. Growth, 55, (1981) 145.

[8] J. Nishijima and T. Kurabayashi, J. Electrchem.Soc.,130, (1983) 413.

[9] T. Ohno, Phys. Rev. B44, (1991) 6306.

[10] R. M. Graves and G. E. Scuseria, J. Chem. Phys., 95 (1991) 6602.

[11] K. Balasubramanian, J. Chem. Phys., 87 (1987) 3518; *ibid* 86 (1987), 3410.

[12] J. Andzelm, N. Russo and D. R. Salahub, Chem. Phys. Lett 169 (1987), 142.

[13] S. Katsuki and S. Huzinaga, Chem. Phys. Lett., 152 (1988), 203

[14] Y. Watanabe, Y. Sakai and H. Kashiwagi, Chem. Phys. lett.,120 (1985), 363.

[15] G. E. Scuseria, J. Chem. Phys., 92 (1990), 6722.

[16] A. A. Bonapasta, M. R. Bruni, A. Lapiccirella, P. Nota, G. Scavia and N. Tomassini, Surf. Sci. 204 (1988) 273.

[17] M. Tsuda, S. Oikawa, M. Morishita and M. Mashita, Jpn. J. Appl. Phys., 26.(1987) L564.

[18] A. Doi, Y. Aoyagi and S. Namba, Appl. Phys. Lett. 48.(1986) 1787; *ibid* 49 (1986) 785.

[19] M. Dupuis, J. D. Watts, H. O. Villar and G. H. B. Hurst, 'HONDO7',Program Libraly No. 1501, Computer Center of the Institute for Molecular Science, (1987).

[20] O. Chesnovsky, S. H. Yang, C. L. Pettiette, M. J. Craycraft, Y. Liu, R. E. Smalley, Chem. Phys. Lett, 138, (1989) 229.

[21] W. Begemann, R. Hector, Y. Y. Liu, J. Tiggesbaumker, K. H. Meiwes-Broer, H. O. Lutz, Z. Phys, D12, (1989) 229.

[22] K. H. Hellwege, W. Pies, A. Weiss: Crystal Structure Data of Inorganic Compounds, Landolt-Börnstein, New Series, Group III, Vol. 7 (Springer-Verlag, Berlin, 1979).

[23] L. C. Snyder and Z. Wasserman, Surf. Sci., 71 (1978) 407; *ibid* 77 (1987)52.

[24] A. C. Kenton and M. W. Ribarsky, Phys. Rev. B23 (1981) 2897 .

[25] K. Hermann and P. S. Bagus, Phys. Rev. B20 (1979) 1603.

[26] J. H. Callomon, E. Hirota, K. Kuchitsu, W. J. Lafferty, A. G. Maki, and C. S. Pote, *Structure Data of Free Polyatomic Molecules*, Landolt-Börnstein, New Series, Group II, Springer-Verlag, Berlin, 1976, V. 7.

[27] W. J. Hehre, R. F. Stewart and J. A. Pople, J. Chem. Phys., 51 (1969) 2567.

[28] W. R. Wadt and P. J. Hay, J. Chem. Phys., 82 (1985) 284.

PART III
Theoretical study of the hydrolysis of guanosine triphosphate in ras-p21 protein

Abstract

We studied the hydrolysis reaction of GTP in p21 by the ab-initio method and molecular dynamics simulation by assuming two reaction mechanisms: GB61 and an alternative reaction proposed by Langen et al.. The only difference between them is the location of the proton in their intermediates; in GB61 the proton is on the glutamine 61, while in anothr mechanism it is on the γ-phosphate. The lower energy barrier is given by mechanism A, and its $\Delta G^{\ddagger}$ of 28 kcal/mol is similar to the observed $\Delta G^{\ddagger}$ of 23 kcal/mol. In contrast, GB61 gives a very high $\Delta G^{\ddagger}$ of 115 kcal/mol and an unstable intermediate. The difference in the free energy of the intermediates was estimated by the free energy perturbation (FEP) method. The results show that, even considering the solvation and protein effect, the intermediate of GB61 is 54 kcal/mol less stable than that of mechanism A. Therefore, we conclude that mechanism A is most likely to occur in the hydrolysis of GTP in ras p21.

1. Introduction

The ras family of protooncogenes are of particular interest, since they have been implicated in the development of numerous tumors. The ras gene products are so-called p21 proteins which bind guanine nucleotides with high affinity and are thought to be involved in various signal transduction pathways in many cell types. The p21-Guanosine diphosphate (GDP) complex receives a signal from an upstream element, and GDP is then exchanged for Guanosine triphosphate (GTP) which converts inactive p21-GDP complex to the active p21-GTP complex. p21-GTP is able to transmit the signal downstream to an appropriate target. The active p21-GTP complex is converted to the inactive GDP complex by hydrolysis of GTP to GDP. A recent study proposed that glutamine 61 (Gln61) helps to facilitate the nucleophilic attack on the γ-phosphate by activating a water molecule (GB61 mechanism) [1]. Although the proposed mechanism was not described in detail, it seems to imply that Gln61 acts as a general base in this hydrolysis. Such a mechanism is consistent with the observation of a water molecule between Gln61 and GTP, perfectly positioned for a direct in-line attack on the γ-phosphate. However, despite the appealing structural evidence, this mechanism has not been fully established. The previous study indicated that Gln61 is not likely to be a general base in the reaction. An alternative mechanism (mechanism A) was proposed by Langen et al.[2] in which the γ-phosphate itself activates a water molecule.

The x-ray structure shows that Gln61 is located at the surface of the protein and can not play any role in the hydrolysis because of its geometry [3]. In contrast, a molecular dynamics simulation has revealed that Gln61 can rotate in the solution and can be positioned in a good conformation for the reaction [4]. Therefore, a molecular dynamics simulation is necessary in this study to obtain a reactive conformation.

Figure 1 shows the hydrolysis mechanism by mechanism A and GB61. In the GB61 mechanism, the initial step is proton transfer from H_2O to an oxygen

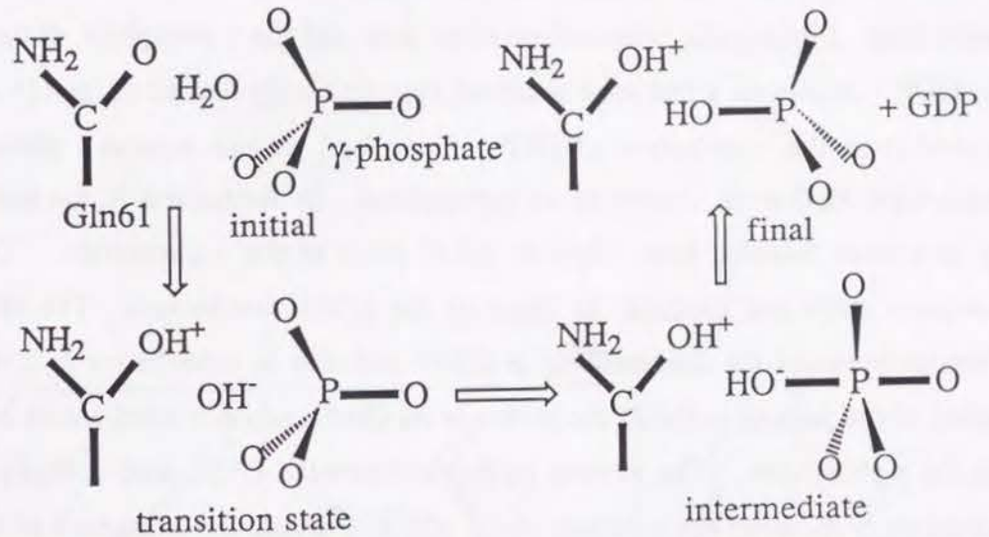

Fig 1. Reaction mechanism GB61 and mechanism A.

atom of Gln61. This is followed by an addition-elimination mechanism, i. e., the reactive species OH^- attacks the γ-phosphate to produce a tetragonal intermediate. Finally, the intermediate turns over and the γ-phosphate desorbs from GDP. However, it has been observed experimentally that all of the H^+ are desorbed from the γ-phosphate of GTP. Therefore, we can assume a proton-transfer from H_2O to an O atom of the γ-phosphate. In mechanism A, the initial step is proton transfer from H_2O to the O atom of the γ-phosphate. The subsequent steps are identical to those of the GB61 mechanism. The only difference between the intermediate in GB61 and that in mechanism A is the location of the proton; in GB61 the proton is on Gln61, while in mechanism A it is on the γ-phosphate. The current study examines the GB61 mechanism and mechanism A by using the structure of ras p21 to evaluate the energetics of the assumed proton-transfer process. This is achieved by the ab-initio method and the molecular dynamics simulation.

2. Computational method

Figure 2 shows the reaction center of the hydrolysis and the cluster model for mechanism A and GB61. The H_2O molecule approaches and reacts with the cluster in one of the two ways shown in Fig 1, which are discussed in Sections 4 and 5, respectively. The H atoms cap the artificial dangling bonds of the NH_3 and P_2O_6 clusters.

The Gaussian basis sets are double zeta (9s5p)/[4s2p] sets [5] with a polarization function for the important atoms and minimal (STO-3G) sets for the less important atoms[6]; the double zeta basis sets are used for the P, O and H atoms located in the reaction center, and the other Mg, P, C, O and H atoms of the cluster are treated with the minimal basis sets. The atoms treated with the double zeta basis are indicated by asterisks in Fig 2.

All of the calculations were performed by the Hartree-Fock (HF) method with the Møller-Plesset second order perturbation (MP2) method using the

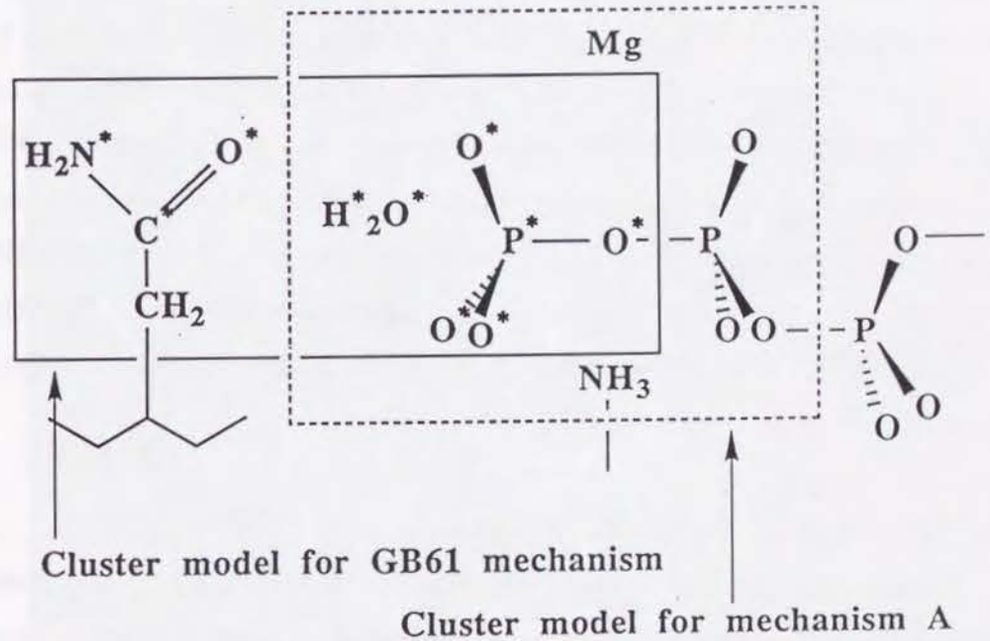

Fig 2. Cluster models representing the reaction centers of GB61 and mechanism A.

GAUSSIAN88 program [7]. The molecular dynamics simulations were carried out using the AMBER version 4 [8], that had been partially modified for this purpose, and COSMOS90 [9] molecular dynamics programs. The simulations used an all-atom force field without any cutt-off of the interactions for minimization and a molecular dynamics simulation. The molecules were immersed in a box of TIP3P water [10]. All of the covalent bonds involving hydrogen were constrained. The simulations were performed at 300 K, at integration step of 0.5 fs. The force field parameters were those given by Cannon [11] for GTP, and the AMBER force field parameters were used for the protein and Mg atoms. To estimate the effect of the protein and the solvent, we estimated the difference in free energy between the intermediates of GB61 and mechanism A using the free energy perturbation method. During the reaction, a reactive water molecule is initially represented by a rigid model (TIP3P), but then becomes OH^- and H^+, which are treated by all-atom model. Therefore, it is difficult to estimate the change in the effect of the solvent throughout the course of the reaction.

3. Hydrolysis of phosphate by mechanism A

To obtain the geometry of the reaction center, a molecular dynamics simulation was performed. A snapshot view of close to the minimized geometry is shown in Figures 3 and 4. Figure 3 shows the p21 protein and the binding GTP; the water molecules are covered and the reaction center, Gln61, the reactive water molecule and the γ-phosphate are shown. Figure 5 shows a cluster model which represents the reaction center and the reaction structures: i.e., initial, transition state and tetragonal intermediate. Since the rate-determining step is the proton transfer from H_2O, the proton transfer from H_2O to the tetragonal-γ-phosphate intermediate is calculated. The binding site for GTP includes a Mg atom which binds with threonine 35 (Thr35) throughout the reaction. NH_4 represents a side chain of lysine 16 (Lys16) which forms a

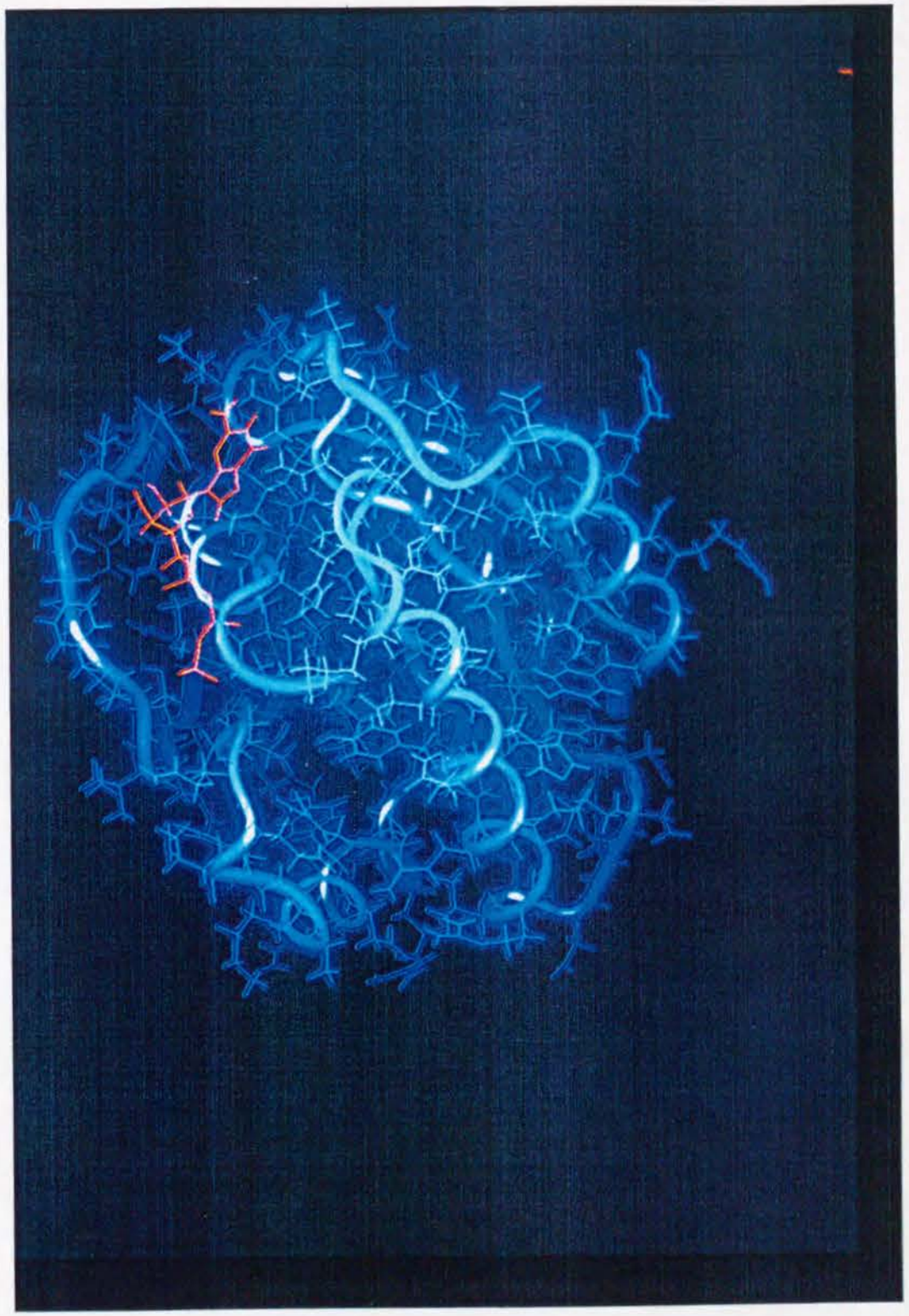

Fig 3.Snapshot of the solution structure of the p21-GTP complex.

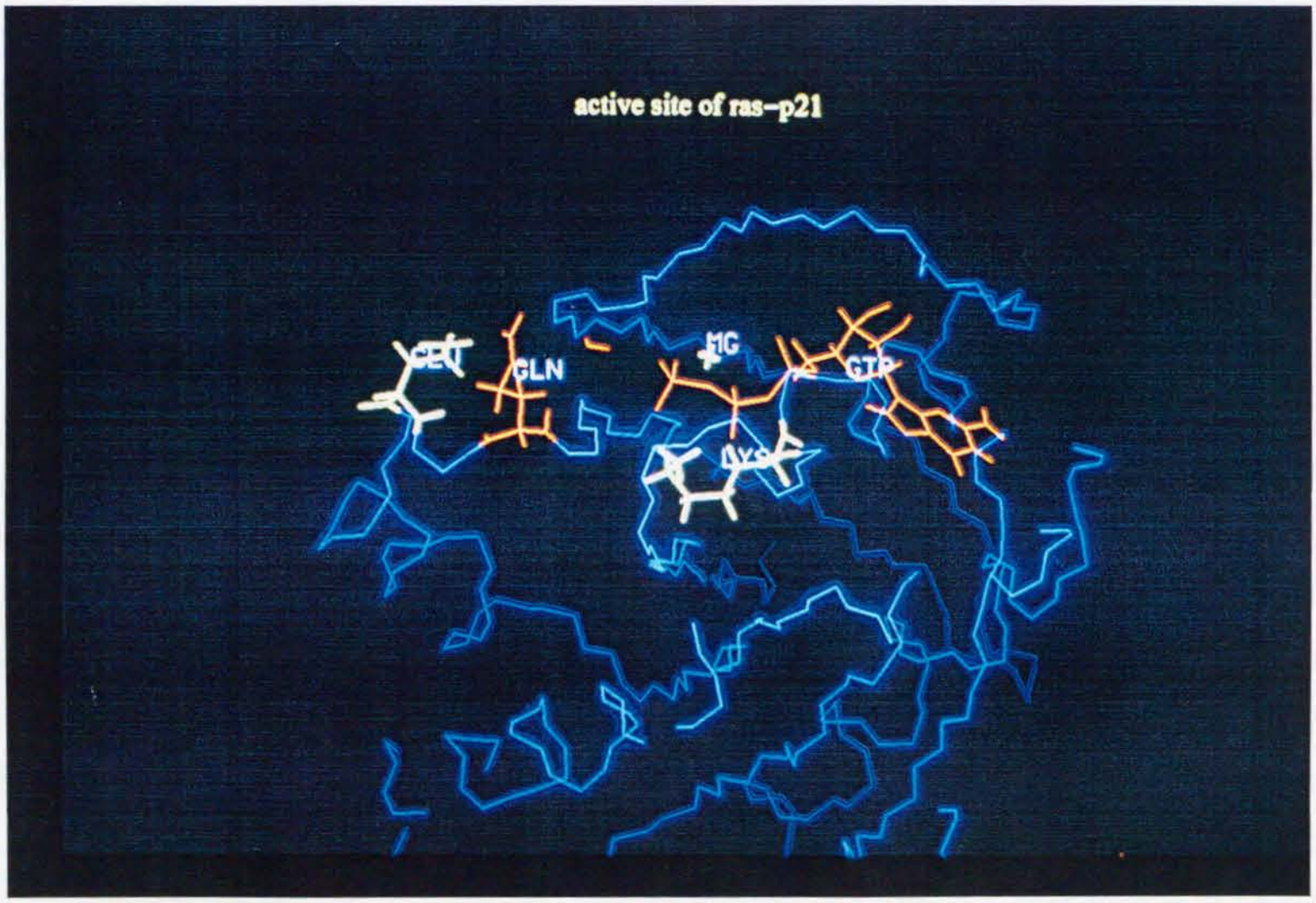

Fig 4.Reaction center of the p21-GTP complex.

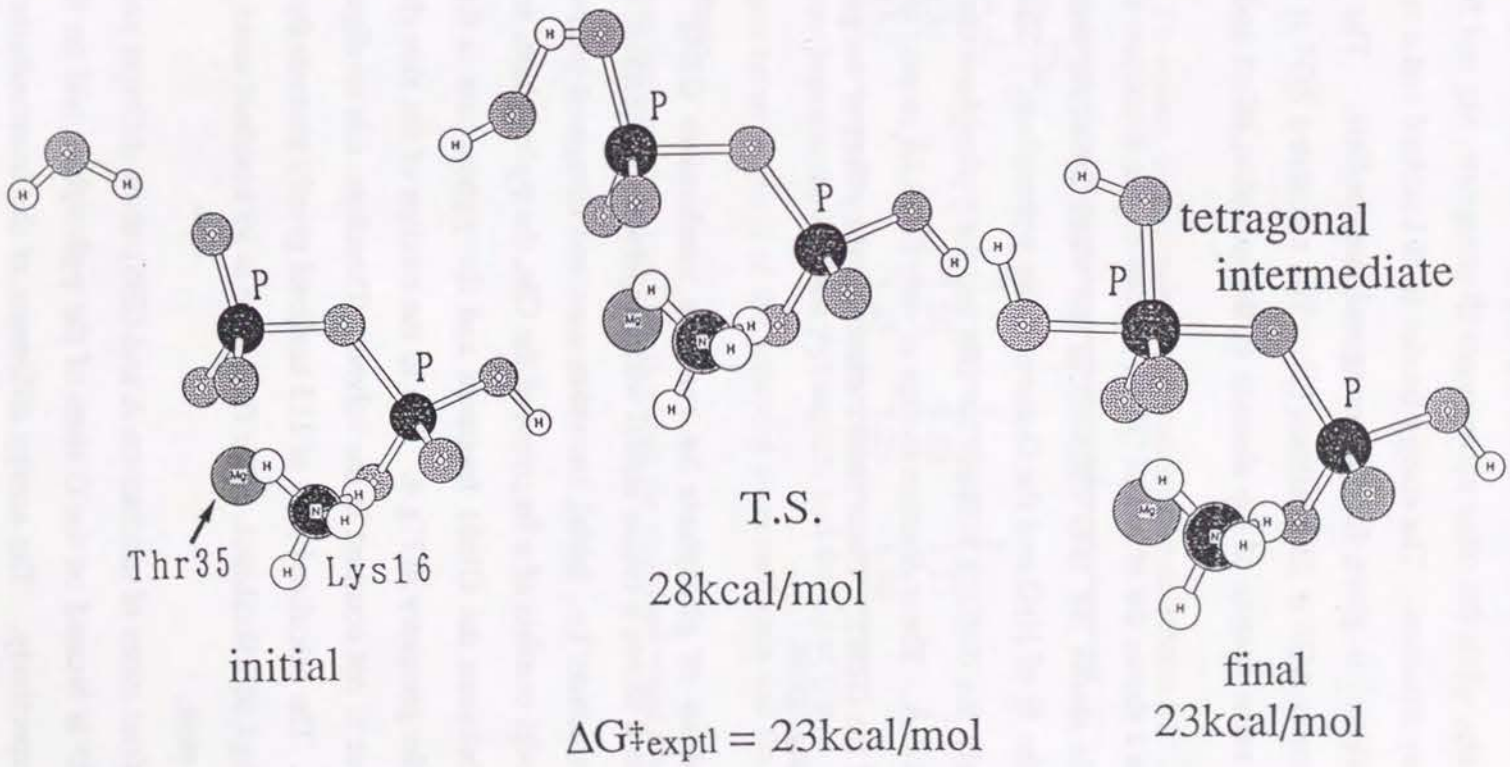

Fig 5. Initial, transition state and intermediate structures, and each energy level in mechanism A.

hydrogen bond with GTP. Only the γ-phosphate and H_2O are optimized in each reaction step, while the other components (β-phosphate, Mg and NH_4) are fixed in the x-ray structure. The energy barrier is 28 kcal/mol and a reaction energy of 23 kcal/mol is given for the tetragonal-intermediate. The experimental energy barrier $\Delta G^{\ddagger}$ is 23 kcal/mol[12]. The calculated $\Delta G^{\ddagger}$ is similar to the observed value despite of the absence of the solvation effect and the dynamic effect.

Table I shows the effect of Gln61 residue on the transition state structure. This Table shows the H-O distance in the water molecule and the distance between the H of H_2O and the O atom of the γ-phosphate. Since Gln61 can rotate freely, the distance between the Gln and the γ-phosphate changes within a range of 4-6 Å. These distance change of only 0.1-0.2Å respect to the geometry change of the Gln61. These results show that the effect of the geometry of the Gln61 is negligible.

4. Hydrolysis of phosphate by reaction mechanism GB61

Figure 6 shows a cluster model which represents the reaction center and the reaction structure: i.e., initial, transition state and tetragonal intermediate. The cluster model consists of a fragment of the Gln, the γ-phosphate, and H_2O. The distance between the Gln61 fragment and the γ-phosphate is fixed at 6 Å to maintain the geometry in Fig 4. Due to the rotation of the side chain of Gln61, the distance is not constant in the solvent. Therefore, this configuration is only expedient. The calculated $\Delta G^{\ddagger}$ of 115 kcal/mol greatly exceeds the experimental value of $\Delta g^{\ddagger}$ of 23kcal/mol. The final state is 99 kcal/mol more unstable than the initial state.

The final states of mechanism A and GB61 show different positions for the H^+: the H^+ is located on the O atom of the γ-phosphate and on the O atom of Gln61, respectively. The energy difference of the intermediates is due to the difference in binding energy between the O-H bond in the γ-phosphate and the

Table I. Geometry dependence of the transition state structure.

phosphate-Gln distance[a] (Å)	4	5	6
R_{OH1}[b] (Å)	1.20	1.20	1.15
R_{OH2}[c] (Å)	1.25	1.25	1.20

a: distance between the P of the γ-phasphate and the Cδ of Gln.

b: distance between the H of the activated water molecule and the O of the γ-phosphate.

c: distance between the O and the H within the activated water molecule.

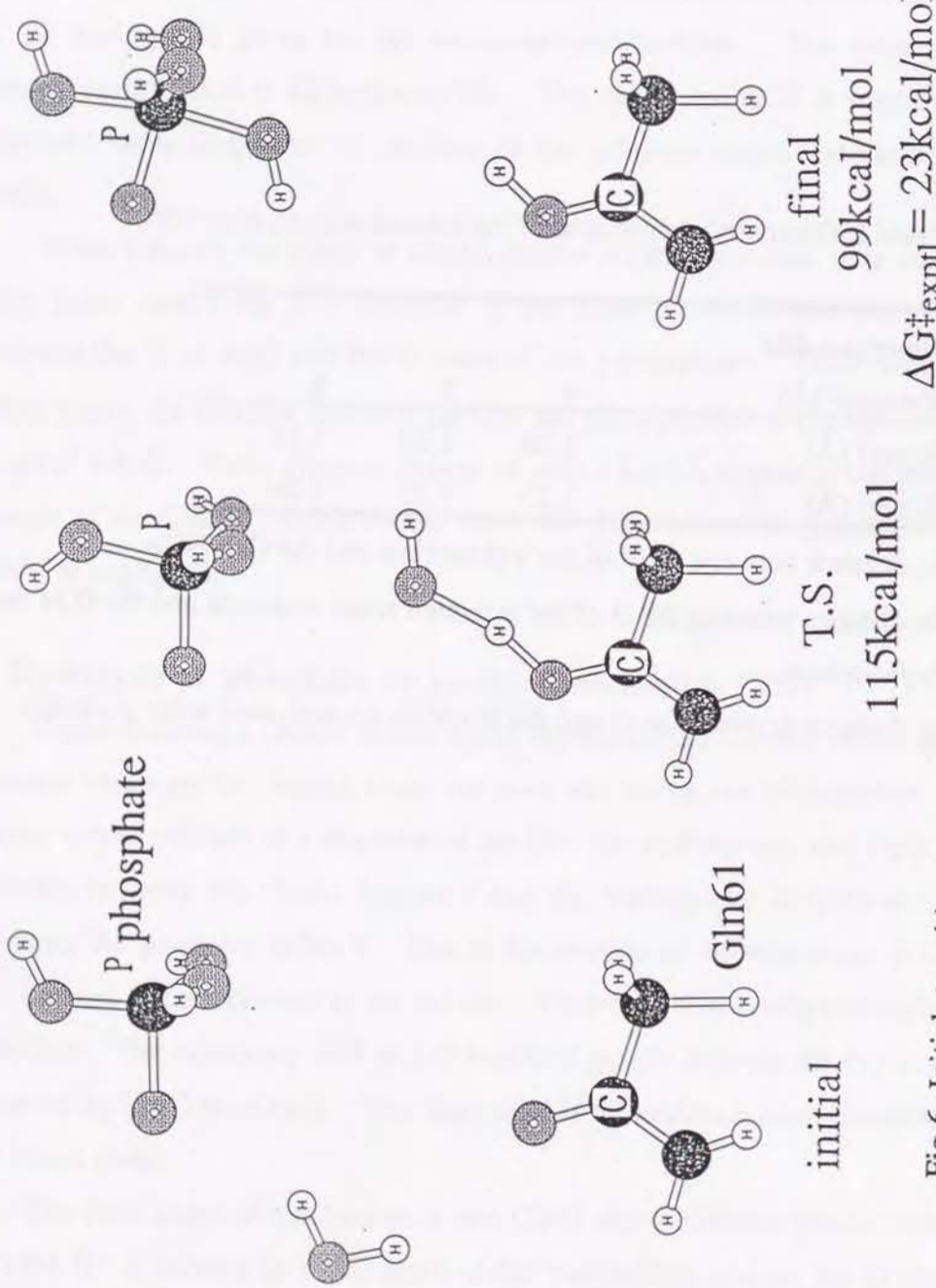

Fig 6. Initial, transition state and intermediate structures, and each energy level in GB61.

O-H bond in the glutamine cation($GlnH^+$). The binding energy of the O-H bond in the γ-phosphate is calculated as 305 kcal/mol, and that of the Gln is calculated as 220 kcal/mol in the gas phase. Since the binding energy difference of 85 kcal/mol(305 - 220 kcal/mol) is very similar to the energy difference of these intermediates (99 - 23 kcal/mol = 77 kcal/mol), the instability of the intermediate in GB61 is not due to the small size of the cluster model, but rather to the unstable O-H bond in $GlnH^+$.

Table II shows the effect of the γ-phosphate on the transition state structure. This Table shows the H-O distance in the water molecule and that between H of H_2O and the O atom of γ-phosphate. Since Gln 61 can rotate freely, the distance between the Gln and the γ-phosphate can changed within a range of 4-6 Å. These distance change only 0.1-0.2Å respect to the geometry change of the Gln61. These results show that the effect of the geometry of the Gln61 is negligible.

In reaction mechanism A, since both the generated H^+ and OH^- attack the γ-phosphate, the γ-phosphate remains neutral. In GB61, the generated H^+ and OH^- attack Gln61 and the γ-phosphate, respectively, which are 6Å apart. The Coulomb interaction between $GlnH^+$ and the γ-phosphate makes this state unstable, and this interaction is strongly affected by solvent molecules. Therefore, the solvation effect reduces the energy difference between the intermediate in GB61 and that in mechanism A.

5. Simulation study

The only difference between the intermediates in GB61 and mechanism A is the location of the proton; in GB61 the proton is on Gln61 and in mechanism A it is on the γ-phosphate. In the gas phase, the ab-initio study showed that the intermediate in GB61 is 77 kcal/mol more unstable than that in mechanism A. Since GB61 shows charge polarization ($GlnH^+$ and PO_5H^-) while mechanism A gives a neutral intermediate (PO_5H_2), a strong solvent effect is expected in

Table II. Geometry dependence of the transition state structure.

phosphate-Gln distance[a] (Å)	4	5	6
R_{OH1}[b] (Å)	1.19	1.22	1.08
R_{OH2}[c] (Å)	1.50	1.40	1.39

a: distance between the P of the γ-phasphate and the Cδ of Gln.

b: distance between the H of the activated water molecule and the O of Gln.

c: distance between the O and the H within the activated water molecule.

GB61, and the energy difference of the intermediate should be reduced in the actual system.

If ΔG is the free energy difference between the intermediates of GB61 and mechanism A, then ΔG is given by the difference of the protonation energy of each intermediate:

$$\Delta G = G(GlnH^+ + PO_5H^-) - G(Gln + PO_5H_2)$$
$$= G(GlnH^+ + PO_5H^-) - G(Gln + PO_5H^-) - G(H^+)$$
$$- (G(Gln + PO_5H_2) - G(Gln + PO_5H^-) - G(H^+))$$
$$= \Delta G_A - \Delta G_B$$

where ΔG_A is the protonation energy of Gln61 and ΔG_B is the protonation energy of the γ-phosphate,

$$\Delta G_A = G(GlnH^+ + PO_5H^-) - G(Gln + PO_5H^-) - G(H^+)$$
$$\Delta G_B = G(Gln + PO_5H_2) - G(Gln + PO_5H^-) - G(H^+).$$

Figure 7 shows a schematic representation of ΔG_A, ΔG_B and the models of these states. We estimated the protonation energy with the effects of the protein and the solvent by the free energy perturbation (FEP) method [13].

$$\Delta G = G_1 - G_0$$
$$= \sum_i G_{\lambda(i+1)} - G_{\lambda(i)}$$
$$G_{\lambda(i+1)} - G_{\lambda(i)} = -k_BT \ln\langle \exp[-(V_{\lambda(i+1)} - V_{\lambda(i)})/k_BT] \rangle_{\lambda(i)}$$

where G_0 and G_1 are the free energies of state 0 and 1, respectively, $V_{\lambda(i)}$ is the potential energy of state λ(i), and $\langle\ \rangle_{\lambda(i)}$ represents the ensemble average of state λ(i). The ensemble is evaluated from an MD trajectory with $V = V_{\lambda(i)}$.

The minimum value of the force field potential is not necessarily equal to the binding energy. Therefore, the force field and the FEP result must be corrected. To do so, the system is divided into two parts; reaction center region I and region O. The interaction E is divided into three components,

$$E = E_{II} + E_{IO} + E_{OO}$$

where the suffixes, II, OO and IO represent the interactions within regions I and O,

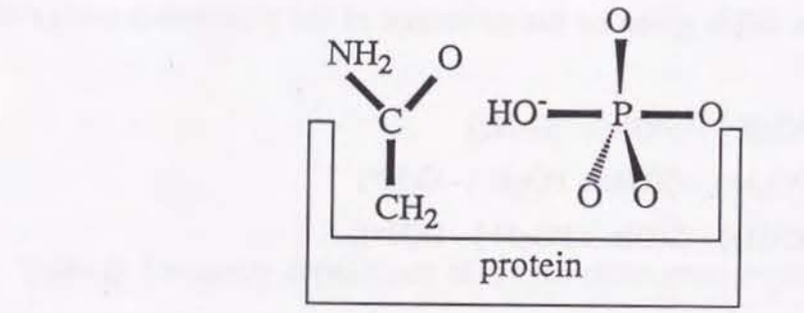

state 0 for GB61 and reaction A

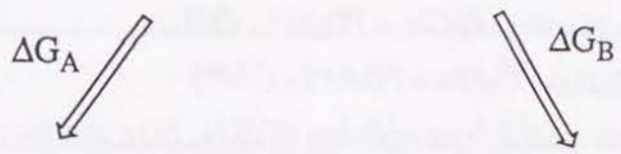

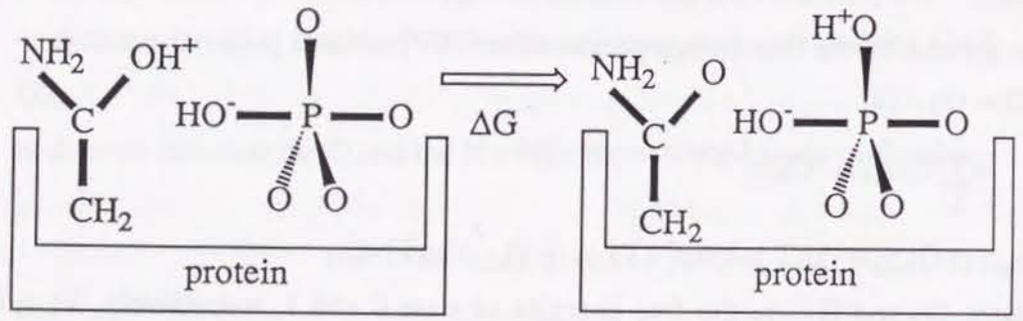

state 1 for GB61 state 1 for mechanism A

Fig 7. Schematic representation of states 0 and 1 for GB61 and mechanism A.

and the interaction between regions I and O. When region I is isolated, the ab-initio method and the empirical force field must give the same bonding energy, $E_{ab\text{-}initio} = E_{emphirical}$. We apply an energy correction E_{corr} to the empirical result,

$E_{ab\text{-}initio} = E_{emphirical} + E_{corr}$.

The addition of the constant to the force field does not influence the MD trajectory, and ΔG ca be easily corrected as,

$\Delta G = \Delta G_{MD} + E_{corr}$

In this study, states 1 and 0 represent [$GlnH^+ + PO_5H^-$] and [$Gln + PO_5H^- + H^+$] for GB61, and [$Gln + PO_5H_2$] and [$Gln + PO_5H^- + H^+$] for mechanism A, respectively (Fig 7; the protein and the solvent molecules are included in each state). Figure 8 shows region I for GB61 and mechanism A. The width of each window, $\Delta\lambda$ is set at 0.2. E_{corr} is estimated by using CH_3CONH_2 and $P_2O_8H_2$ for region I in GB61 and mechanism A, respectively.

$E_{corr} = E_{ab\text{-}initio} - E_{emphirical}$

= 192 kcal/mol for CH_3CONH_2

= 153 kcal/mol for $P_2O_8H_2$,

FEP gives the corrected ΔG_A and ΔG_B as 173 and 227 kcal/mol, respectively,.and the energy difference is

$\Delta G = \Delta G_A - \Delta G_B = 54$ kcal/mol

The effect of the solvent and the protein field reduce the energy difference of the respective intermediates. However, the intermediate of GB61 is still 54 kcal/mol less stable than that of mechanism A. This result shows that GB61 is not likely to occur during hydrolysis.

6. Conclusion

We studied the mechanism of hydrolysis of GTP in p21 by the ab-initio method and molecular dynamics simulation by assuming two reaction mechanisms: GB61 and mechanism A. Figure 9 shows the energy diagram obtained with the ab-initio method. The lower energy barrier is given by mechanism A, and its $\Delta G^{\ddagger}$ of 28

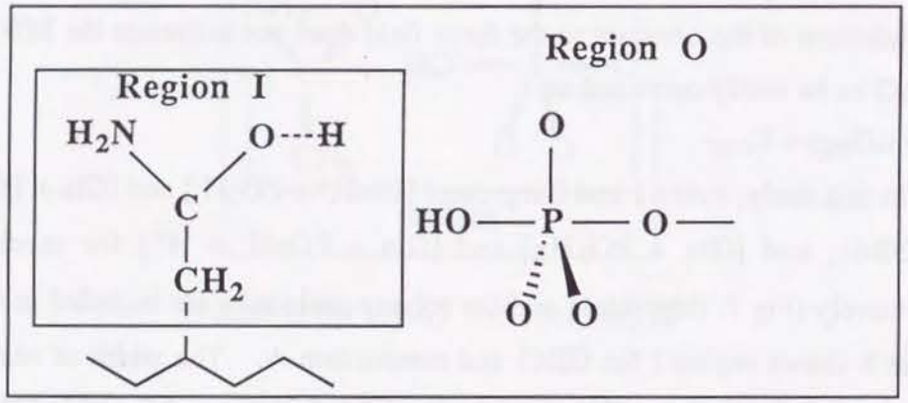

Regions I and O for GB61 mechanism

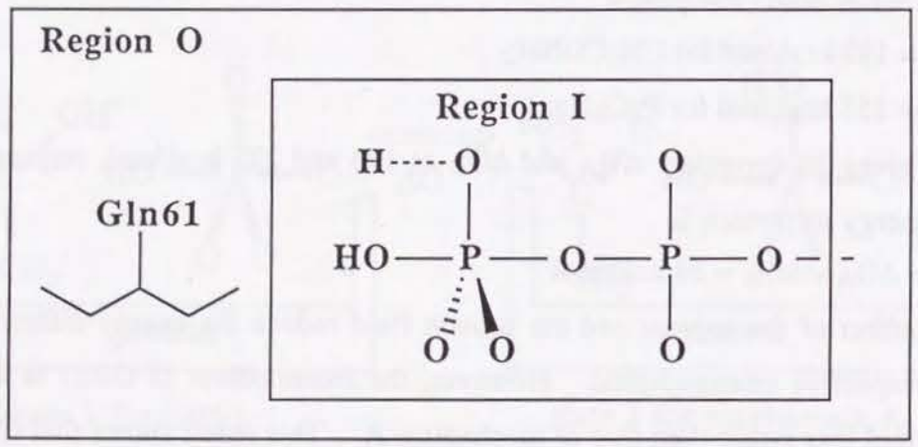

Regions I and O for mechanism A

Fig 8. Schematic representation of the regions I and O.

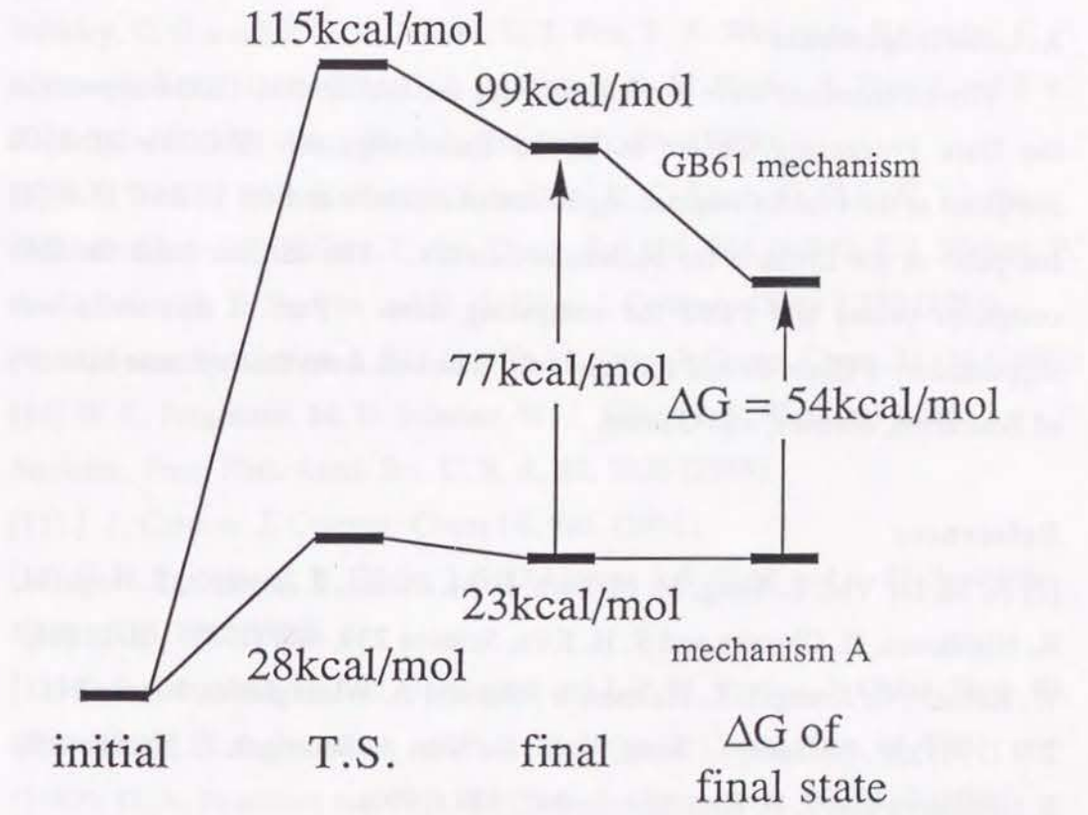

Fig 9. Energy diagram of GB61 and mechanism A. The reference of the free energy is arbitrary.

kcal/mol is similar to the observed $\Delta G^{\ddagger}$ of 23 kcal/mol. In contrast, GB61 gives a very high $\Delta G^{\ddagger}$ and an unstable intermediate. The free energy difference is estimated by the FEP method. The results show that, even considering the solvation and protein effects, the energy of the intermediate of GB61 is 54 kcal/mol higher than that of mechanism A. Therefore, we conclude that mechanism A is more likely to occur in the hydrolysis of GTP in ras p21.

Acknowledgements

The calculations were carried out with the FACOM M-1800 computer at the Data Processing Center of Kyoto University, the FACOM VP-2600 computer at the Protein Engineering Research Institute and the HITAC M-680H computer at the Institute for Molecular Science. The authors thank the IMS computer center and PERI for computing time. Part of this study was supported by a Grant-in-Aid for Scientific Research from the Japanese Ministry of Education, Science, and Culture.

References

[1] A. M. De Vos, L. Tong, M. Milburn, P. M. Matias, J. Jancarik, S. Noguchi, K. Nishimura, E. Ohtsuka and S. H. Kim, Science 239, 888 (1988) ; E. F. Pai, W. Kabsch, U. Krengel, K. Holmes, J. John and A. Wittinghofer, Nature 341, 209 (1989);M. Milburn, L. Tong, A. M. De Vos, A. Bruenger, Z. Yamaizumi, S. Nishimura and S. H. Kim Science 247, 939 (1990).

[2] R. Langen, T. Schweins and A. Warshel, Biochemistry 31, 8691 (1992).

[3] E. F. Pai, U. Krengel, G. A. Petsko, R. S. Goody, W. Kabsch and A. Wittinghofer, EMBO J.9, 2351 (1990);U. Krengel, I. Schlichting, A. Scherer, R. Schumann, M. Frech, J. John, E. F. Pai, and A. Wittinghofer, Cell 62, 539 (1990);G. G. Prive, M. V. Milburn, L. Tong, A. M. De Vos, Z. Yamaizumi, S. Nishimura and S. H. Kim, Proc. Natl. Acad. Sci. U. S. A. 89, 3649 (1992).

[4] C. K. Foley, L. G. Pedersen, P. S. Charifson, T. A. Darden, A. Wittinghofer, E. F. Pai and M. W. Anderson, Biochemistry 31, 4951 (1992).

[5] S. Huzinaga, J. Andzelm, M. Klobukowski, E. R. Andzelm, Y. Sakai and H. Tatewaki, "Gaussian basis sets for molecular calculations, Physical science data Vol 16", (Elsevier Science Publishers, Amsterdam, 1984).

[6] W. J. Hehre, R. F. Stewart and J. A. Pople, J. Chem. Phys. 51, 2567 (1969).

[7] M. J. Frisch, M. Head-Gordon, H. B. Schlegel, K. Raghavachari, J. S. Binkley, C. Gonzalez, D. J. Defrees, D. J. Fox, R. A. Whiteside, R. Seeger, C. F. Melius, J. Baker, L. R. Kahn, J. J. P. Stewart, D. M. Fluder, S. Topiol, and J. A. Pople, Gaussian88, Gaussian, Inc., Pittsburgh, PA, (1988).

[8] S. J. Weiner, P. A. Kollman, D. A. Case, U. C. Singh, C. Chio, C. Alagona, S. Profeta Jr and P. Weiner, J. Am. Chem. Soc 106, 765 (1984); S. J. Weiner, P. A. Kollman, D. T. Nguyen and D. A. Case, J. Comput. Chem 7,230 (1986).

[9] M. Saito, Simulation, 8, 321 (1992); M. Saito, J. Comp. Chem.,11, 76 (1990).

[10] W. L. Jorgensen, M. D. Schaber, W. J. Allard, I. S. Sigal and E. M. Scolnick, Proc. Natl. Acad. Sci. U. S. A. 85, 5026 (1988).

[11] J. F. Cannon, J. Comput. Chem 14, 995, (1993).

[12] G. L. Temeles, J. B. Gibbs, J. S. D'Alonzo, I. S. Sigal and E. M. Scolnick, Nature 313, 700 (1985).

[13] T. P. Straatsma, H. J. C. Berendsen and J. P. M. Postma, J. Chem. Phys. 85, 6720 (1986); D. A. Pearlman and P. A. Kollman, J. Chem. Phys. 91, 7831 (1989); D. A. Pearlman and P. A. Kollman, J. Chem. Phys. 90, 2460 (1989).

PART IV
Fourier transformation of the Hartree-Fock equation.

Abstract

Fourier transformation of the Hartree-Fock equation is presented. This method combines the N one-electron simultaneous equations of the Hartree-Fock method, where N is the number of electrons in the system, into a single differential equation which includes only two variables: i.e., one spatial coordinate $\boldsymbol{x}$ (x, y, z) and a parameter t . This transformation also provides a new representation for the spatial distribution of the exchange interaction.

1. Introduction

If we suppose an N-electron system using the Hartree-Fock approximation, then each electron moves in an electric field produced by the other N - 1 electrons, and N one-electron wave-functions (orbitals) are required to describe the total wave function. The time-independent N-electron Schrödinger equation is defined in 3N-dimensional space as [1]

$$(\mathbf{H}(\Phi) - E)\,\Phi(x_1,..,x_N) = 0\,, \qquad (1)$$

where **H** is the Hamiltonian , E is the eigen value, and Φ is the total wave function in 3N-dimensional space. On the other hand, with the Hartree-Fock method, $\Phi(x_1,..,x_N)$ is decomposed into N one-electron wave functions (orbitals) in a three-dimensional space, which are defined by the simultaneous N-order equation as

$$(\mathbf{f}(\phi_1,\phi_N) - \varepsilon_i)\,\phi_i(x) = 0 \quad (i=1,...,N) \qquad (2)$$

where **f** is the Fock operator and ε_i is the orbital energy. This representation is somewhat cumbersome since the Hamiltonian and the number of one-electron wave functions depend on the number of electrons.

We aim in this study to rewrite this formula into the one which do not depend on the number of electrons. Several theories which incorporate this feature have been proposed, including the one-particle Green's function method, the field theory and the density equation or functional theory. The Green's function does not depend on the number of electrons, and it includes only two variables : i.e., the space coordinate and the electron energy [2]. In the field theory, the creation and annihilation operators are introduced, and these operators produce the Hamiltonian which does not depend on the number of particles, and wave functions which include only one spatial coordinate as a variable [3]. In the density equation theory, the fourth-order density function is introduced which does not depend on the number of electrons but depends on only eight spatial coordinates [4]. The density function satisfies the density equation which corresponds to the Schrödinger equation [5]. This theoretical cencept is very charming in spite of the problem, so-called N representability [6].

In this study, we use a Fourier transformation to rewrite the Hartree-Fock equation (eq.(2)) into a form which has a wave function Φ and an operator **H** that are described by only two variables: i.e., one spatial coordinate x and a parameter t, such that

$$-i\,\frac{\partial}{\partial t}\Phi(x,t) = \mathbf{H}(x,t)\,\Phi(x,t). \qquad (3)$$

The density functional theory estimates the electron exchange energy (Exc) based on the electron density [7,8]. Since this estimation makes this theory easily solved and quite useful, several other methods of estimating Exc have been proposed, like the local temperature and gradient corrections [9-12]. In this study, we show that the Fourier transformation also provides another representation of the spatial distribution of the exchange interaction.

2. Methodology of transformation

We consider a 2N-electron closed-shell system described by a restricted Hartree-Fock approximation. In addition, we assume that there is no degeneracy of the orbitals. Let $\{\phi_i(x)\}$ and $\{\varepsilon_i\}$ be the eigen vectors and the eigen values, respectively, of the Hartree-Fock equation, eq.(2) under the orthonormality condition of eq.(4).

$$\int dx\,{}^3\phi_i(x)\phi_j(x) = \delta_{ij} \qquad (4)$$

where δ_{ij} denotes Kronecker's delta. An explicit representation of the Fock operator **f** is,

$$\mathbf{f} = \mathbf{H}^{core} + \sum_{a}^{occ} [2\,\mathbf{J}\,(\phi_a) - \mathbf{K}(\phi_a)] \qquad (5)$$

$$\mathbf{H}^{core} = -\frac{1}{2}\nabla 2 + v(x) \qquad (6)$$

$$\mathbf{J}(\phi_a)\,\phi_i(x) = \int dx'3\frac{|\phi_a(x')|2\,\phi_i(x)}{r_{xx'}} \qquad (7)$$

$$\mathbf{K}(\phi_a)\,\phi_i(x) = \int dx'\frac{\phi_a{}^*(x')\,\phi_a(x)}{r_{xx'}}\,\phi_i(x') \qquad (8)$$

where $\mathbf{H}^{core}$, **J** and **K** represent the bare Hamiltonian, Coulomb repulsion and exchange repulsion operators, respectively. We can rewrite eq.(2) as

$$\sum_{i}^{occ} (\,\mathbf{f} - \varepsilon\,)\phi_i(x)\,\delta(\varepsilon_i - \varepsilon) = 0. \qquad (9)$$

Here, we impose a condition on the orbital energies: If the differences between two pairs of eigen values are equal to each other: $\varepsilon_i - \varepsilon_j = \varepsilon_k - \varepsilon_l$, then i = k and j = l. In other words, if $i \neq k$ and $j \neq l$ then $\varepsilon_i - \varepsilon_j \neq \varepsilon_k - \varepsilon_l$.

Under this condition, the Fourier transformation of eq.(9) is given as

$$F\Big(\sum_i^{occ} (\mathbf{f} - \varepsilon)\phi_i(\boldsymbol{x})\, \delta(\varepsilon_i - \varepsilon)\Big) = (\mathbf{H} + i\frac{\partial}{\partial t})\Phi \qquad (10)$$

where the pseudo-wave function $\Phi(\boldsymbol{x},t)$ and the pseudo-Hamiltonian $\mathrm{H}(\boldsymbol{x},t)$ include a new parameter t. They are defined as

$$\Phi(\boldsymbol{x},t) = \sum_i^{occ} \phi_i(\boldsymbol{x})\, \exp(i\varepsilon_i t) \qquad (11)$$

where each ϕ_i satisfies eq.(4).

In other words, the function Φ which is defined by eqs.(4) and (11) satisfies the Schrödinger-like equation, eq. (3).

The explicit representation of the **H** operator in eq.(3) is

$$\mathbf{H}(\boldsymbol{x},t) = \mathbf{H}^{core} + \int d\boldsymbol{x}'^3 \frac{2\,\rho(\boldsymbol{x}') - \sigma(\boldsymbol{x}',t) - \mathbf{R}(\boldsymbol{x}',t)}{r_{\boldsymbol{x}\boldsymbol{x}'}} \qquad (12)$$

where $\mathbf{H}^{core}$ is defined by eq. (6) and ρ, σ and **R** are given by,

$$\rho(\boldsymbol{x}) = \lim_{T\to\infty} \int_0^T \frac{dt}{T}\, \Phi^*(\boldsymbol{x},t)\, \Phi(\boldsymbol{x},t) \qquad (13)$$

$$\sigma(\boldsymbol{x},t) = \Phi^*(\boldsymbol{x},t)\, \Phi(\boldsymbol{x},t) - \rho(\boldsymbol{x}) \qquad (14)$$

$$\mathbf{R}(\boldsymbol{x},t) = \sum_j^{occ} \phi_j(\boldsymbol{x})\phi_j^*(\boldsymbol{x})\, \exp(2i\varepsilon_j t)\, \mathbf{I}, \qquad (15)$$

where **I** is the inversion operator on t such that

$$\Phi(\boldsymbol{x},-t) = \mathbf{I}\, \Phi(\boldsymbol{x},t). \qquad (16)$$

We note that $\Phi(\boldsymbol{x},t)$ and $\mathbf{H}(\boldsymbol{x},t)$ are described by two variables: i.e., the 3-dimensional positional vector, $\boldsymbol{x}$ = (x, y, z), and the parameter t. The number of variables in Φ and **H** does not depend on the number of electrons. Although the parameter t does not represent time, the dimension of t is the same as that of time. Only **R** includes the HF orbitals, $\phi_j(\boldsymbol{x})$ and its complex conjugate. Furthermore, instead of excluding the exchange operator, this equation includes the time inversion operator **I** which can not be represented by the classical normal calculation.

We now give a prof for eq.(10). We decompose the right-hand side of eq.(10) into the following four terms and perform a Fourier transformation on the terms in sequence, as follows:

(step 1) transformation of the bare Hamiltomian part gives

$$F\Big(\sum_i^{occ} \mathbf{H}^{core}\, \phi_i(\boldsymbol{x})\, \delta(\varepsilon_i - \varepsilon)\Big) = \mathbf{H}^{core}\, \Phi(\boldsymbol{x},t)\,. \qquad (17)$$

(step 2) transformation of the orbital energy part gives

$$F\Big(\sum_i^{occ} \varepsilon\, \phi_i(\boldsymbol{x})\, \delta(\varepsilon_i - \varepsilon)\Big) = -\,i\,\frac{\partial}{\partial t}\Phi(\boldsymbol{x},t). \qquad (18)$$

(step 3) transformation of the Coulomb repulsion part gives

$$F\Big(\sum_i^{occ}\sum_a^{occ} \mathbf{J}(\phi_a)\phi_i\, \delta(\varepsilon_i - \varepsilon)\Big) = \mathbf{J}(\Phi)\, \Phi(\boldsymbol{x},t). \qquad (19)$$

(step 4) transformation of the exchange repulsion part gives

$$F\Big(\sum_i^{occ}\sum_a^{occ} \mathbf{K}\,(\phi_a)\,\phi_i\, \delta(\varepsilon_i - \varepsilon)\Big) = \int d\boldsymbol{x}'^3 \frac{\sigma(\boldsymbol{x}',t) + \mathbf{R}(\boldsymbol{x}',t)}{r_{\boldsymbol{x}\boldsymbol{x}'}}\, \Phi(\boldsymbol{x},t). \qquad (20)$$

3. Transformation of the Fock operator

(step 1) Transformation of the bare Hamiltonian $\mathbf{H}^{core}$

Since $\mathbf{H}^{core}$ does not include the orbital energy or the exchange operator, this step is easily performed,

$$F\Big(\sum_i^{occ} \mathbf{H}^{core}\, \phi_i(\boldsymbol{x})\, \delta(\varepsilon_i - \varepsilon)\Big)$$

$$= \int d\varepsilon \sum_i^{occ} \mathbf{H}^{core}\, \phi_i(\boldsymbol{x})\, \delta(\varepsilon_i - \varepsilon)\, \exp(i\varepsilon t)$$

$$= \mathbf{H}^{core} \sum_i^{occ} \phi_i(\boldsymbol{x}) \exp(i\varepsilon_i t). \qquad (21)$$

Using eq.(11), the right-hand side of eq.(21) is reduced, and eq. (17) is confirmed.

(step 2) Transformation of the orbital energy component ε

Since this term clearly includes the orbital energy, this transformation is slightly difficult:

$$F\Big(\sum_{i}^{occ} \varepsilon\ \phi_i(x)\ \delta(\varepsilon_i - \varepsilon)\Big)$$

$$= \int d\varepsilon \sum_{i}^{occ} \varepsilon\ \phi_i(x)\ \delta(\varepsilon_i - \varepsilon)\ \exp(i\varepsilon t)$$

$$= \sum_{i}^{occ} \varepsilon_i\ \phi_i(x)\ \exp(i\varepsilon_i t). \qquad (22)$$

Here, the relation is obviously satisfied:

$$\varepsilon_i\ \phi_i \exp(i\varepsilon_i t) = -\,i\,\frac{\partial}{\partial t}\phi_i \exp(i\varepsilon_i t). \qquad (23)$$

Replacing the each term in eq. (22) by eq. (23), then

$$\text{eq. (22)} = -\,i\,\frac{\partial}{\partial t}\sum_{i}^{occ} \phi_i(x)\ \exp(i\varepsilon_i t). \qquad (24)$$

Putting eq. (11) into the right-hand side of eq.(24), we obtain the expected form eq. (18).

(step 3) Transformation of the Coulomb repulsion term **J**

Since the Coulomb repulsion term does not include the energy or the exchange operator, this transformation is easy:

$$F\Big(\sum_{i}^{occ}\sum_{a}^{occ} \mathbf{J}(\phi_a)\phi_i\ \delta(\varepsilon_i - \varepsilon)\Big)$$

$$= \int d\varepsilon \sum_{i}^{occ} \mathbf{J}(\rho)\ \phi_i\ \delta(\varepsilon_i - \varepsilon)\ \exp(i\varepsilon t)$$

$$= \int dx'^3 \frac{\rho(x')}{r_{xx'}} \sum_{i}^{occ} \phi_i(x)\ \exp(i\varepsilon_i t)$$

$$= \int dx'^3 \frac{\rho(x')}{r_{xx'}}\ \Phi(x,t). \qquad (25)$$

Furthermore, the electron density $\rho(x)$ in eq.(25) can be represented by Φ. We can show that the average of $\Phi^*\Phi$ on t gives ρ:

$$\lim_{T\to\infty} \int_0^T \frac{dt}{T}\ \Phi^*(x,t)\ \Phi(x,t)$$

$$= \lim_{T\to\infty} \int_0^T \frac{dt}{T} \sum_{i}^{occ} \phi_i(x)^*\ \phi_j(x) \exp(i(\varepsilon_i - \varepsilon_j)t)).$$

If $\varepsilon_i \neq \varepsilon_j$ then the integral of $\exp(i(\varepsilon_i - \varepsilon_j)t))))/T$ is zero, and the integral is non-zero only when $\varepsilon_i = \varepsilon_j$, then we can further transform the above equation as,

$$= \sum_{i}^{occ} \phi_i(x)^*\ \phi_i(x)$$

$$= \rho(x). \qquad (26)$$

Here, the electron density ρ in eq.(25) is represented by Φ and we obtain eq. (19).

(step 4) Transformation of the exchange repulsion term **K**

Since the Fourier transformation is reversible, we examine the inverse Fourier transform F^{-1} of eq. (20), instead of examining the Fourier transform F.

The inverse transformation of the first term of eq. (20) is

$$F^{-1}\Big(\int dx'^3 \frac{\sigma(x',t)\ \Phi(x,t)}{r_{xx'}}\Big) = \int dt\ \exp(-i\varepsilon_a t) \int dx'^3\ \frac{\sigma(x',t)}{r_{xx'}}\Phi(x,t). \qquad (27)$$

Here, $\sigma(x,t)$ is defined by eq. (14) and the explicit expression is,

$$\sigma(x,t) = \sum_{a\neq l}^{occ} \phi_a(x)\phi_l^*(x)\exp(i(\varepsilon_a - \varepsilon_l)t). \qquad (28)$$

Substituting σ in eq. (27) by eq. (28), then

$$\text{eq. (27)} = \int dt \sum_{a\neq l}^{occ}\sum_{i}^{occ} \int dx'^3 \frac{\phi_a(x')\phi_l^*(x')\phi_i(x)}{r_{xx'}} \exp(i(\varepsilon_a - \varepsilon_l + \varepsilon_i - \varepsilon)t)$$

$$= \sum_{a\neq l}^{occ}\sum_{i}^{occ} \int dx'^3 \frac{\phi_a(x')\phi_l^*(x')\phi_i(x)}{r_{xx'}}\ \delta(\varepsilon_a - \varepsilon_l + \varepsilon_i - \varepsilon). \qquad (29)$$

In section 2, we assume that all eigen values $\{\varepsilon_i\}$ satisfy the following condition: If the differences between two pairs of eigen values are equal to each other: $\varepsilon_i - \varepsilon_j = \varepsilon_a - \varepsilon_l$, then i = a and j = l. Applying this condition to eq.(29), we obtain,

$$\text{eq. (29)} = \sum_{i\neq a}^{occ} \int dx' \frac{\phi_i^*(x')\ \phi_i(x)}{r_{xx'}}\ \phi_a(x')\delta(\varepsilon_i - \varepsilon)$$

$$= \sum_{i\neq a}^{occ} \mathbf{K}\ (\phi_a)\ \phi_i\ \delta(\varepsilon_i - \varepsilon). \qquad (30)$$

Eq.(30) corresponds to the exchange interaction term in cases where $i \neq a$.

We next attempt to transform the second term of eq.(20). Performing the inverse Fourier transformation as in the previous discussion, we obtain,

$$F^{-1}\left(\int dx'^3 \frac{R(x',t)}{r_{xx'}}\Phi(x,t)\right)$$

$$= \int dt\, \exp(-i\varepsilon t)\int dx'^3 \frac{R(x',t)}{r_{xx'}}\Phi(x,t)$$

$$= \int dt \sum_{i}^{occ}\sum_{a}^{occ}\int dx'^3 \frac{\phi_a(x')\phi_a(x')^*\phi_i(x)}{r_{xx'}}\exp(i(2\varepsilon_a - \varepsilon - \varepsilon_i)t). \qquad (31)$$

If we let l = a in the condition mentioned above, we find that if $\varepsilon_a - \varepsilon_j = \varepsilon_k - \varepsilon_a$, namely $2\,\varepsilon_a = \varepsilon_j + \varepsilon_k$, then a = j and a = k.

Using this condition, eq.(31) becomes,

$$\text{eq. (31)} = \int dx'^3 \frac{\phi_a(x')\phi_a(x')^*\phi_a(x)}{r_{xx'}}\delta(\varepsilon_a - \varepsilon)$$

$$= \sum_{a}^{occ} \mathbf{K}(\phi_a)\phi_a\,\delta(\varepsilon_a - \varepsilon). \qquad (32)$$

Eq.(30) plus eq. (32) gives the complete transformation of the exchange term, and eq. (20) is confirmed. All of the terms which must be transformed are given in eqs. (21), (24), (25), (30), and (32) and the Fourier transformation of eq. (11) is confirmed.

4. Additional feature

The Hartree-Fock total energy E_0 can be derived from eqs. (3) and (11), and it is given by

$$E_0 = \lim_{T\to\infty}\int_0^T \frac{dt}{T}\int dx^3\,\Phi(x,t)^*\,[\mathbf{H}^{core} - i\frac{\partial}{\partial t}]\Phi(x,t). \qquad (33)$$

It is easy to prove eq.(33):

$$\text{eq. (33)} = \lim_{T\to\infty}\int_0^T \frac{dt}{T}\sum_{i}^{occ}\sum_{j}^{occ}\int dx^3\,\phi_i(x)^*\,[\mathbf{H}^{core} - i\frac{\partial}{\partial t}]\phi_j(x)\exp(i(\varepsilon_i - \varepsilon_j)t)$$

$$= \lim_{T\to\infty}\int_0^T \frac{dt}{T}\sum_{i}^{occ}\sum_{j}^{occ}\int dx^3\,\phi_i(x)^*[\,\mathbf{H}^{core} + \varepsilon_j]\,\phi_j(x)\exp(i(\varepsilon_i - \varepsilon_j)t)$$

$$= \sum_{i}^{occ}[<\phi_i(x)^*\,\mathbf{H}^{core}\,\phi_i(x)> + \varepsilon_i\,]. \qquad (34)$$

Eq.(34) is the explicit representation of the Hartree-Fock total energy.

$\sigma(x,t)$ represents the density which yields the exchange interaction and $\mathbf{R}(x,t)$ represents the density which yields the electron self-energy. The average of $\sigma(x,t)$ on

t is regarded as the representation of the spatial distribution of the exchange interaction.

$$\overline{\sigma(x)} = \left(\int_0^T \sigma(x,t)^2\,\frac{dt}{T}\right)^{1/2}$$

using eq. (28) then,

$$= \Big(\sum_{i\neq j}^{occ}(\phi_i(x)\phi_i(x)^*)\,(\phi_j(x)\phi_j(x)^*)^{1/2}$$

$$= \Big(\sum_{i\neq j}^{occ}\rho_i(x)\rho_j(x)\Big)^{1/2}, \qquad (35)$$

where $\rho_i(x) = \phi_i(x)\phi_i(x)^*$.

5. Concluding remarks

If the argument t is taken to be the time, then the $\Phi(x,t)$ is regarded as the wave in the 3-dimensional space. Each $\exp(i\varepsilon_i t)$ in eq. (11) gives the excitation of the each wave whose energy is ε_i, and the linear combination of these waves gives the total wave function $\Phi(x,t)$. The complex conjugate of $\exp(i\varepsilon_i t)$, $\exp(-i\varepsilon_i t)$ annihilates the each wave. Thus, these $\exp(-i\varepsilon_i t)$ and $\exp(i\varepsilon_i t)$ are similar to the annihilation and creation operators in the second quantization theory. Since both the $\exp(-i\varepsilon_i t)$ and $\exp(i\varepsilon_i t)$ are classical number, the anti-commutation relation of the creation and annihilation operators are reflected to the time dependent electron density, eqs. (14) and (15).

If all of the orbital energies satisfy the condition mentioned in the text, then Fourier transformation combines the simultaneous equations of the Hartree-Fock method into a single differential equation. The new wave-function and equation are described by two variables: i.e., one spatial coordinate x = (x, y, z) and a parameter t. Eq.(3) is not useful for practical applications. It includes the time inversion operator **I** instead of the exchange operator, and the decomposed equation(eq.(2)) is generally easier to solve. In addition, since the electrons are distinguished only by their energies, eq. (3) is useless in a degenerated system. However, we should note that the density $\overline{\sigma(x)}$ that is derived by this transformation, represents the spatial density distribution which yields the exchange interaction. Eq. (35) shows that the overlaps

of the different orbitals contributes the exchange repulsion. This results is different from that of the Xa method, in that theory, the exchange repulsion is estimated by the total electron density based on the free electron gas model. Eqs. (5) and (8) shows that the exchange repulsion comes from the summation of the overlaps of the different orbitals, in this sense, the definition eq. (35) is somewhat natural.

6. Acknowledgement

The author is grateful to professor H. Nakatsuji for the valuable discussions especially on the physical images of this work and warm encouragements.

References

[1] Dirac PAM (1953) The principles of quantum mechanics. Oxford University Press, London.

[2] Economou EN (1983) Green's functions in quantum physics, Springer-Verlag, Berlin.

[3] Avery J (1976) Creation and Annihilation Operators, McGraw-Hill, New York.

[4] Löwdin PO (1955) Phys. Rev.(97):1474.

[5] Nakatsuji H (1976) Phys. Rev. A14:41.

[6] Coleman AJ (1963) Rev. Mod. Phys.35:668.

[7] Parr RG and Yang W (1989) Density-Functional Theory of Atoms and Molecules, Oxford University Press, New York.

[8] Kohn W and Sham LJ (1965) Phys. Rev. A140:1133.

[9] Ghosh SK and Parr RG (1986) Phys. Rev. A34:785.

[10] Ghosh SK, Berkowitz M and Parr RG (1984) Proc. Natl. Acad. Sci. (U.S.A.)81:8028.

[11] Ghosh SK and Berkowitz M (1985) J. Chem. Phys. 2976:83.

[12] Yang W (1986) Phys. Rev. A34:4575.

LIST OF PUBLICATIONS

PART I

Chapter 1

Theoretical study on hydrogen adsorption on a ZnO surface

H.Nakatsuji and Y.Fukunishi, Int.J.Quantum.Chem., 42, 1101 (1992)

Chapter 2

Modifications for ab-initio calculations of the moderately large-embedded-cluster model. Hydrogen adsorption on a lithium surface

Y.Fukunishi and H.Nakatsuji, J.Chem.Phys.97, 6535 (1992)

PART II

Chapter 1

Cluster model study on GaAs crystal epitaxial growth by arsenic molecular beam.I.: As_2 adsorption on GaAs surface

Y.Fukunishi and H.Nakatsuji, Surf. Sci. 291, 271 (1993).

Chapter 2

Cluster model study on GaAs crystal epitaxial growth by arsenic molecular beam.II.: Mechanism involving a $GaAs_2$ intermediate cluster

Y.Fukunishi, H.Nakatsuji, Surf. Sci.,291, 281 (1993).

Chapter 3

Cluster model study on GaAs crystal epitaxial growth by arsenic molecular beam.III.:As_4 molecular beam

Y.Fukunishi, H.Nakatsuji, Surf. Sci. submitted for publication.

PART III

Theoretical study on the hydrolysis of Guanosine Triphosphate in ras-p21 protein

Y.Fukunishi, M. Saitoh and H. Nakatsuji, in preparation.

PART IV

Fourier transformation of the Hartree-Fock equation

Y. Fukunishi, Theoritica. Chimica. Acta., submitted for publication.

Other publications

(1)

Direct modification of orientational opacity function for the CF_3H + Ar(3P) reaction using information entropy

Y.Fukunishi,T.Kasai and K.Kuwata, Chem.Phys, 177, 85 (1993).

(2)

Electronic structure and reaction mechanisms of chemisorbed hydrogen and occluded hydrogen in metal

Y.Fukunishi, M.Hada, and H.Nakatsuji, Syokubai, 33, 270 (1991)

(3)

Dipped adcluster model for chemisorptions and catalytic reactions on a metal surface.

H.Nakatsuji,H.Nakai and Y.Fukunishi, J.Chem.Phys.95, 640 (1991)

(4)

Formation of an intense pulsed beam of CH_3Cl in the |111> state using a 2-m electrostatic hexapole field

T.Kasai,T.Fukawa,T.Matsunami,D-C Che,K. Ohashi, Y.Fukunishi, H.Ohoyama, and K.Kuwata, Rev.Sci.Instrum, Rev. Sci. Instrum. 64, 1150, (1993).

(5)

Chemisorption and catalysis on a metal surface

H.Nakai,Y.Fukunishi and H.Nakatsuji, Kikan-kagaku-sosetsu:Inorganic Quantum Chemistry, 13, 158 (1991)

(6)

Theoretical studies on the surface-molecule interactions and reactions

H.Nakatsuji, M.Hada, H.Nakai and Y.Fukunishi, Syokubai, in press.